AFOSR-TR- 78-1028   FOR FURTHER TRAN

J. H. WAGNER
T. H. OKIISHI
DECEMBER 1977

D D C

JUN 22 1978

E

ANALYSIS OF MULTISTAGE, AXIAL FLOW TURBOMACHINE WAKE PRODUCTION, TRANSPORT, AND INTERACTION

TURBOMACHINERY
COMPONENTS RESEARCH PROGRAM

ENGINEERING RESEARCH INSTITUTE
IOWA STATE UNIVERSITY
AMES, IOWA 50010 USA

78 06 19 068

SECURITY CLASSIFICATION OF THIS PAGE (When Data Entered)

REPORT DOCUMENTATION PAGE	READ INSTRUCTIONS BEFORE COMPLETING FORM

1. REPORT NUMBER AFOSR-TR-78-1028	2. GOVT ACCESSION NO.	3. RECIPIENT'S CATALOG NUMBER

4. TITLE (and Subtitle)
ANALYSIS OF MULTISTAGE, AXIAL FLOW TURBOMACHINE WAKE PRODUCTION, TRANSPORT, AND INTERACTION.

5. TYPE OF REPORT & PERIOD COVERED
INTERIM rept.
1 Oct 76 - 30 Sep 77

6. PERFORMING ORG. REPORT NUMBER
ISU-ERI-AMES-78173, TCRL-10

7. AUTHOR(s)
J. H. WAGNER
T. H. OKIISHI

8. CONTRACT OR GRANT NUMBER(s)
AFOSR-76-2916

9. PERFORMING ORGANIZATION NAME AND ADDRESS
IOWA STATE UNIVERSITY
ENGINEERING RESEARCH INSTITUTE
AMES, IOWA 50011

10. PROGRAM ELEMENT, PROJECT, TASK AREA & WORK UNIT NUMBERS
2307A4
61102F

11. CONTROLLING OFFICE NAME AND ADDRESS
AIR FORCE OFFICE OF SCIENTIFIC RESEARCH/NA
BLDG 410
BOLLING AIR FORCE BASE, D C 20332

12. REPORT DATE
Dec 77

13. NUMBER OF PAGES
113p.

14. MONITORING AGENCY NAME & ADDRESS(if different from Controlling Office)

15. SECURITY CLASS. (of this report)
UNCLASSIFIED

15a. DECLASSIFICATION/DOWNGRADING SCHEDULE

16. DISTRIBUTION STATEMENT (of this Report)

Approved for public release; distribution unlimited.

17. DISTRIBUTION STATEMENT (of the abstract entered in Block 20, if different from Report)

18. SUPPLEMENTARY NOTES

19. KEY WORDS (Continue on reverse side if necessary and identify by block number)
AXIAL-FLOW COMPRESSOR
AXIAL-FLOW TURBOMACHINE
AXIAL-FLOW FAN
AXIAL-FLOW BLOWER
AXIAL-FLOW PUMP
WAKE
TURBOMACHINE FLUID FLOW
MULTISTABE AXIAL-FLOW TURBOMACHINE

20. ABSTRACT (Continue on reverse side if necessary and identify by block number)
A periodic-average flow measurement technique involving a hot-wire anemometer system was used to measure the periodically unsteady and three-dimensional fluid velocity field between blade rows in the first stage of a low-speed, multistage, axial-flow research compressor. These data suggest that the fluid flow through the imbedded rotor and stator rows is appreciably unsteady, in a periodic fashion in portions of the compressor annulus. Illustrative examples of periodic-average fluid flow field variation with rotor blade sampling position in stop-action sequence are presented for different locations in the compressor. A

DD FORM 1473 1 JAN 73
404 418

UNCLASSIFIED
SECURITY CLASSIFICATION OF THIS PAGE (When Data Entered)

simple, first order approximation physical description of the blade wake flow transport and interaction process largely based on experimental data interpretation is proposed to organize and to help explain the observations made. Blade span variations of flow data reflect end-wall effects. Inlet guide vane exit flow data involve some unusual unsteady flow effects.

ENGINEERING
RESEARCH

**ANALYSIS OF MULTISTAGE, AXIAL FLOW
TURBOMACHINE WAKE PRODUCTION,
TRANSPORT, AND INTERACTION**

J. H. Wagner
T. H. Okiishi
December 1977

78 06 19 068

ACKNOWLEDGMENTS

SUMMARY

A periodic-average flow measurement technique involving a hot-wire anemometer system was used to measure the periodically unsteady and three-dimensional fluid velocity field between blade rows in the first stage of a low-speed, multistage, axial-flow research compressor. These data suggest that the fluid flow through the imbedded rotor and stator rows are appreciably unsteady, in a periodic fashion, in portions of the compressor annulus. Illustrative examples of periodic-average fluid flow field variation with rotor blade sampling position in stop-action sequence are presented for different locations in the compressor. A simple, first order approximation physical description of the blade wake flow transport and interaction process largely based on experimental data interpretation is proposed to organize and to help explain the observations made. Blade span variations of flow data reflect end-wall effects. Inlet guide vane exit flow data involve some unusual unsteady flow effects.

TABLE OF CONTENTS

LIST OF FIGURES

LIST OF TABLES

SYMBOLS AND NOTATION

A	cross section area, m^2
$\vec{A}$	unit vector along hot-wire sensor (Figure 8)
b_0, b_1, $b_2 \ldots b_9$	effective cooling velocity/actual velocity ratio correlation coefficients
c	blade chord length (Figure 3), meters
E_ℓ	linearized anemometer bridge voltage, volts
g	local acceleration of gravity, 9.8026 m/s^2
g_c	conversion factor, 1.0 kgm/Ns^2
h_{hg}	height of barometer mercury column, meters
K_1, K_2, K_3	effective cooling velocity equation constants (Equation B-9)
m	constant hot-wire probe turning measurement angle increment (Figure 9), degrees
P_{atm}	barometric pressure (Equation B-1), N/m^2
PHH	percent passage height from hub (Equation B-4), percent
Q_v	Venturi metered volume flow rate (Equation B-5), m^3/s
r	radius from compressor axis, meters
R	gas constant, Nm/kg^oK
R_{cb}	cable resistance, ohms
R_{ph}	probe holder resistance, ohms
R_{p1}	probe lead resistance, ohms
$R_{s,c,d}$	cold resistance read off anemometer deck, ohms
$R_{s,op,d}$	sensor operating resistance anemometer deck setting (Equation 17), ohms
RPM	rotor rotational speed, rpm
R,Y,Z	compressor coordinate system (Figure 10)

S   circumferential space between blades, blade pitch (Figure 3), meters or degrees

t   temperature, ^{o}K

t_{baro} barometer ambient temperature, ^{o}K

t_{max} blade section maximum thickness (Figure 3), meters

U   rotor blade velocity (Equation B-6), m/s

V   calibration nozzle jet velocity (Equation B-7), m/s

$\vec{V}$ absolute velocity (Figure 10), m/s

V'   relative velocity (Equation B-17), m/s

V_e hot-wire effective cooling velocity (Equation 5b), m/s

V_z axial component of fluid velocity (Figure 10; Equation B-15), m/s

V_θ tangential component of absolute fluid velocity (Figure 10; Equation B-16), m/s

V'_θ tangential component of relative fluid velocity (Equation B-17), m/s

x,y,z   hot-wire probe coordinates fixed to probe (Figure 8)

Y   circumferential traversing position, degrees

YO   circumferential blade row setting position when Y is equal to zero, circumferential distance from the probe traversing measurement stations to blade stacking axis, positive in the direction of rotation, degrees

α   sensor yaw angle, angle between the velocity vector and hot-wire sensor (Figure 8; Equation 4), degrees

β_{mv} approximate tangential flow angle (Figure 9), degrees

β_r radial flow angle (Figure 10; Equation B-13), degrees

β_θ absolute tangential flow angle with respect to axial direction (Figure 10; Equation B-12), degrees

β'_θ relative tangential flow angle with respect to axial direction (Equation B-19), degrees

γ   blade stagger angle (Figure 3), degrees

γ_{H_2O} specific weight of water (Equation B-3), N/m^3

γ_{hg} specific weight of mercury, N/m^3

ΔP_n differential pressure between calibration nozzle plenum pressure and atmospheric pressure, meters of water

ΔP_{vent} differential pressure across venturi, meters of water

θ_0 hot-wire sensor angle with respect to a plane normal to the probe axis (Figure 8), degrees

θ_{off} measurement off-set angle (Figure 9)

θ_p probe pitch angle (Figure 9), degrees

θ_y probe yaw angle (Figure 8), degrees

ρ density of air (Equation B-2), kg/m^3

ϕ_v venturi flow coefficient (Equation B-8)

Additional General Subscripts

a,b,c   hot-wire probe measurement positions

h   annulus inner surface, hub

IGV   inlet guide vane

off   offset

R   rotor

S   stator

t   annulus outer surface, tip

1. INTRODUCTION

Modern design systems for turbomachines rely on, to a great
extent, empirical correlations to reflect real fluid flow effects.
This state of design competence often leads to good machines.
However, more often than can be afforded, the resultant hardware
involves undesirable deficiencies that can be related to insufficient
knowledge about the fluid mechanics involved. For example, mis-
understanding of the substantial relationships between the unsteadiness
of turbomachine flow and the efficiency, aerodynamic and aeroelastic
stability, and noise production of such machines can result in costly
disappointments. Mikolajczak [1] suggests that further significant
improvements in turbomachine technology should be sought through
better understanding and control of the unsteady flows involved.

Progress in fluid flow measurement has resulted in the develop-
ment of a variety of techniques (see, for example, References 2-27)
for observing the unsteady aspects of turbomachine flows. Precise
coordination of data acquisition with rotor sampling position has made
possible the extraction of the periodically unsteady flow (periodic-
average flow) data from the entire collection of information. The
periodic-average flow is important because of the role it plays with
respect to forced blade vibration, discrete frequency noise generation,
and turbomachine energy transfer. Data yielding detailed information
about the sequential variation of periodic-average flow with rotor
sampling position are rare [14,15,16,24,26].

In this report are offered detailed periodic-average,three-

dimensional flow data for the first stage of a low-speed, multistage,
axial-flow research compressor that demonstrate flow field variation
with sequential change in rotor sampling position. A physical
description of the complicated fluid mechanical processes involved
is proposed.

2. RESEARCH COMPRESSOR FACILITY

The research compressor facility of the Iowa State University
Engineering Research Institute/Mechanical Engineering Department
Turbomachinery Components Research Laboratory was used for the
present study. Briefly reviewed below is the research compressor and
related equipment and instrumentation. For more detailed information
see Reference 28.

2.1. Axial Flow Research Compressor

Figure 1 is a sketch of the entire research compressor apparatus.
Figure 2 depicts, in more detail, the compressor portion only. The
inlet guide vane (IGV) row and three identical rotor-stator stages
were within an annulus having constant hub (0.284 m) and tip (0.406 m)
diameters. All stationary blade rows had the same number of blades
(37) and were mounted on separate ring assemblies which could be
moved independently or in desired combinations. The rotor blade rows
each included the same number of blades (38) and were assembled
together so that all of the respective blade stacking axes were aligned
axially. All of the blades were constructed of a plastic material
(Monsanto ABS) with British C4 sections reflecting a free vortex design.
Blade characteristics are summarized below:

Number of blades per row	IGV and stator rows - 37
	rotor rows - 38
Blade span (constant)	6.10 cm (2.4 in.)
Blade chord (constant), c	3.05 cm (1.2 in.)
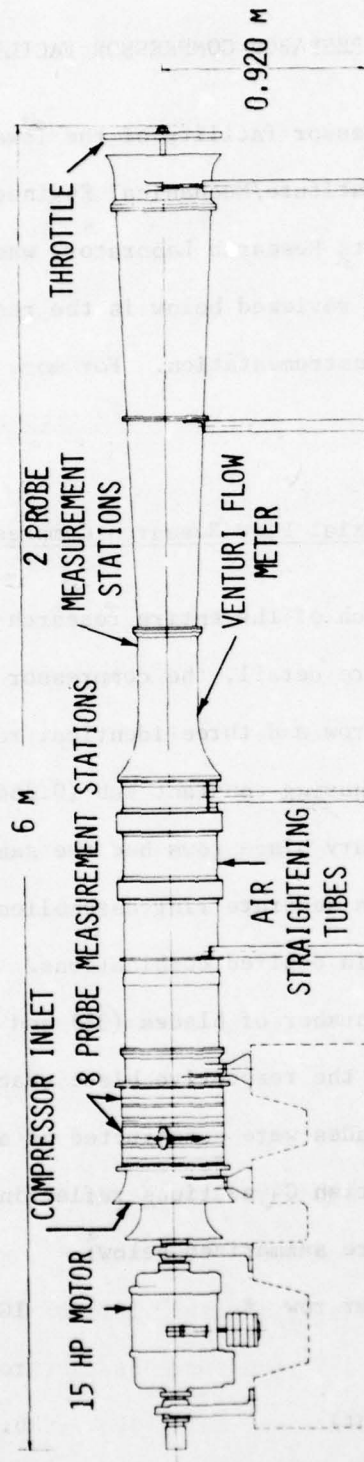
Figure 1. Research compressor apparatus side view.

PROBE
MEASUREMENT
STATIONS
1 2 3 4 5 6 7 8
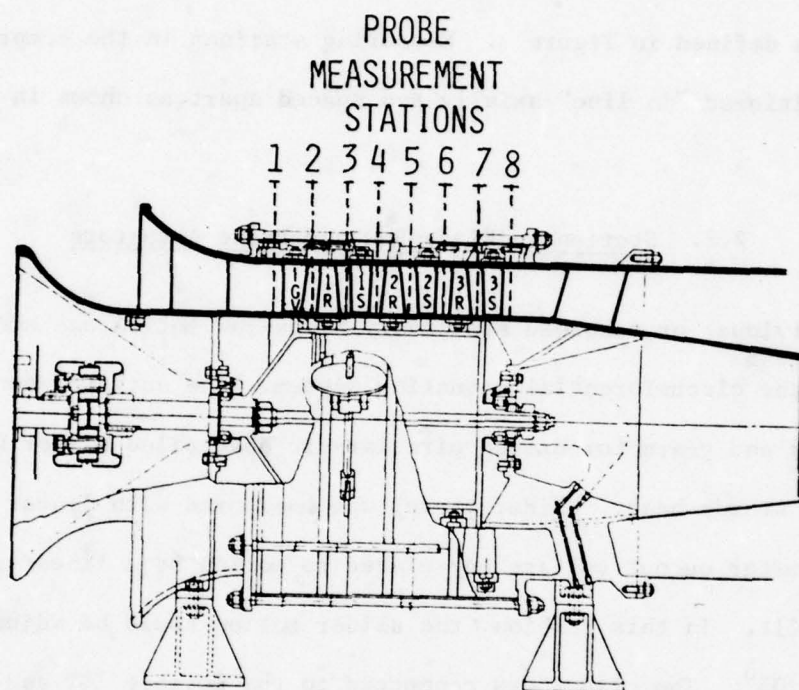
Figure 2.   Research compressor with probe measurement stations.

Blade section maximum thickness/   10%

chord ratio, t_{max}/c

Blade geometry details are tabulated in Table 1 with associated variables defined in Figure 3. Measuring stations in the compressor were positioned "in line" axially and spaced apart as shown in Figure 4.

2.2. Stationary Blade-Row and Probe Actuators

Individual or combined stationary blade-row motion was accomplished with the circumferential actuating system. The actuator consisted of a rack and gearmotor-driven circular-arc dovetailed slider moving within a sturdy base. Slider travel was monitored with linear potentiometer output voltage correlated to motion by a linear least squares fit. In this fashion, the slider motion could be adjusted to within 0.05^{o}. The slider was connected to the movable IGV and stator blade row rings with adjustable linkages so that a variety of stationary blade row positioning schedules could be achieved. Scales on each blade-row ring and the outer compressor casing were used for ascertaining the precise location of each blade row. The scales were calibrated in terms of degrees, positive in the direction of rotation. A reading of 0.0^{o} corresponded to the stacking axis of a predetermined reference blade in each row being "in line" with the measurement stations of the compressor. Any circumferential distance of a reference blade stacking axis from this zero location was denoted as YO, its circumferential position. Throughout these tests, IGV and stator blade row rings were positioned for minimum sound as follows:
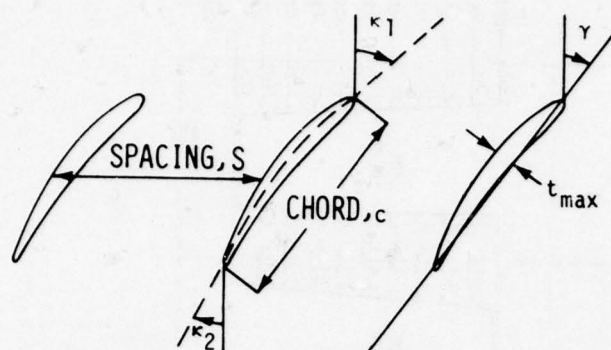
Figure 3. Blade nomenclature.

Table 1. Geometric blade tables for ICV, rotors, and stators at several radial locations.

Blade Row	Percent Passage Ht. From Hub PHH	Solidity c/S	Stagger γ degrees	Blade Angles Inlet κ_1 degrees	Outlet κ_2 degrees	Camber $\kappa_1 - \kappa_2$ degrees
IGV	0	1.263	20.35	0.00	42.10	-42.10
	10	1.211	20.05	0.00	40.77	-40.77
	20	1.164	19.69	0.00	39.47	-39.47
	30	1.121	19.25	0.00	38.23	-38.23
	40	1.080	18.65	0.00	37.08	-37.08
	50	1.041	18.15	0.00	36.05	-36.05
	60	1.004	17.63	0.00	35.02	-35.02
	70	0.971	17.05	0.00	33.93	-33.93
	80	0.940	16.45	0.00	32.92	-32.92
	90	0.913	15.65	0.00	32.10	-32.10
	100	0.887	14.15	0.00	31.40	-31.40
Rotor	0	1.299	-20.54	-42.40	3.90	-46.30
	10	1.250	-24.39	-44.76	- 2.84	-41.92
	20	1.205	-28.11	-46.85	- 9.51	-37.34
	30	1.164	-31.70	-48.53	-15.96	-32.57
	40	1.123	-35.15	-49.82	-21.88	-27.94
	50	1.078	-38.47	-50.81	-27.06	-23.75
	60	1.035	-41.66	-51.77	-31.64	-20.13
	70	0.999	-44.71	-52.90	-35.78	-17.12
	80	0.968	-47.63	-53.98	-39.26	-14.72
	90	0.939	-50.41	-54.82	-41.91	-12.91
	100	0.909	-53.07	-55.50	-44.10	-11.40
Stator	0	1.263	40.24	54.80	26.70	28.10
	10	1.211	39.32	53.48	25.67	27.81
	20	1.164	38.39	52.36	24.68	27.68
	30	1.121	37.46	51.43	23.74	27.69
	40	1.080	36.54	50.25	22.77	27.48
	50	1.041	35.61	48.56	21.72	27.84
	60	1.004	34.68	47.13	20.76	26.37
	70	0.971	33.75	46.65	20.01	26.64
	80	0.940	32.83	46.36	19.34	27.02
	90	0.913	31.90	45.59	18.62	26.97
	100	0.887	30.97	44.50	17.85	26.65

PROBE MEASUREMENT STATIONS

TIP 100%
90%
80%
70%
60%
50%
40%
30%
20%
10%
0% HUB

IGV

FIRST ROTOR

FIRST STATOR

SECOND ROTOR

SECOND STATOR

THIRD ROTOR
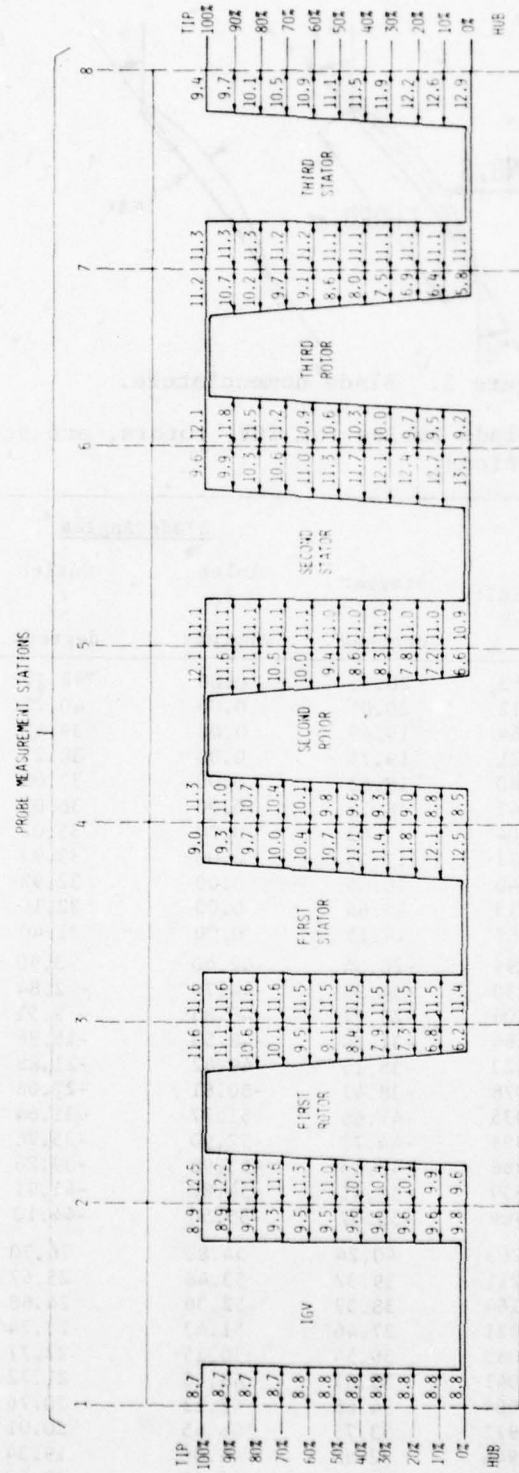
THIRD STATOR

Figure 4. Schematic diagram showing axial location of probe measurement stations (dimensions in mm).

Inlet Guide Vanes	YO_{IGV}/S_S	= 0.00
First Stator	YO_{1S}/S_S	= 0.17
Second Stator	YO_{2S}/S_S	= 0.56
Third Stator	YO_{3S}/S_S	= 0.77

The relative positioning of some of these blades may be seen in Figure 5. As will be explained later, the circumferential actuator was the key to providing the means for measuring the blade-to-blade variations of flow in the compressor. Since the probes used could not be actually traversed in the circumferential direction, the stationary and "sampled" rotor blades had to be moved circumferentially relative to a fixed probe.

The probe actuator (L. C. Smith Company model 6180) was used with the control indicator (L. C. Smith Company model DI-3R) and actuator switch box (L. C. Smith Company model DI-4R-SB) to vary the probe yaw angle and immersion depth. Probe angles and positions in the compressor annulus were monitored by observing mechanical digital counter readings and linear potentiometer output voltages. Each potentiometer's output voltage was correlated with motion with a linear least squares fit which allowed probe angles and immersion positions to be measured within 0.05^{o} and 0.15 mm respectively.

2.3. Pressure and Temperature Measurement Instrumentation

All working fluid pressure measurements were made with precision water-in-glass manometers (Meriam type Incl.) which were calibrated with a micromanometer (Meriam type Micro.). Room air temperature was
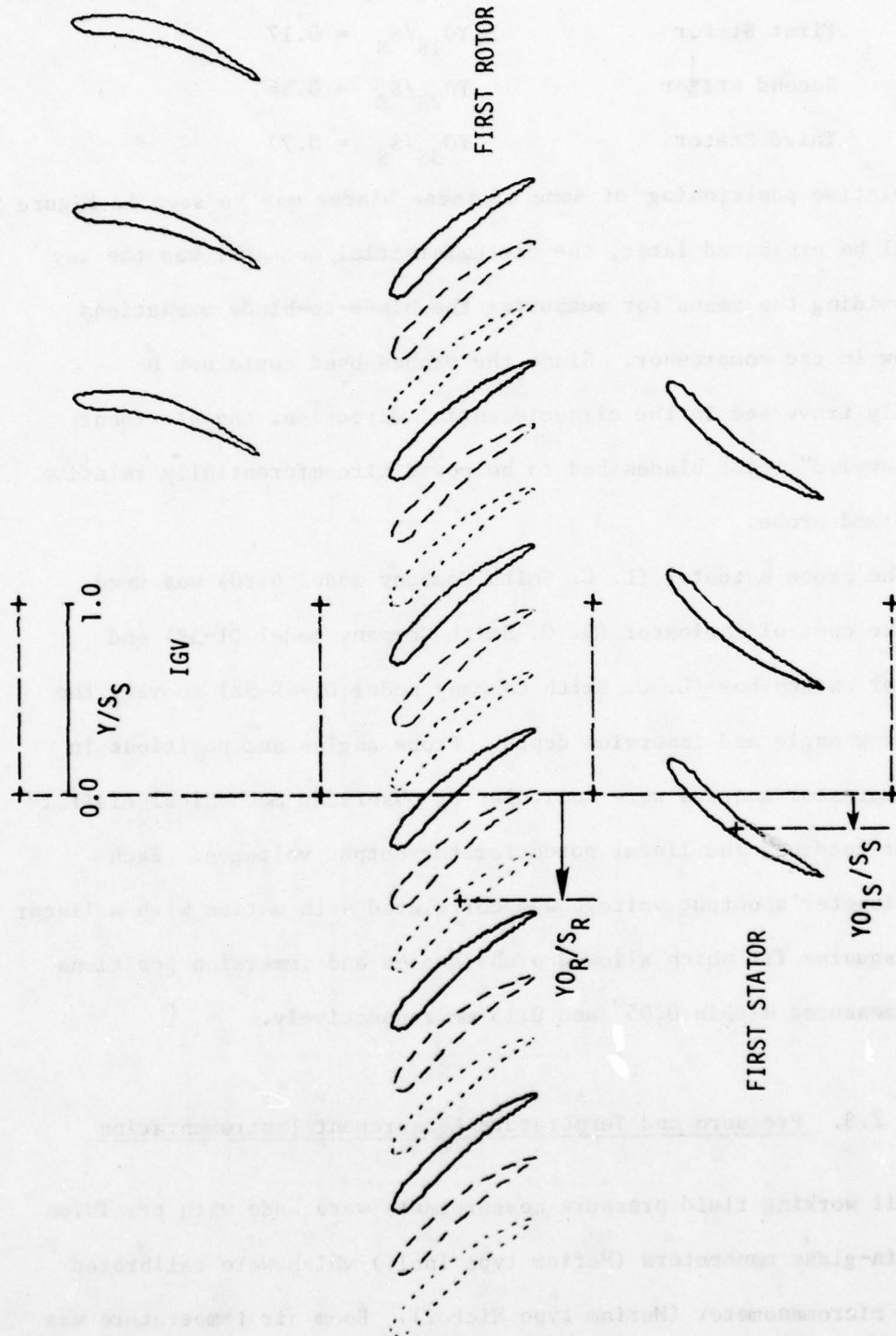
Figure 5. Blade cascade showing relative positions of blades for several rotor sampling positions.

measured with mercury-in-glass thermometers, while working fluid
temperature was measured with a copper-constantan thermocouple and
a precision millivolt potentiometer (Leeds and Northrup model 8686).
Barometric pressure was measured using a mercury-in-glass barometer
(Princo Instruments, Inc. model B-222).

2.4. Periodic-Average Measurement System

The periodic-average measurement system, shown schematically
in Figure 6, was composed of the following components:

    (1) Single slanted hot-wire probe (Disa model 55P02 Modified)

    (2) Constant temperature anemometer (Thermo-Systems, Inc.
        [TSI] model 1010A)

    (3) Linearizer (TSI model 1072)

    (4) Periodic sample-and-hold circuit

    (5) Photoelectric triggering circuit

    (6) Signal averaging circuit

    (7) Digital scanning voltmeter (Hewlett-Packard model 3480D)

    (8) Desk-top calculator (Hewlett-Packard model 9821A)

    (9) Oscilloscopes (Tektronix Inc.)

The hot-wire probe involved a 5 μm diameter platinum-plated
tungsten wire with a 1.25 mm sensing portion centered on the probe axis.
The wire was copper and gold plated at the ends and positioned at
an angle of 54.7^{o} from the probe axis. The hot-wire anemometer and
linearizer were used to produce a linear relationship between air
velocity and output voltage. The periodic sample-and-hold circuit was
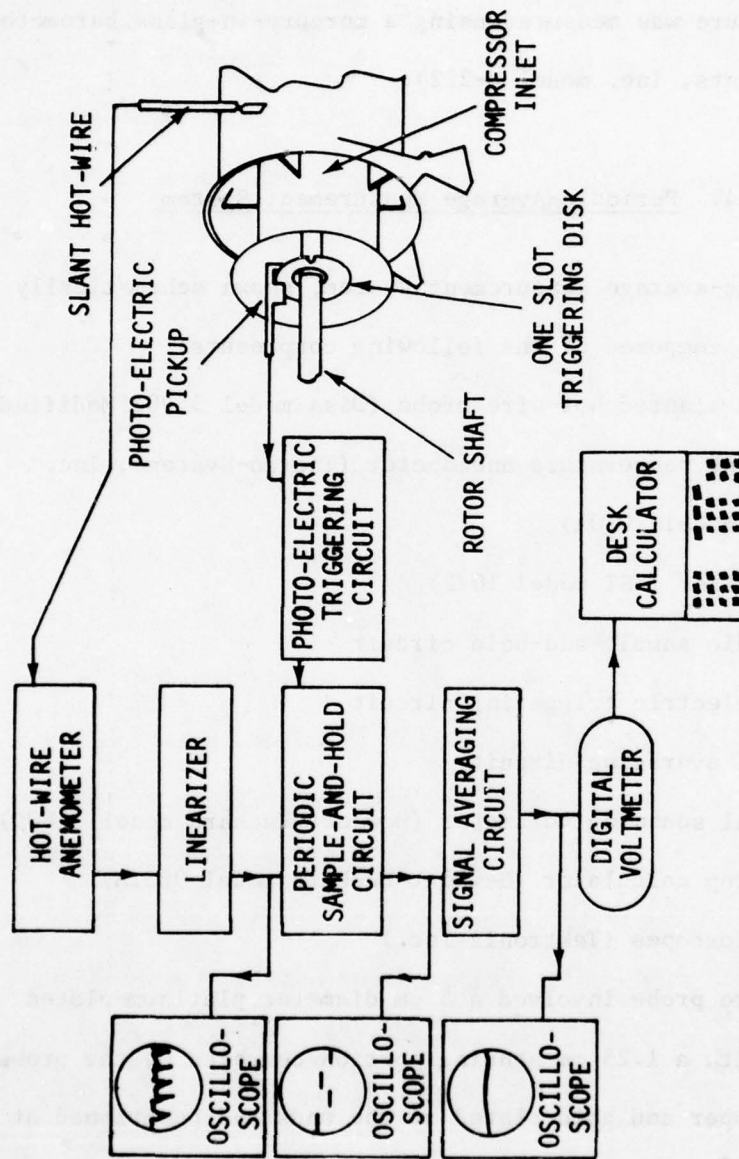
Figure 6. Schematic set-up diagram of periodic-average flow measurement system.

phase locked with the compressor rotor by the photoelectric pickup which was triggered by a slot in a disc rotating with the compressor shaft. The photoelectric pickup was connected to the stationary blade row actuator with an adjustable arm so that any desired rotor sampling position, YO_R, could be obtained. The rotor sampling position was measured, in degrees, from the line of measurement stations, with the stationary blade rows set as indicated earlier (see section 2.2.). Figure 5 shows the relative position of the stationary blades and several rotor sampling positions. The sample-and-hold circuit was designed and constructed by the Iowa State University Engineering Research Electronic Shop to obtain a 5 μsec* sample with each revolution of the rotor shaft. Two scribe marks, one on the rotating portion of the hub surface and the other on the stationary portion of the hub, were used to set the rotor phase lock reference position $YO_R/S_R = 0.0$. Once the reference condition was established, other rotor sampling positions were obtained, by moving the photoelectric pickup with respect to the stationary blade row actuator and by observing the amount of movement with mechanical scales. The reference setting was checked daily and set with an electronic time delay provision in the sample-and-hold circuit. The periodically sampled signal was electronically smoothed with the signal averaging circuit, subsequently read by the digital voltmeter, and finally arithmetically averaged and stored in the calculator for further reduction and tape storage.

---

*The typical rotor wake period is 1.1 msec.

A desk-top calculator and an associated multiple channel scanning digital voltmeter were used to read, store, and reduce data. The interfacing between the calculator and voltmeter enabled the calculator to selectively read different channels and store readings. The calculator possessed over 1400 memory registers. Additionally, with tape cassette capability, the calculator could be extended to store permanently on tape any data and programs to be recalled at the user's convenience. The plotting and tabulating of results were done with the Iowa State University Computation Center computing system (IBM 360/65, 370/158).

2.5. Calibration Nozzle

An air nozzle was used for the calibration of hot-wire sensors. The nozzle has a throat diameter of 25.4 mm (1.0 in.) and a contraction ratio of 144 to 1. The flow at the nozzle involved a uniform velocity profile for values of velocity from 0.0 to 50 m/s. Regulated compressed air provided the supply air and a variable-current heater, blower, and heat exchanger arrangement was used for air temperature control. A special probe holder permitted the sensing portion of the probe to remain in the same position in the nozzle flow while the probe yaw and pitch angles were varied. A telescope was used to visually align wires.

3. EXPERIMENTAL PROCEDURES AND DATA REDUCTION

All measurements presently involved were obtained with the periodic-average measurement system described earlier. The compressor operating point was held constant at the condition indicated in Figure 7 (1400±1 rpm, 0.42 flow coefficient) with frequent monitoring and adjusting.

The standards for velocity, pressure, and temperature instrument calibrations were provided by the calibration nozzle, the micromanometer, and mercury-in-glass thermometers. Calibration of all electronic equipment was performed by the ISU Engineering Research Institute Electronic shop.

The desk-top programmable Hewlett-Packard calculator was used extensively for calibration, data acquisition, and data reduction. Programs were used to control step-by-step data acquisition, to make preliminary calculations, to print out data and preliminary results, and to record on tapes for further data reduction. Data reduction programs accepted the preliminary results and produced final results. A list and brief description of each data acquisition and reduction program used may be found in Appendix A.

3.1. Periodic-Average Sampling Technique

The hot-wire anemometer output signal is composed of a periodic component and a random component. With controlled sampling and data averaging the random fluctuation influence can be made as small as desired, depending on the number of samples taken [4,7,18,23,25,
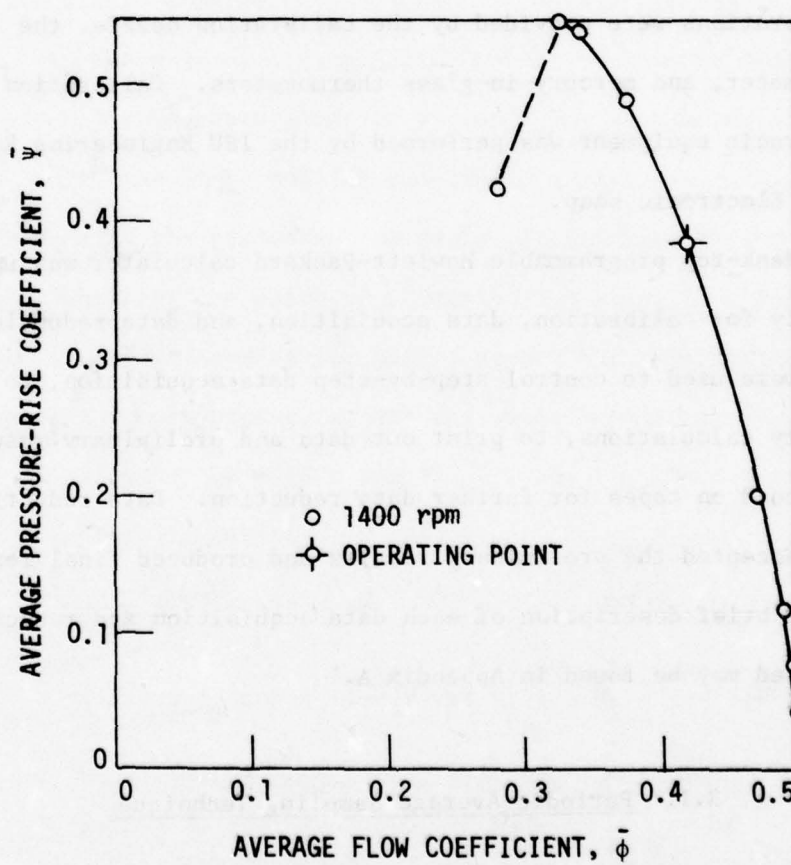
Figure 7. Research compressor performance curve and
operating point.

26,28]. With the system used presently, electronic and arithmetic averaging of data could be accomplished. The electronic averaging was done with a low pass filter having a time constant of 1 sec. Schmidt and Okiishi [28] found the arithmetic average of 180 samples of electronically-smoothed data to be approximately equal to the arithmetic average of 1200 unfiltered data points. More current data indicated that 180 samples of electronically-smoothed data were sufficient to make the random component of the unsteady flow negligibly small except at the IGV row exit where 360 samples were needed because of the separated flow activity involved.

The data sampling system was triggered by a photoelectric pickup, connected to the circumferential actuator slider, and by a single-slot disc rotating with the compressor shaft. The photoelectric pickup could be moved relative to the stationary blade rows so that periodic-average "snapshots" of the flow field could be obtained for each of several time sequenced positions of the sampled rotor blades. Thus, periodic-average flow field changes could be measured for various sampled rotor positions. This kind of measurement was accomplished by moving the stationary blade rows and the photoelectric pickup relative to the stationary probe so that the probe was effectively made to traverse the flow field over one stator blade pitch spacing.

3.2. Single, Slanted Hot-Wire Three-Dimensional Velocity Measurement Technique

A single, slanted hot-wire was used to obtain three-dimensional flow field parameters. Before the measurement technique can be

discussed, some relationships linking probe geometry and hot-wire
cooling velocities must be presented.

3.2.1. Probe Geometry

The hot-wire sensor, the probe coordinate system, and a general
velocity vector are shown in Figure 8. The coordinate system is
fixed to the probe with the x-z plane lying on the sensing portion
of the probe and the probe axis and with the y-axis perpendicular to
the x-z plane and centered on the sensor. The wire is slanted at an
angle, θ_0, to the x-axis. The velocity vector, $\vec{V}$, can be resolved
into orthogonal components along x, y, and z for each orientation of
the wire. When the probe and its coordinate system are rotated
about the z-axis, the projected yaw angle, θ_y, changes by the amount
of turning, whereas, the pitch, θ_p, remains the same. The sensor
yaw angle, α, was defined as the angle between the intersection of
the probe sensor unit vector, $\vec{A}$, and the velocity vector, $\vec{V}$. To
obtain a relationship between α and θ_0, θ_p, and θ_y, the dot product
of the two vectors is taken:

$$\vec{A} = \cos\theta_0 \; \vec{i} + \sin\theta_0 \; \vec{k} \tag{1}$$

$$\vec{V} = -V \cos\theta_p \cos\theta_y \; \vec{i} - V \cos\theta_p \sin\theta_y \; \vec{j} - V \sin\theta_p \; \vec{k} \tag{2}$$

$$\vec{A}\cdot\vec{V} = |\vec{A}||\vec{V}| \cos(180 - \alpha) = -|\vec{V}| \cos\theta_0 \cos\theta_p \cos\theta_y$$
$$-|\vec{V}| \sin\theta_0 \sin\theta_p \tag{3}$$

$$\therefore \cos\alpha = \cos\theta_0 \cos\theta_p \cos\theta_y + \sin\theta_0 \sin\theta_p \tag{4}$$
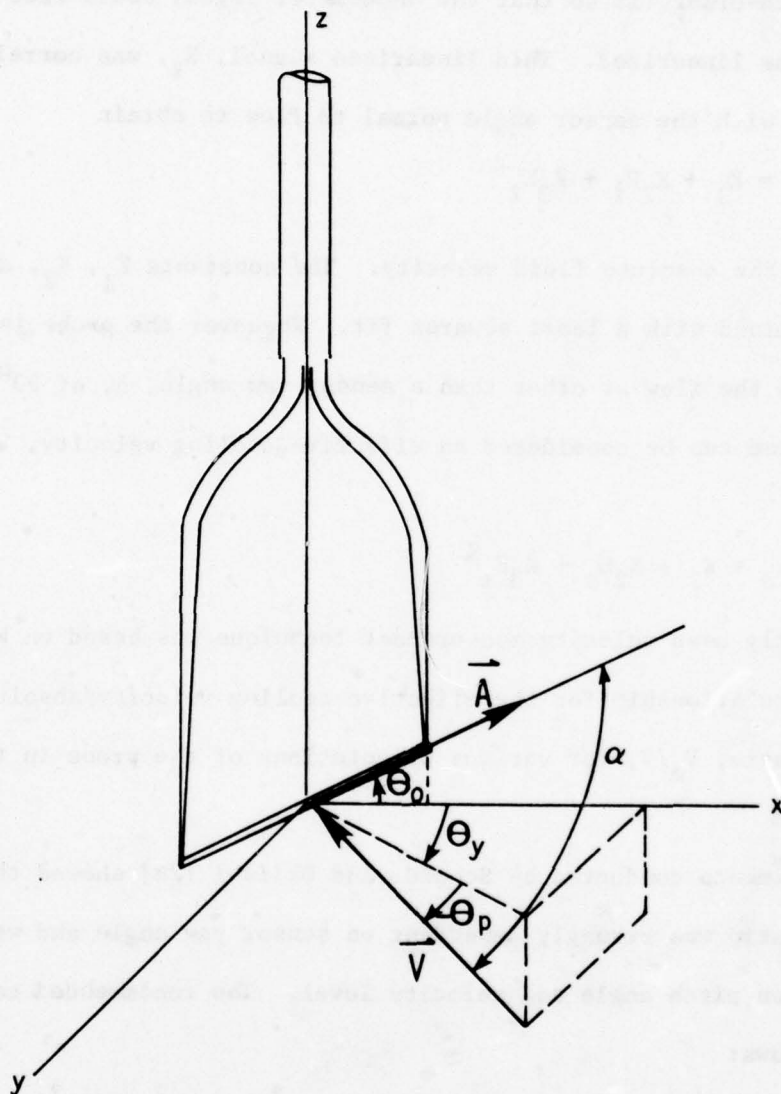
Figure 8. Hot-wire configuration relating velocity vector, $\vec{V}$, to hot-wire sensor and probe coordinates x, y, z.

3.2.2. Effective Cooling Velocity Ratio

The hot-wire anemometer output was correlated to fluid velocity with a fourth-order fit so that the anemometer signal could electronically be linearized. This linearized signal, E_ℓ, was correlated to velocity with the sensor angle normal to flow to obtain

$$V = K_1 + K_2 E_\ell + K_3 E_\ell^2 \tag{5a}$$

where V is the absolute fluid velocity. The constants K_1, K_2, and K_3 were determined with a least squares fit. Whenever the probe is oriented to the flow at other than a sensor yaw angle, α, of 90°, the velocity read can be considered an effective cooling velocity, V_e, where

$$V_e = K_1 + K_2 E_\ell + K_3 E_\ell^2 \tag{5b}$$

The presently used velocity measurement technique was based on knowing a precise relationship for the effective cooling velocity/absolute velocity ratio, V_e/V, for various orientations of the probe in the flow stream.

Experiments conducted by Schmidt and Okiishi [28] showed this velocity ratio was strongly dependent on sensor yaw angle and weakly dependent on pitch angle and velocity level. The recommended correlation is as follows:

$$V_e/V = b_0 + b_1 \alpha + b_2 \theta_p + b_3 V + b_4 \alpha^2 + b_5 \theta_p^2 + b_6 V^2$$
$$+ b_7 \alpha \theta_p + b_8 \alpha V + b_9 \theta_p V \tag{6}$$

The coefficients b_0 through b_9 were determined from a least squares fit of data as described in the calibration procedure section (see section 3.3.3.).

3.2.3. Measurement Technique

The wire was rotated in the flow field to three different positions denoted as a, b, and c (see Figure 9). These probe positions relate to yaw angles of $\theta_{y,a}$, $\theta_{y,b}$, and $\theta_{y,c}$ which were set as indicated below:

$$\theta_{y,a} = \theta_y \tag{7}$$

$$\theta_{y,b} = \theta_y - m_b \tag{8}$$

$$\theta_{y,c} = \theta_y - m_c \tag{9}$$

where m_b and m_c are probe turning angle increments from the a location. For each orientation of the wire, effectively 1200 samples were taken and electronically and arithmetically averaged to obtain a time-average effective cooling velocity for that particular probe position. For each periodic-average velocity vector measurement, a total of six equations like Eqs. (4) and (6) were obtained for the orientations of the wire. These equations are:

For position a

$$V_{e,a}/V = b_0 + b_1 \alpha_a + b_2 \theta_p + b_3 V + b_4 \alpha_a^2 + b_5 \theta_p^2$$
$$+ b_6 V^2 + b_7 \alpha_a \theta_p + b_8 \alpha_a V + b_9 \theta_p V \tag{10}$$

$$\cos \alpha_a = \cos \theta_0 \cos \theta_p \cos \theta_{y,a} + \sin \theta_0 \sin \theta_p \tag{11}$$

For position b

$$V_{e,b}/V = b_0 + b_1 \alpha_b + b_2 \theta_p + b_3 V + b_4 \alpha_b^2 + b_5 \theta_p^2$$
$$+ b_6 V^2 + b_7 \alpha_b \theta_p + b_8 \alpha_b V + b_9 \theta_p V \tag{12}$$

$$\cos \alpha_b = \cos \theta_0 \cos \theta_p \cos \theta_{y,b} + \sin \theta_0 \sin \theta_p \tag{13}$$

22

Figure 9. Hot-wire measurement positions and nomenclature,
viewed from above along probe axis.
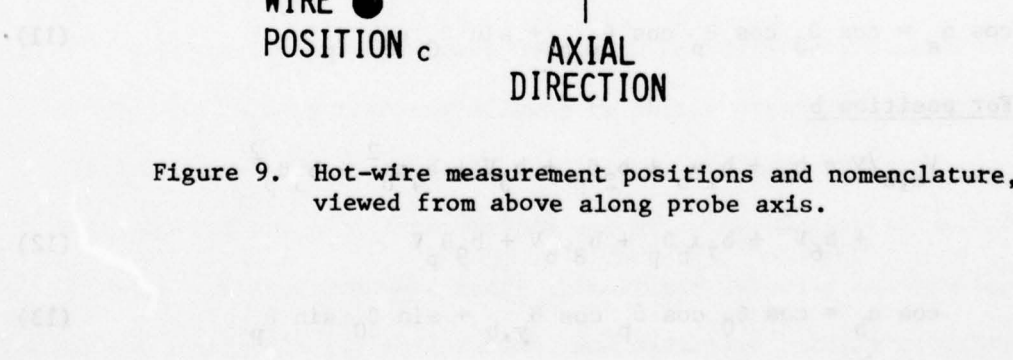
For position c

$$V_{e,c}/V = b_0 + b_1\alpha_c + b_2\theta_p + b_3V + b_4\alpha_c^2 + b_5\theta_p^2$$

$$+ b_6V^2 + b_7\alpha_c\theta_p + b_8\alpha_cV + b_9\theta_pV \tag{14}$$

$$\cos\alpha_c = \cos\theta_0 \cos\theta_p \cos\theta_{y,c} + \sin\theta_0 \sin\theta_p \tag{15}$$

By substituting Eqs. (7), (8), and (9) into Eqs. (11), (13), and (15), the six unknown variables α_a, α_b, α_c, θ_p, θ_y, and V remain in the six equations, (10) through (15). These equations were solved simultaneously using the Newton-Raphson method. The three-dimensional velocity vector is completely described with the variables θ_p, θ_y, and V known relative to the probe position, a.

To set the three wire orientations, a minimum effective velocity angle, β_{mv}, was obtained as shown in Fiure 9. From this minimum effective velocity angle position, the probe was rotated to positions a, b, and c according to the following schedule:

$$\theta_{a,off} = 20^o$$

$$\theta_{b,off} = 60^o$$

$$\theta_{c,off} = -20^o$$

From Figure 9, it can be seen that

$$\theta_{y,a} = \theta_y \simeq -20^o$$

$$\theta_{y,b} = \theta_y - m_b \simeq -60^o$$

$$\theta_{y,c} = \theta_y - m_c \simeq 20^o$$

and

$$m_b = 40^o$$

$$m_c = -40^o$$

This positioning of the probe was done for each velocity vector
obtained. For all of the measurements, the probe was positioned so
that the longer wire support was downstream of the sensing portion
of the wire to minimize prong interference.

3.3. Calibration Procedures

The calibration nozzle was used to provide a uniform velocity air
stream for velocity calibration. Plenum pressures were observed with
inclined water-in-glass manometers. Velocity was calculated using the
following equation:

$$V = \sqrt{\frac{2g_c \; \gamma_{H_2O} \; \Delta P_n}{\rho}} \tag{16}$$

where

$\quad$ V = velocity, m/s

$\quad$ g_c = gravitational constant 1.0 kg m/Ns^2

$\quad$ γ_{H_2O} = specific weight of water, N/m^3

$\quad$ ρ = density of air, kg/m^3

$\quad$ ΔP_n = differential pressure between plenum pressure and
$\quad\quad\quad$ atmospheric pressure, meters of water

Calibration programs were used with the desk-top calculator.
Sufficient warm-up time was allowed to obtain steady state conditions.
Fluid temperatures, barometric conditions, and test conditions were
entered into the calculator before and after each calibration. Three
hot-wire calibrations were made: linearizer velocity calibration,
second order velocity calibration, and effective cooling velocity ratio
calibration.

3.3.1. Linearizer Velocity Calibration

The linearizer was used to approximate the anemometer output with a fourth order polynomial. The "zero" degree term of the polynomial was set equal to zero, and coefficients were determined by a least squares curve fit, thus producing a linear relationship between velocity and anemometer output with the wire positioned normal to the flow of the calibration nozzle.

The wire was optically positioned 6.35 mm (0.25 in.) away from the nozzle exit plane. With the air velocity set close to the average value of the range of velocities anticipated, the cold combined resistance of the sensor, cables, and leads was measured, $R_{s,c,d}$. The operating resistance of the sensor was calculated with an overheat ratio of 1.8. Because the cable and lead resistances were not involved with the overheat calculation, they were subtracted from the cold resistance reading at the anemometer deck and then subsequently added back on as demonstrated in Eq. (17).

$$R_{s,op,d} = 1.8 \, (R_{s,c,d} - R_{cb} - P_{ph} - R_{pl})$$
$$+ \, R_{cb} + R_{ph} + R_{pl} \tag{17}$$

where

$R_{s,op,d}$ = deck setting of sensor operating resistance, ohms

$R_{s,c,d}$ = deck reading of combined sensor, cable, and lead resistance, ohms

R_{cb} = cable resistance, ohms

R_{ph} = probe holder resistance, ohms

R_{pl} = probe lead resistance, ohms

Probe holder and cable resistance were measured with an impedence
bridge while the probe lead resistance was taken as furnished by the
manufacturer. The linearizer calibration system included the hot-wire,
anemometer, DVM, and desk-top calculator only. The linearizer was
correlated over a range of nozzle air velocities (0.0 to 23 m/s) in
fifteen increments. The linearized polynomial velocity was compared
to the actual nozzle velocity. The acceptance criterion for the points
was that the error should be less than or equal to 1%. Linearizer
calibration was performed with every effective cooling velocity ratio
calibration.

3.3.2. Second Order Velocity Calibration

A second order correlation, Eq. (5), between the linearized
anemometer output and velocity level with the wire normal to the flow
was performed before and during effective cooling velocity calibration
and data acquisition to avoid error due to electronic equipment drift.

The second order calibration was done with the wire positioned
normal to the nozzle flow. Any other wire yaw angle does not indicate
an absolute velocity but rather an effective cooling velocity, V_e.
The second order calibration system included the probe, anemometer,
linearizer, DVM, and desk-top calculator. Fourteen points were
taken for each calibration for air velocities ranging from 4 to 23 m/s.
Acceptable error was confined to less than 1% in the velocity working
range.

3.3.3. Effective Cooling Velocity Calibration

The effective cooling velocity calibration was performed to
obtain the coefficients in the effective cooling velocity ratio equation:

$$V_e/V = b_0 + b_1\alpha + b_2\theta_p + b_3V + b_4\alpha^2 + b_5\theta_p^{\ 2}$$
$$+ b_6V^2 + b_7\alpha\theta_p + b_8\alpha V + b_9\theta_p V \tag{6}$$

The calibration was made over the range of expected compressor yaw and pitch angles and velocities.

The probe was positioned in the nozzle jet stream in the same manner as for the linearizer calibration. For a particular velocity level, the probe was set at each of six pitch angles and rotated from 0 to 90° in yaw angle increments of 5°. This procedure was continued until data for all of the velocity levels (11.6, 15.2, 19.2, 22.3 m/s) and pitch angles (-9 to 6°, in increments of 3°) were acquired. This procedure was also used for probe yaw angles of 0 to -90° because of the lack of perfect symmetry wire response to yaw angle. Thus, during data reduction, two sets of coefficients (b_0 through b_9) were used depending on the yaw orientation of the wire. Positions a and b involved the 0 to -90 calibration coefficients while position c used the 0 to +90 calibration coefficients.

After all the data were taken, the coefficients were solved using a least squares method. Acceptable error was limited to being less than 2% with the majority of the errors less than 1%.

3.4. Data Acquisition

The data acquisition system used was presented earlier in schematic form in Figure 6. Prior to taking data, equipment and room temperature equilibrium were established, inclined manometers zeroed, cold resistance of the wire at the deck set, flow coefficient set, linearizer

coefficients adjusted, second order calibration performed, probe
actuator positioned in the compressor, and radial location set. After
setting and adjusting the time delay device for $YO_R/S_R = 0.0$, the
desired rotor sampling position could be set by adjusting the photo-
electric pickup position relative to the stationary blade rows.

With the probe sensor positioned at 90° (normal to the compressor
axis), a trace of the blade-to-blade variation of effective cooling
velocity was made with an x-y storage oscilloscope where x was the
potentiometer reading from the circumferential actuator, and y was
the time-averaged hot-wire sampled signal. This survey was made by
moving the stationary blade rows and photoelectric pickup relative
to the probe. By using this procedure, the probe was effectively made
to traverse the flow field for one stator blade pitch. From this
x-y trace, the position of the wake could be detected and test points
appropriately scheduled. The circumferential actuator system was
then set back to zero, $Y/S_s = 0.0$, for the first test data point. With
another x-y storage oscilloscope, a trace of effective cooling velocity
against probe yaw angle was repeatedly obtained by rotating the probe
about its axis. In this fashion, a minimum effective cooling velocity
angle, β_{mv}, could be discerned. From this minimum angle position, the
probe could be appropriately positioned to locations a, b, and c,
discussed earlier (see Figure 9). After periodically sampled data
were obtained, with the probe at each position (a, b, and c), the
circumferential actuator was shifted to a new position, Y/S_s, and the
above described procedure was repeated. Thirty velocity vectors from
blade-to-blade were measured for each test run. After the last velocity

vector of a set of thirty was measured, the acquired data were stored
on tape for further reduction. The probe was then removed from the
compressor and a new second order velocity calibration was made. Second
order velocity calibrations were performed before each set of thirty
velocity vectors was measured.

3.5. Data Reduction

Data reduction programs for the desk-top calculator were used to
accept and reduce stored data. The six equations, Eqs. (10) through
(15), were solved simultaneously with the Newton-Raphson method.
Usually, less than five iterations were necessary for convergence.

The compressor coordinate system is shown in Figure 10. The R
coordinate direction is positive outward from the hub, while the θ
coordinate is positive in the direction of rotation. The Z-axis is
aligned axially, positive in the direction of fluid motion. Also
shown are the sign conventions relating to β_θ, β_r, V_r, V_z, and V_θ.
With the probe immersed in the compressor annulus, the probe coordinates
x and y (see Figure 8) are always in the same plane as Y and Z of
the compressor coordinate system, and z from the probe coordinate
system coincides with the R compressor coordinate direction.

The calculated pitch angle and radial angle are related by:

$$\beta_r = -\theta_p$$

The tangential angle is related to the calculated yaw, θ_y, by:

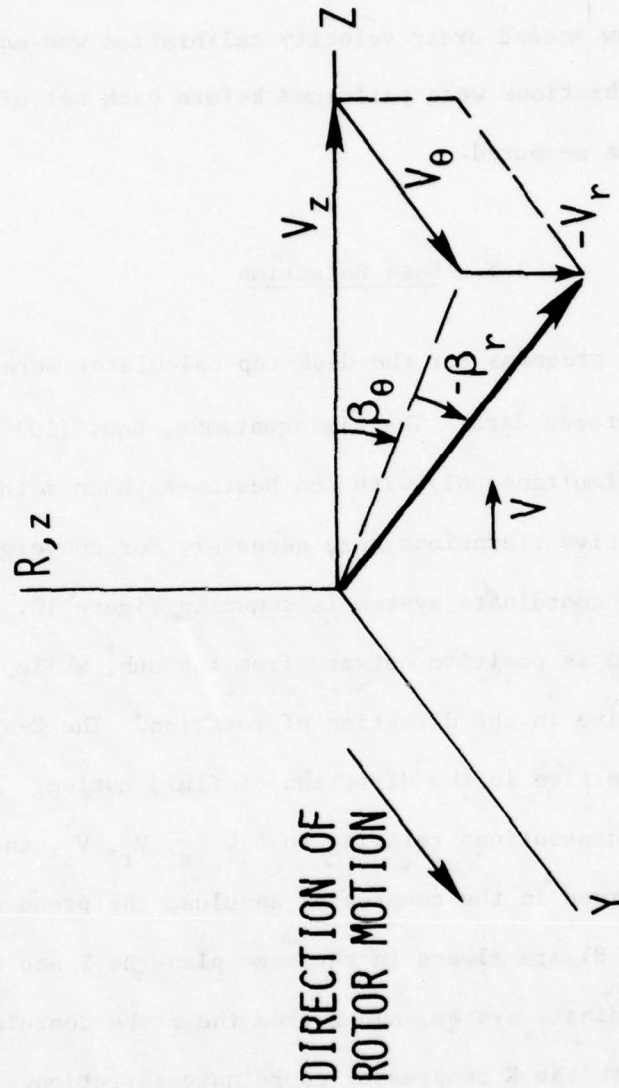$$\beta_\theta = \beta_{mv} + \theta_{a,off} + \theta_y$$

Figure 10. Compressor coordinate system showing nomenclature and sign convention for three-dimensional periodic-average velocity and angle parameters.

The values of β_{mv} and $\theta_{a,off}$ were known from data acquisition. The other flow parameters calculated are presented below:

(1) Axial velocity, m/s, Eq. (B-15)

(2) Absolute tangential velocity, m/s, Eq. (B-16)

(3) Radial velocity, m/s, Eq. (B-14)

(4) Relative velocity, m/s, Eq. (B-17)

(5) Relative tangential velocity, m/s, Eq. (B-18)

(6) Relative tangential angle, degrees, Eq. (B-19)

A complete list of equations used appears in Appendix B.

33

4. PRESENTATION AND DISCUSSION OF DATA

The test results are presented and discussed in this section.
Primary flow variables involved are tabulated in Appendix C. Velocity
and flow angle component variation graphs (scalar plots) are used to
present the periodic-average data (see Figures 11, 12, and 13). The
scalar plots include axial, tangential, and radial velocities supple-
mented with tangential, radial, and, when useful, relative tangential
angles. Uncertainty and accuracy are previously discussed by Schmidt
and Okiishi [28]. To reflect and facilitate data interpretation,
blade-to-blade plane flow plots (cascade plots), showing the periodic-
average location of blade wake flows at different radii for several
distinct orientations of the rotor blades, were constructed (see
Figure 14). The procedure used to construct the cascade plots is
explained in detail below. A physical explanation of the wake trans-
port and interaction effects involved is proposed.

4.1. Construction of Cascade Wake Plots

Stationary blade section profiles were positioned on the plots to
scale according to the minimum sound schedule (see section 2.2.).
The rotor blade sections were located at their periodic sampling
positions.

The obvious wake region locations suggested by the periodic-average
flow data were drawn on the cascade plots first. It should be noted
that periodic-average flow data collection was limited to thirty points
along the broken lines connecting crosses between blade rows, Y/S_S =

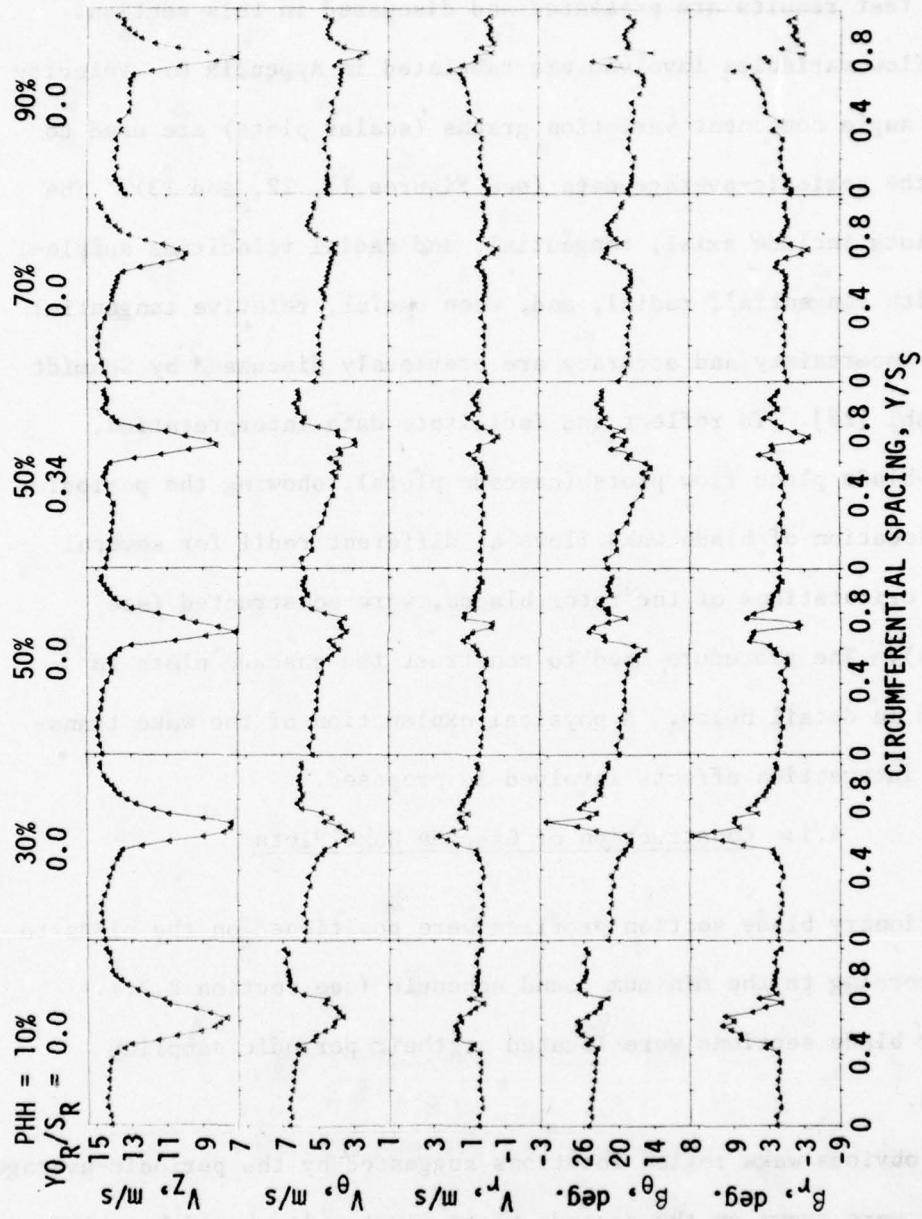Figure 11. Blade-to-blade distribution of periodic-average flow-field parameters. Inlet guide vane exit flow.

(a) First rotor exit flow at
50% passage height from hub.

Figure 12. Blade-to-blade distribution of periodic-average
flow-field parameters. First rotor exit flow.

36

(a) (Continued).

Figure 12. (Continued).

(b) First rotor exit flow at 10% passage height from hub.

Figure 12. (Continued).

$YO_R/S_R = 0.0$ 0.42

CIRCUMFERENTIAL SPACING, Y/S_S

(c) First rotor exit flow at 30% passage height from hub.

Figure 12. (Continued).

39

(d) First rotor exit flow at 70% passage height from hub.

Figure 12. (Continued).
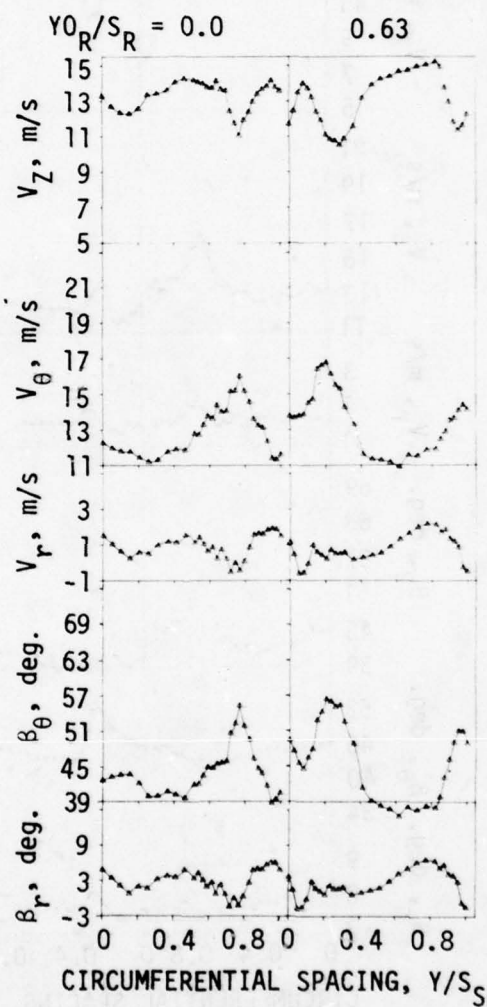
(e) First rotor exit flow at 90% passage height from hub.

Figure 12. (Continued).
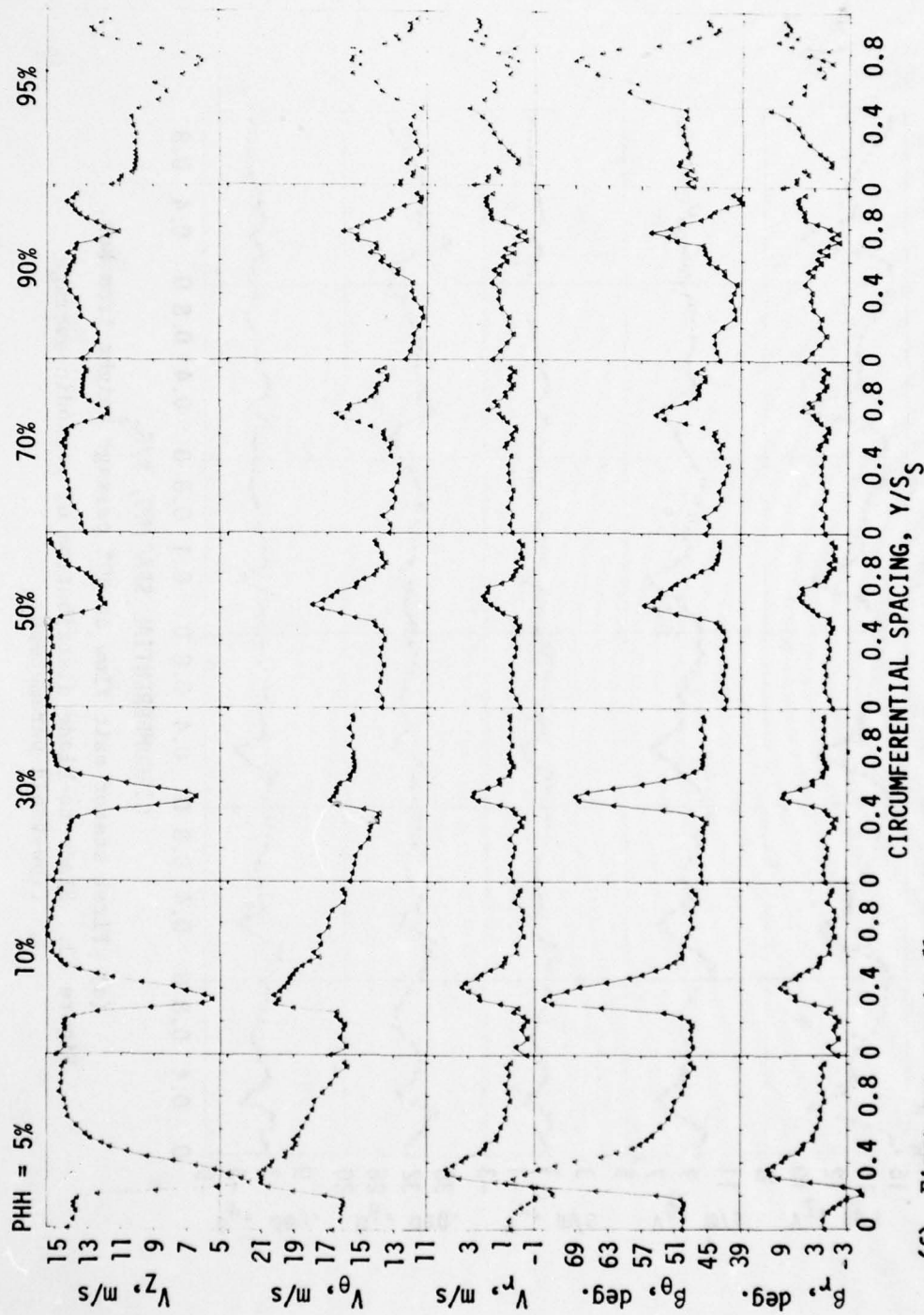
(f) First rotor exit flow at rotor sampling position $YO_R/S_R = 0.0$ and seven different passage heights.

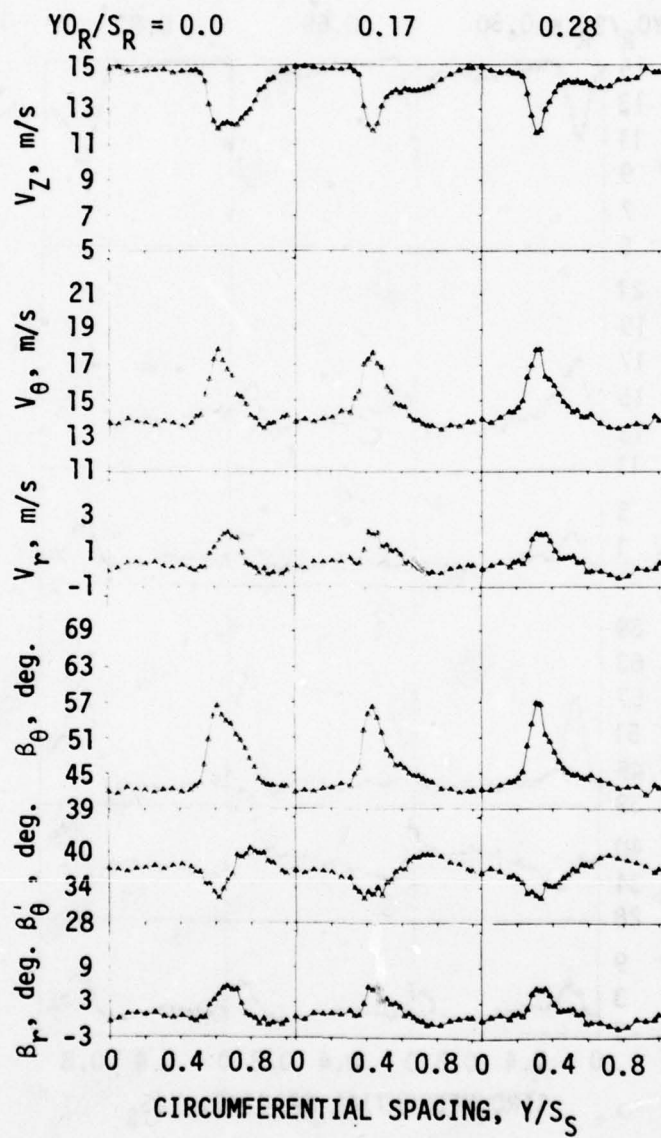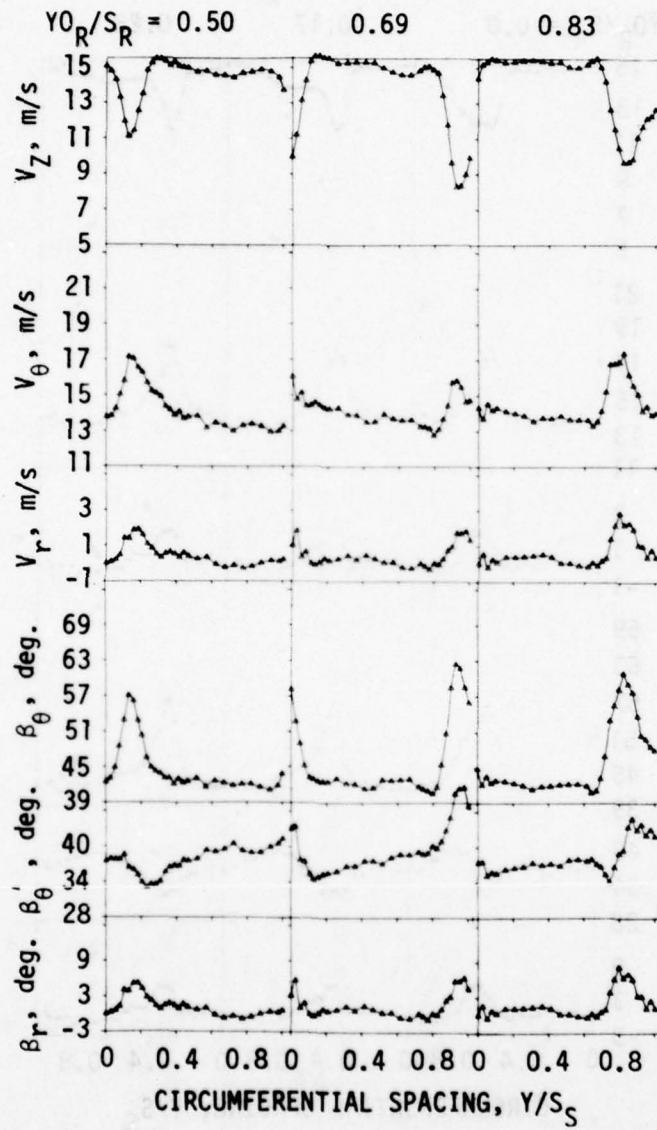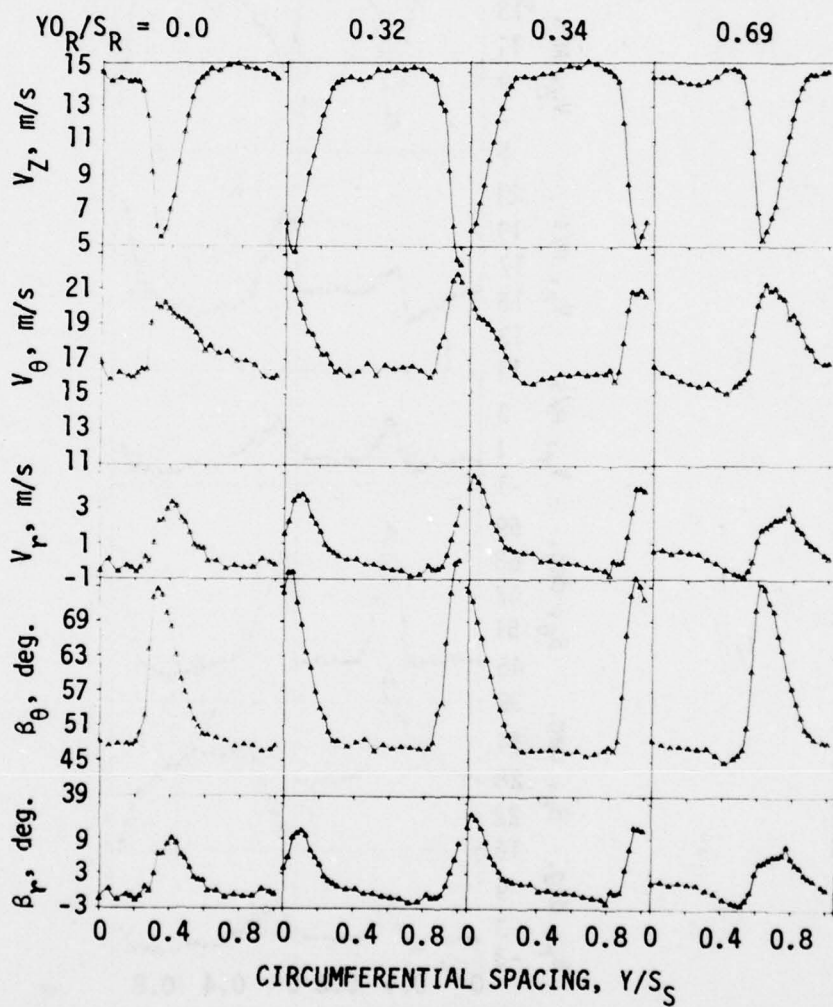Figure 12. (Continued).
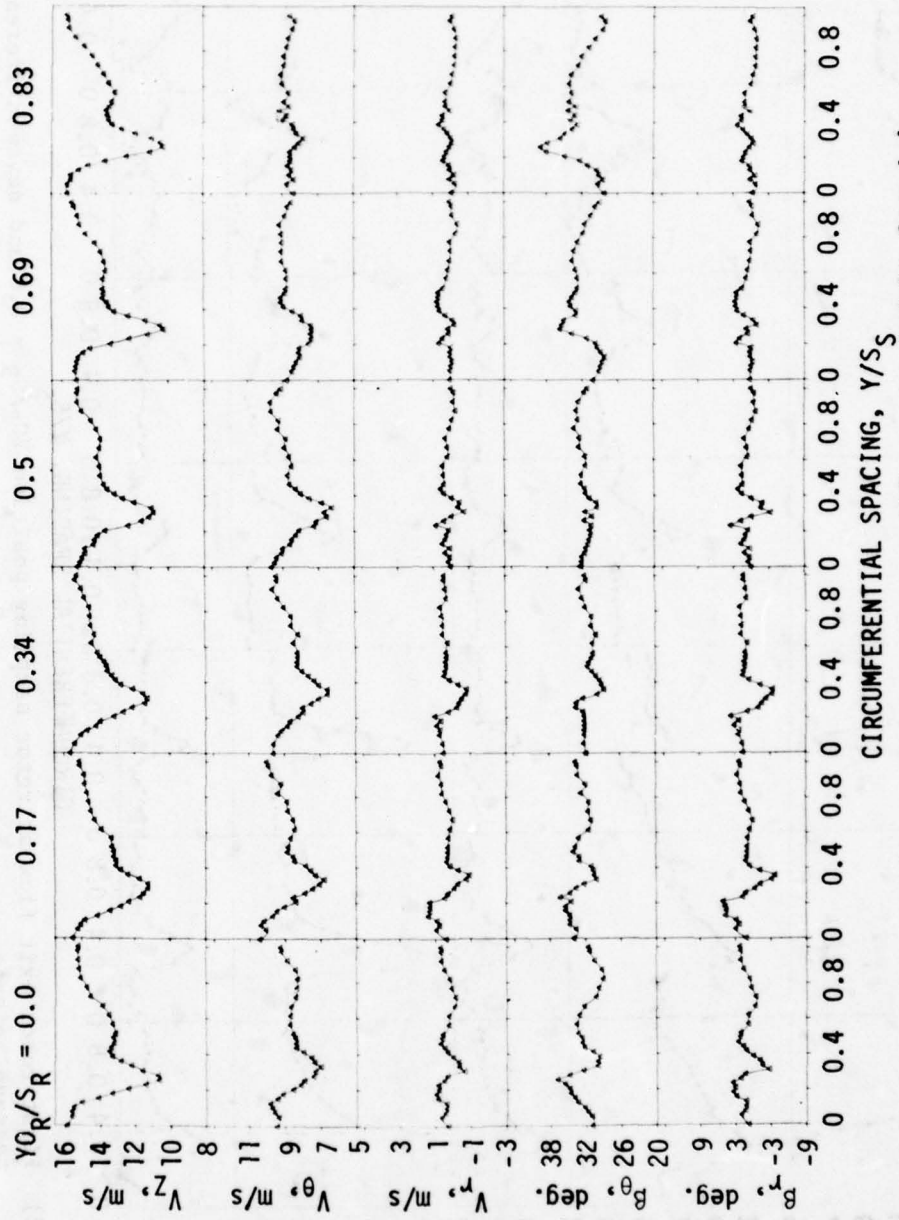
(a) First stator exit flow at 50% passage height from hub.

Figure 13. Blade-to-blade distribution of periodic-average flow-field parameters.
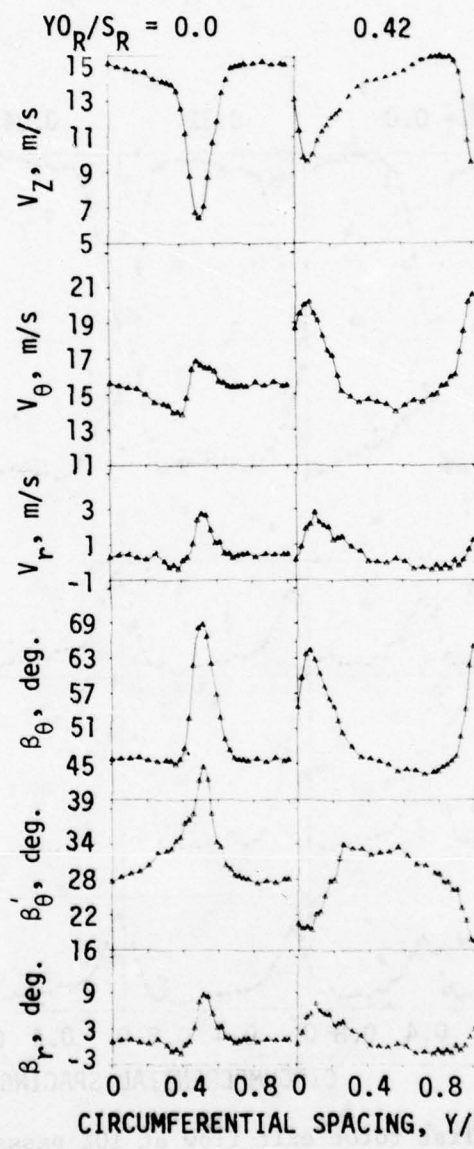
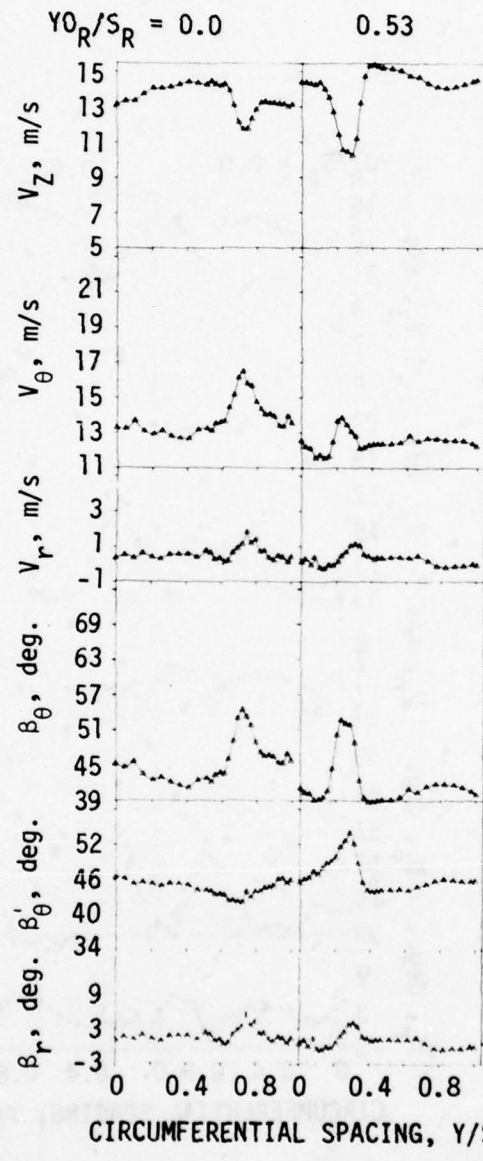(b) First stator exit flow at 10% passage height from hub.

(c) First stator exit flow at 30% passage height from hub.

Figure 13. (Continued).

(d) First stator exit flow at 70% passage height from hub.

(e) First stator exit flow at 90% passage height from hub.
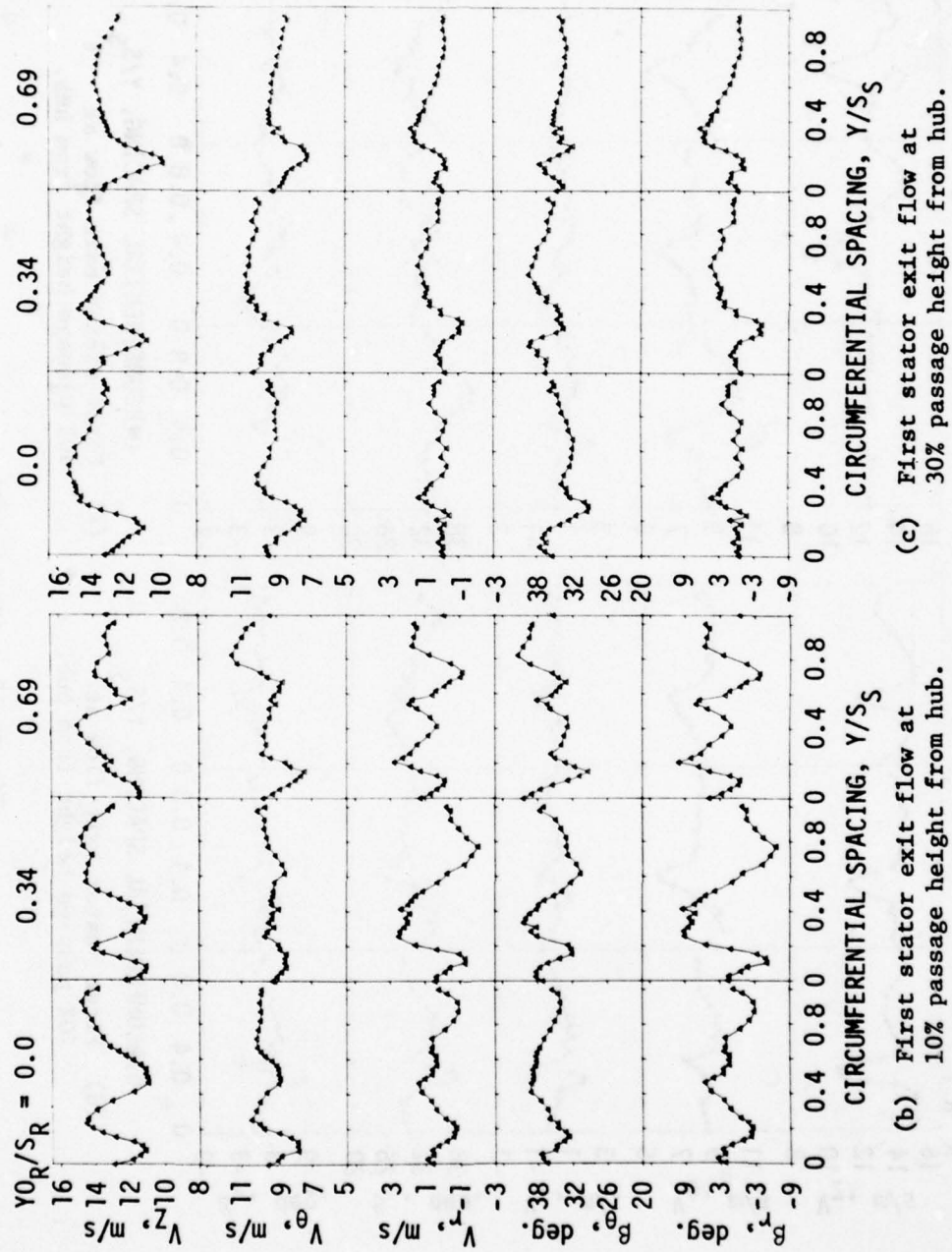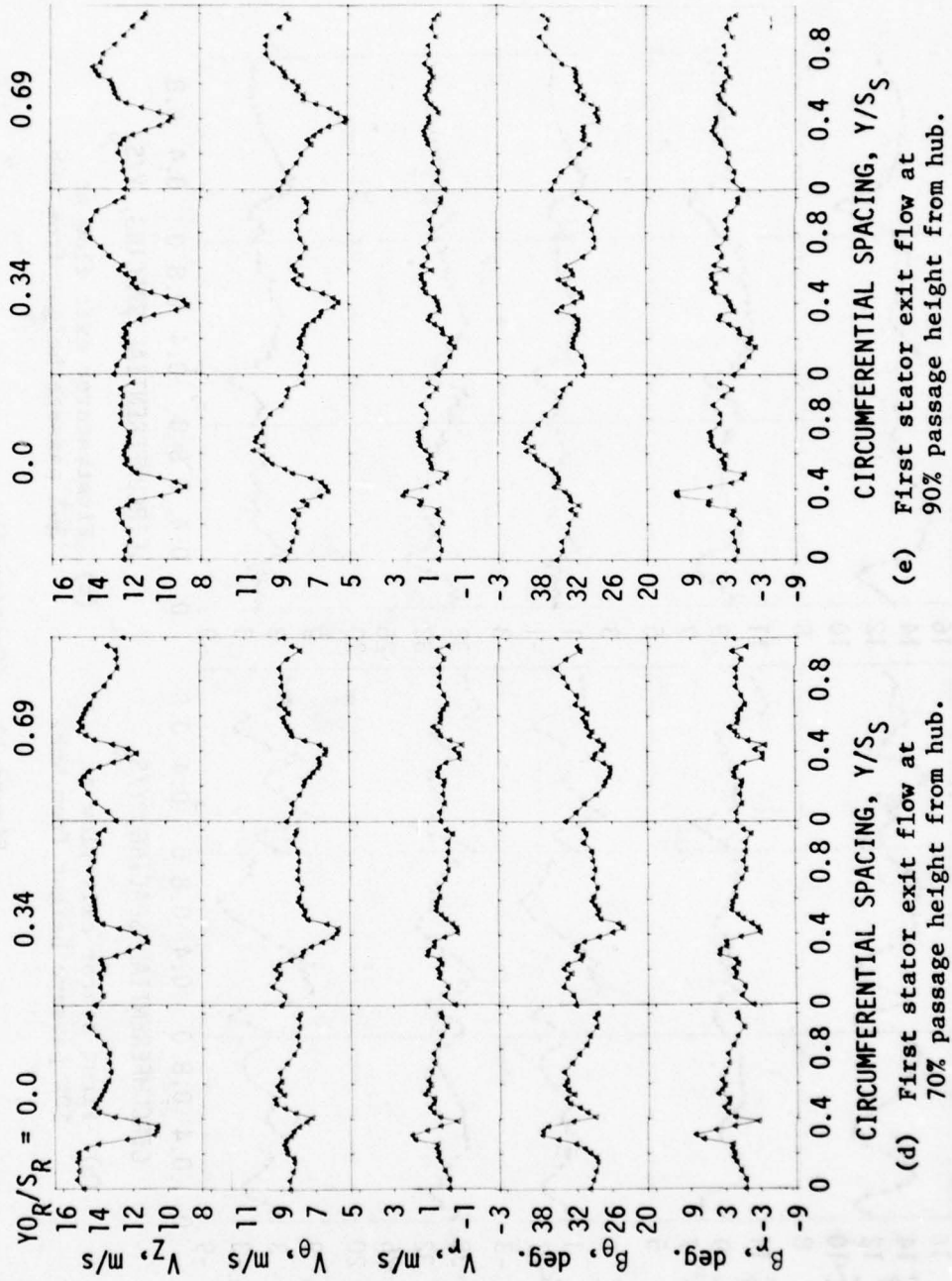
Figure 13. (Continued).
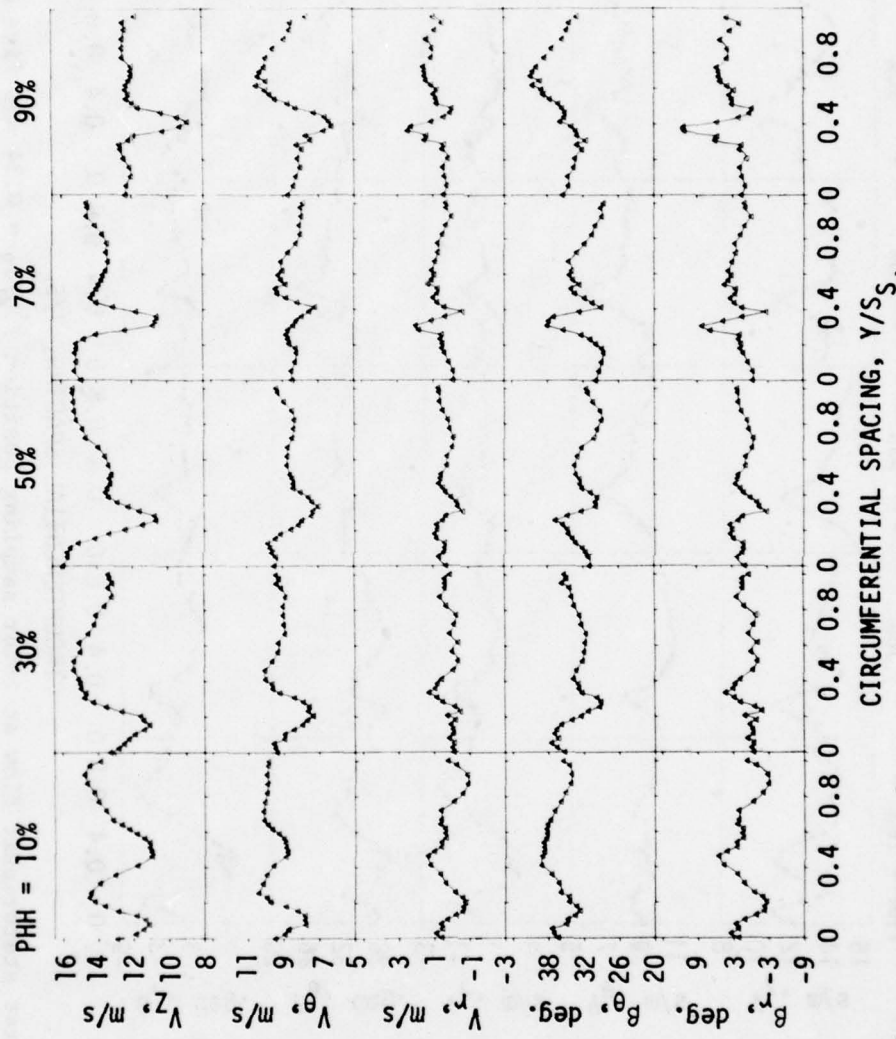
(f) First stator exit flow at rotor sampling position $YO_R/S_R = 0.0$ and five different passage heights.

Figure 13. (Continued).
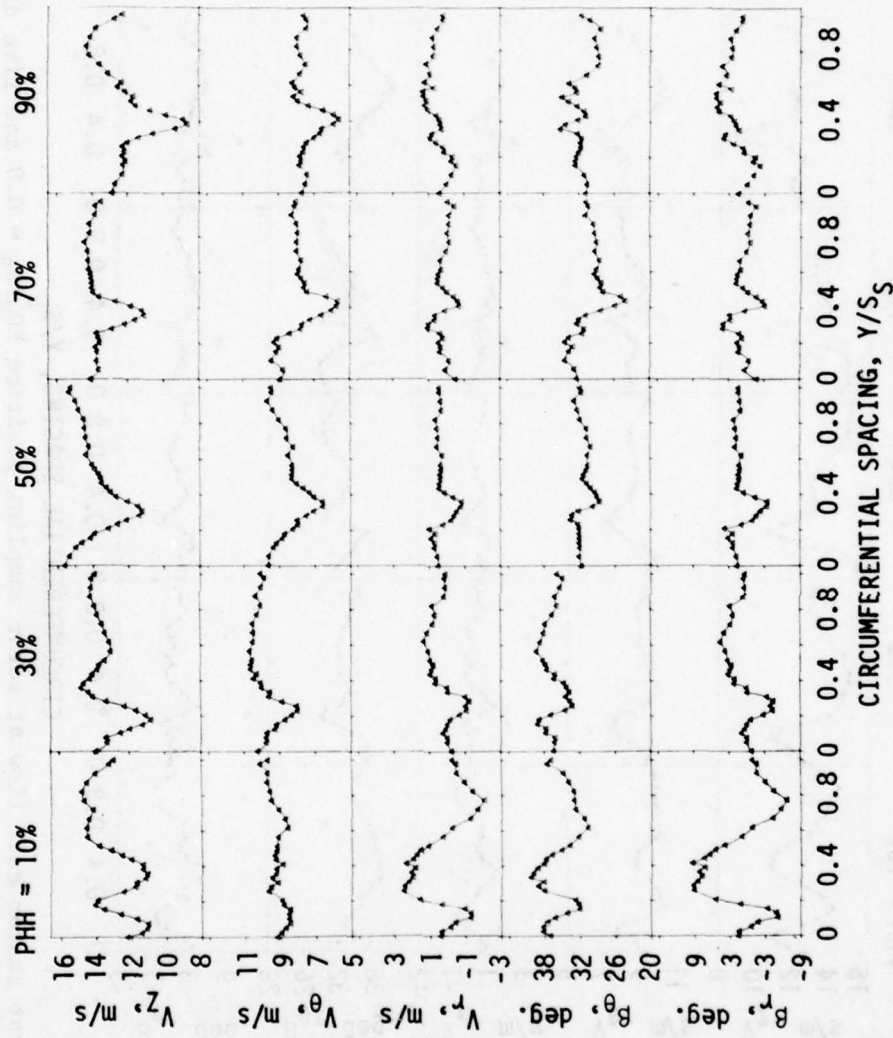
(g) First stator exit flow at rotor sampling position $YO_R/S_R = 0.34$ and five different passage heights.

Figure 13. (Continued).
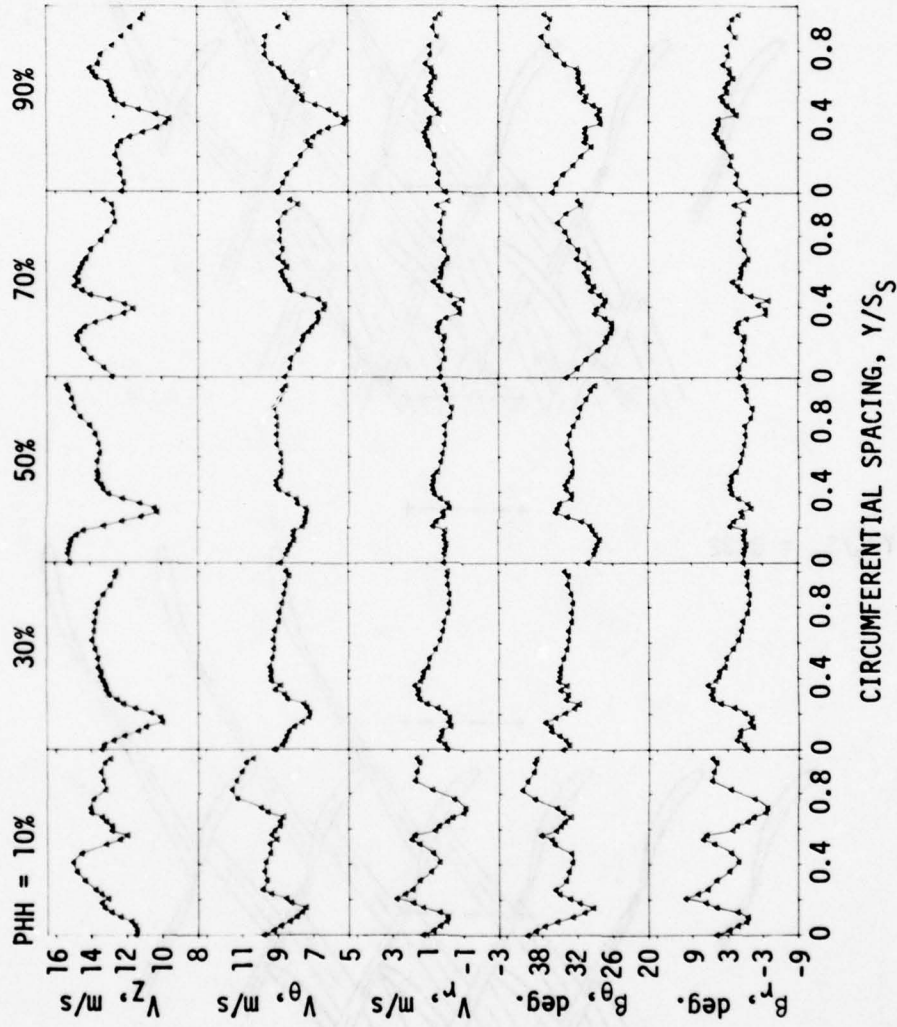
(h) First stator exit flow at rotor sampling position $YO_R/S_R = 0.69$ and five different passage heights.

Figure 13. (Continued).
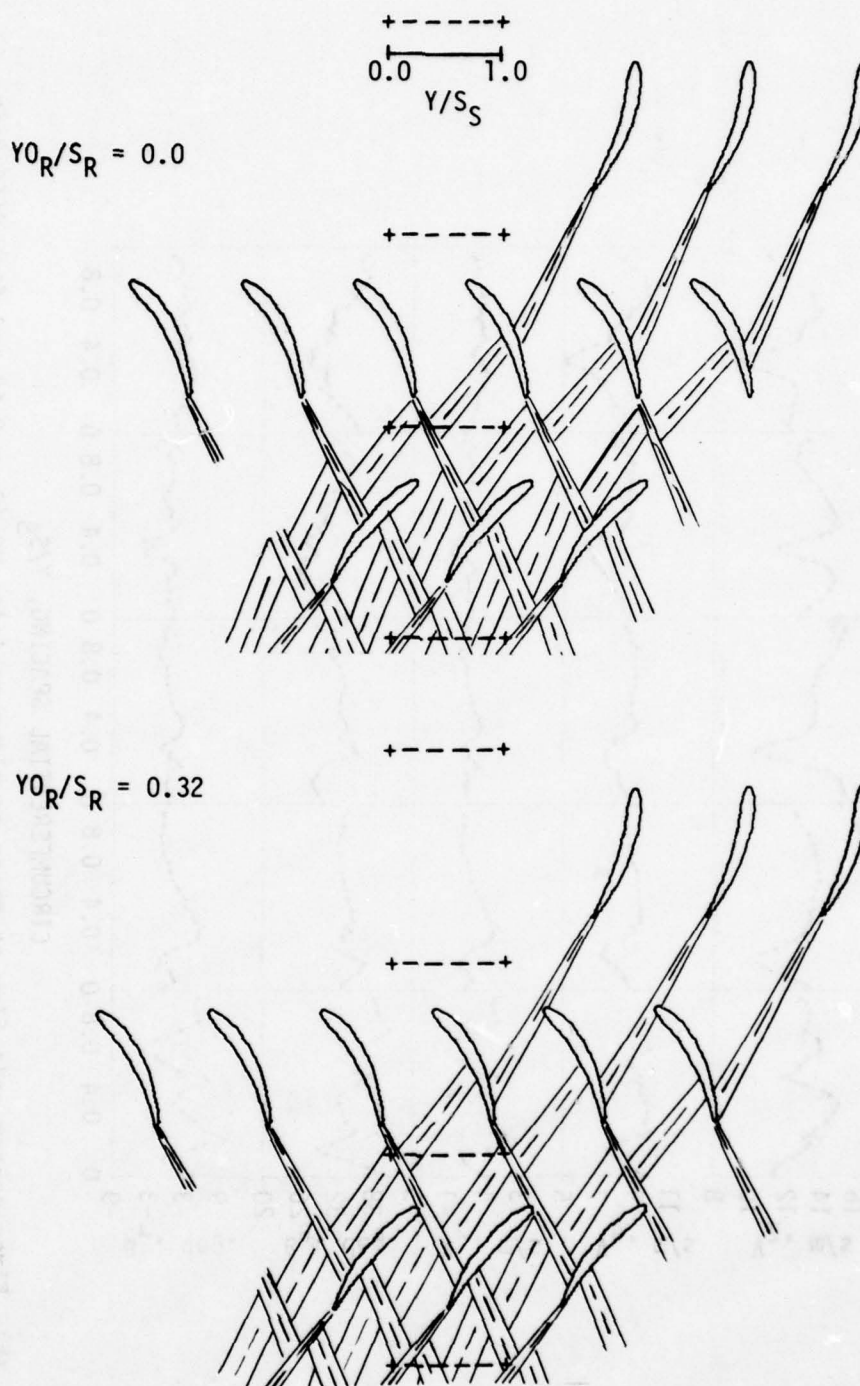
(a) Cascade plots for 10% passage height from hub.

Figure 14. Periodic-average cascade wake interaction plots for the first stage of the research compressor for minimum sound.

$YO_R/S_R = 0.34$
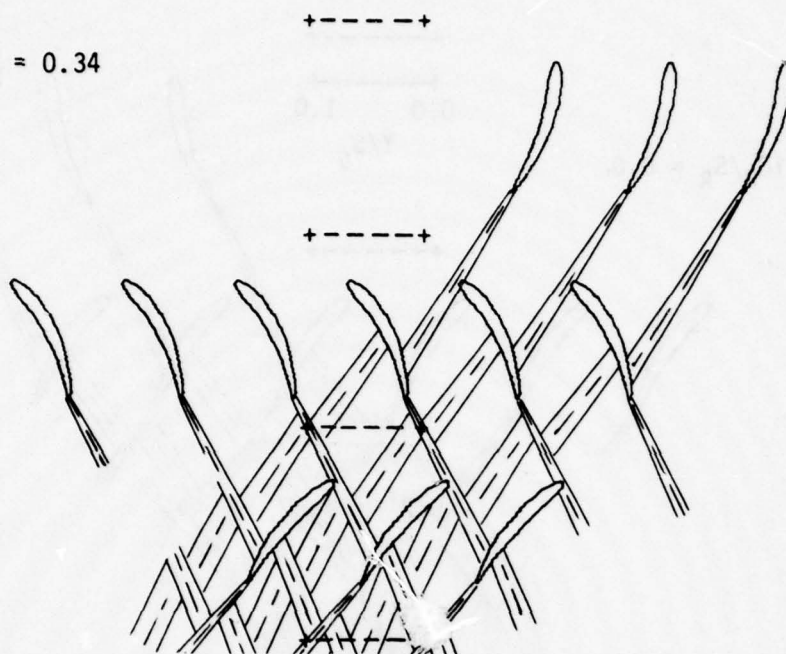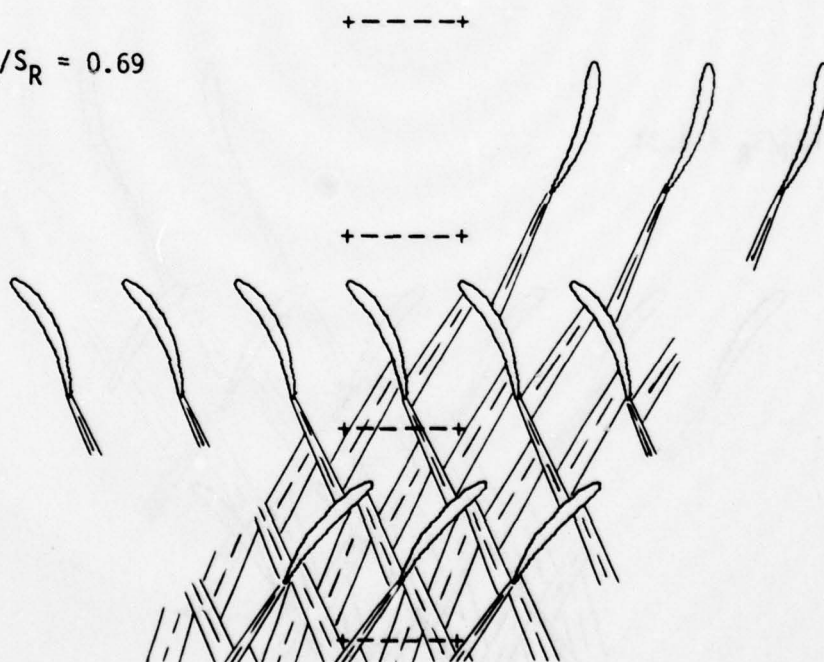
$YO_R/S_R = 0.69$

(a) (Concluded).

Figure 14. (Continued).

50
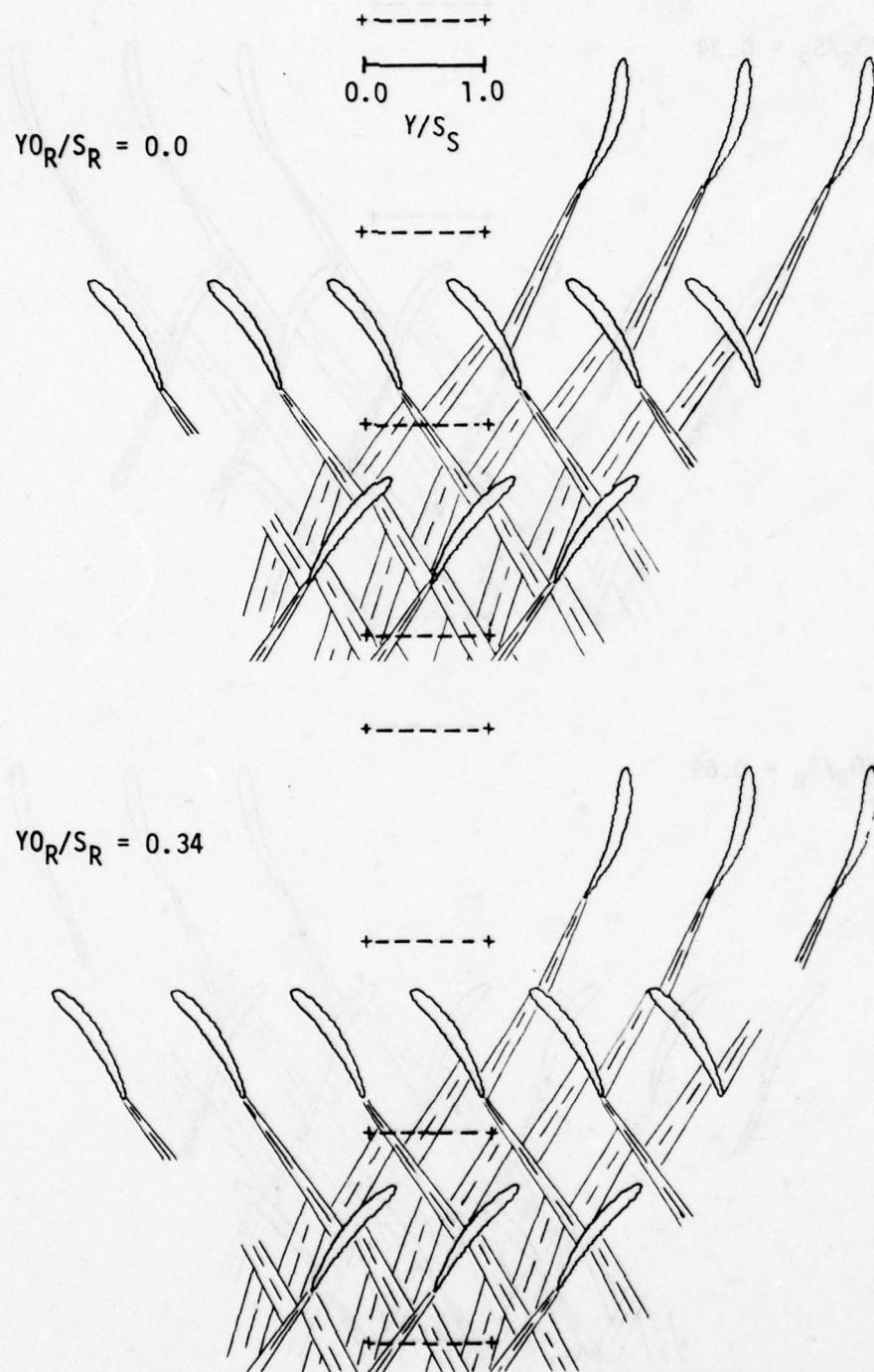
(b) Cascade plots for 30% passage height from hub.

Figure 14. (Continued).

(b) (Concluded).

Figure 14. (Continued).

$YO_R/S_R = 0.0$

$0.0 \qquad 1.0$

Y/S_S

$YO_R/S_R = 0.17$
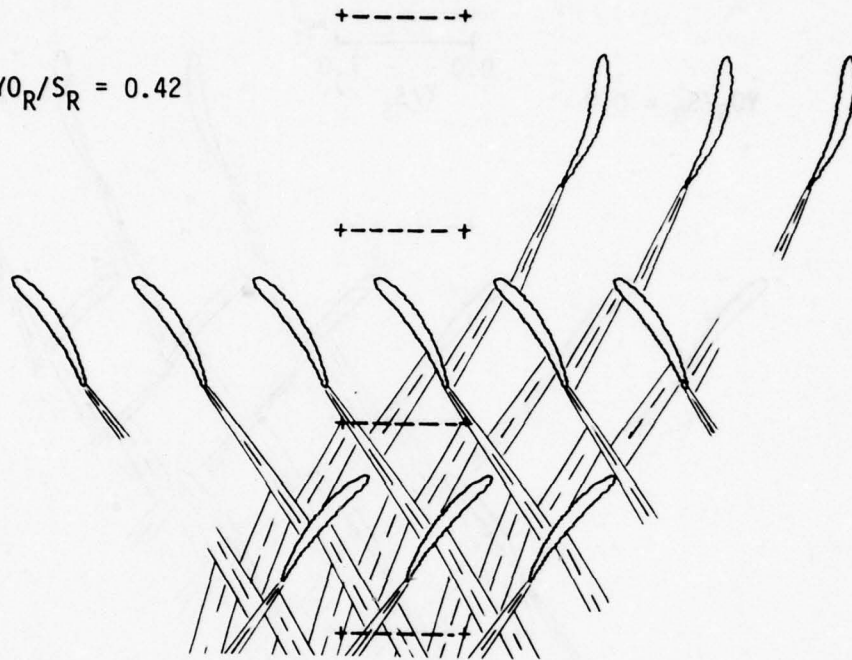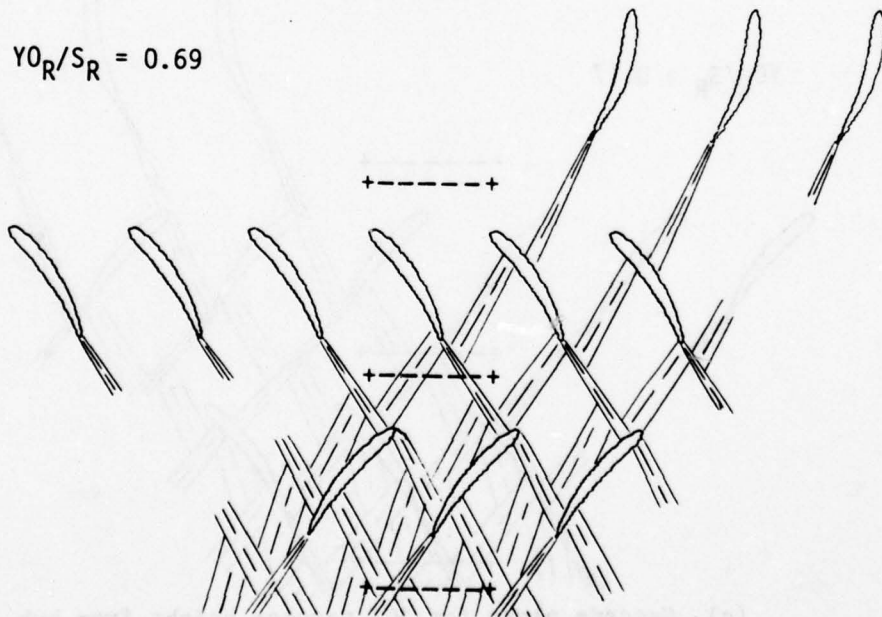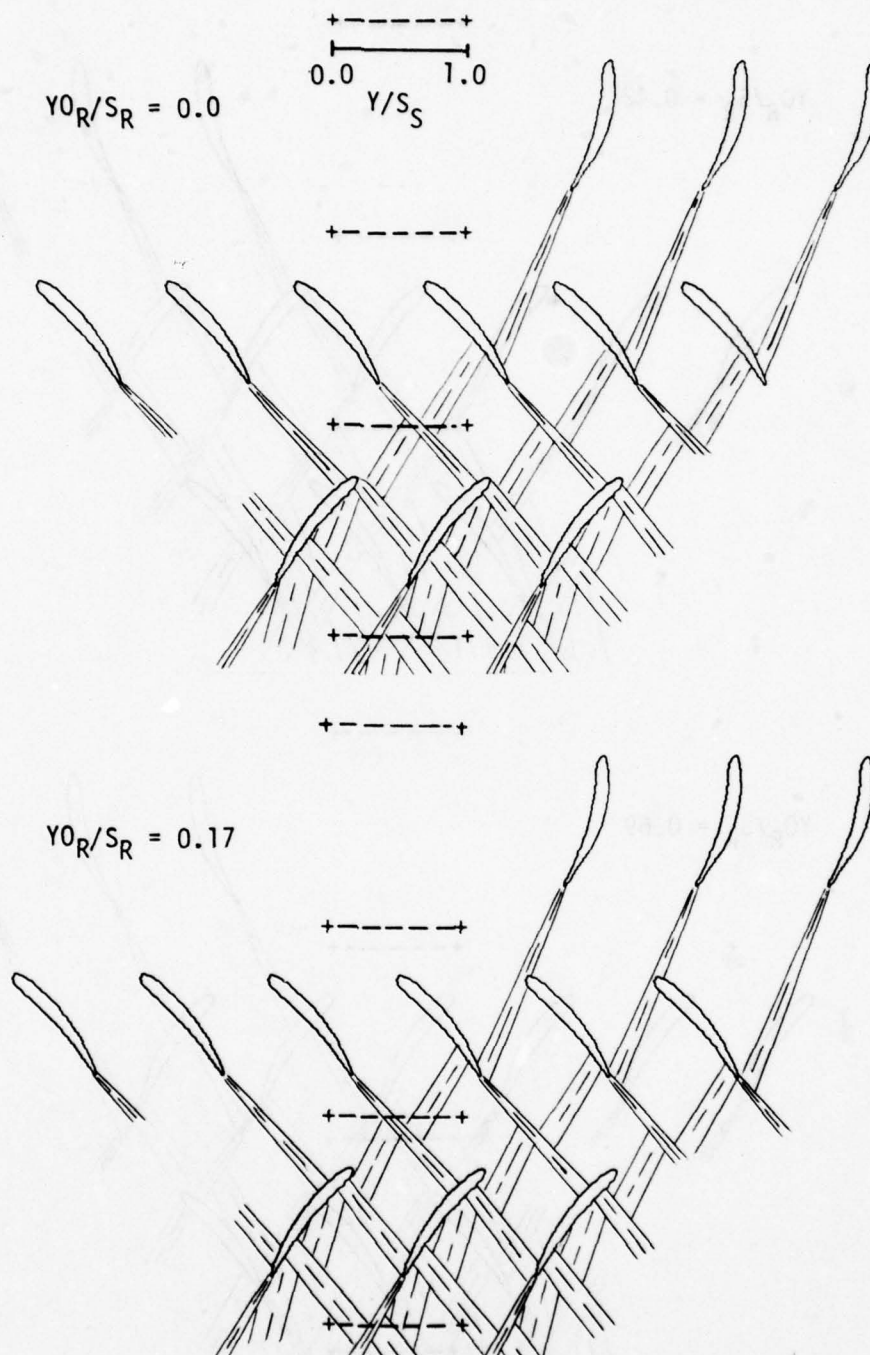
(c) Cascade plots for 50% passage height from hub.
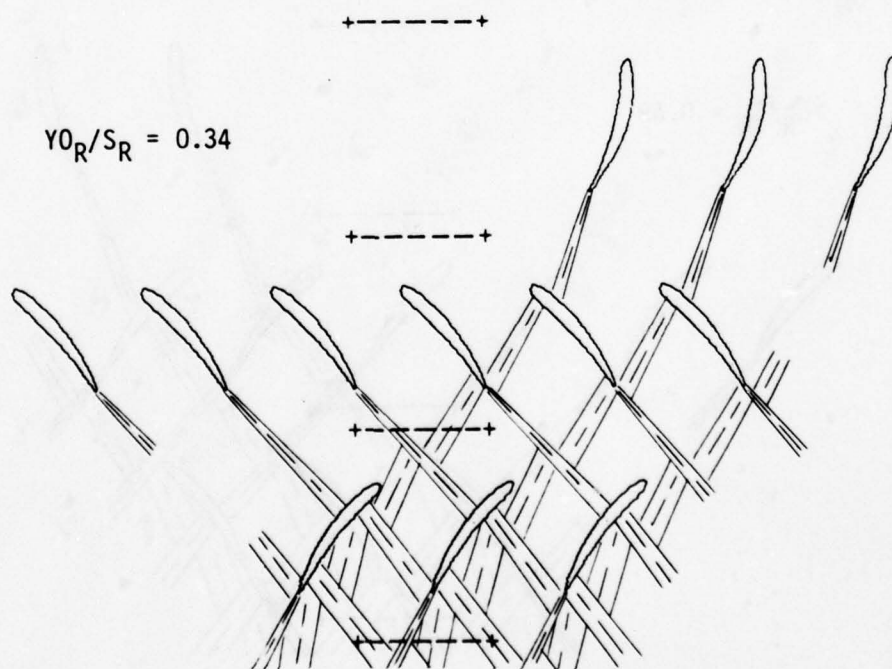
Figure 14.   (Continued).

$YO_R/S_R = 0.28$

$YO_R/S_R = 0.34$

(c) (Continued).

Figure 14. (Continued).

$YO_R/S_R = 0.50$

$YO_R/S_R = 0.69$

(c) (Continued).

Figure 14. (Continued).

$YO_R/S_R = 0.83$

(c) (Concluded).

Figure 14. (Continued).

56

YO$_R$/S$_R$ = 0.0

0.0   1.0

Y/S$_S$

YO$_R$/S$_R$ = 0.34
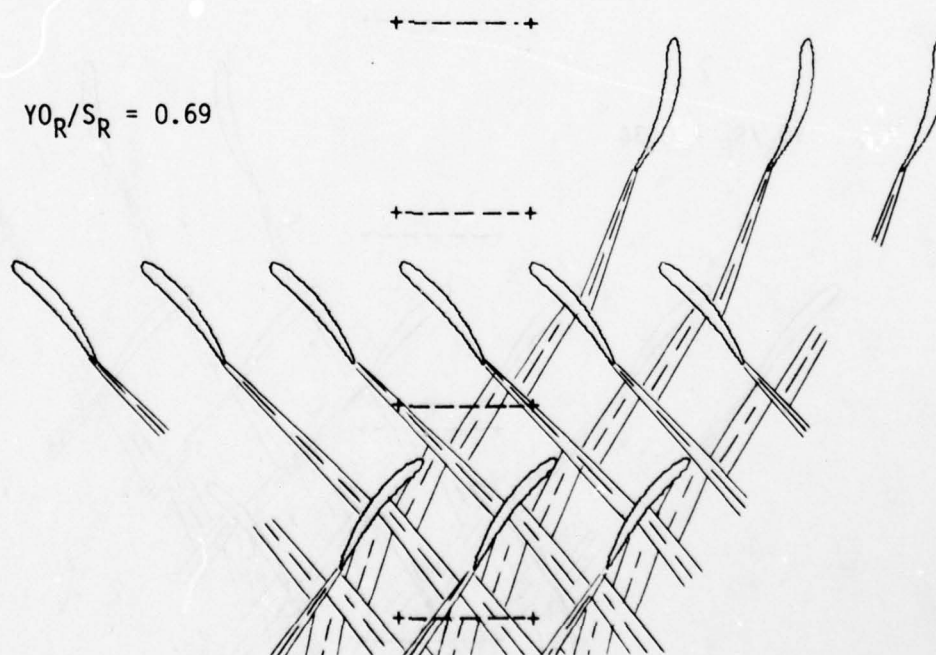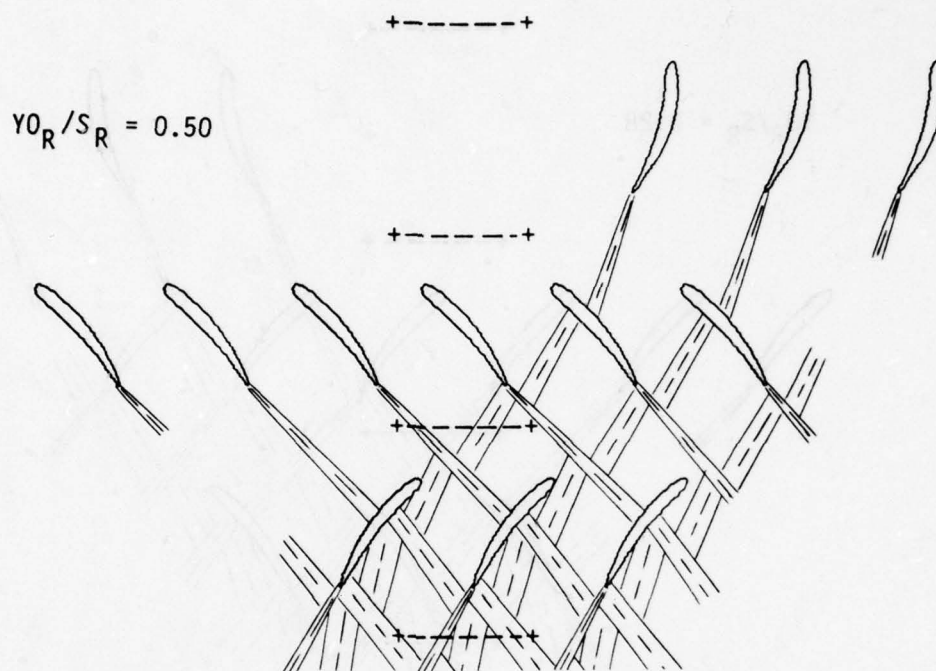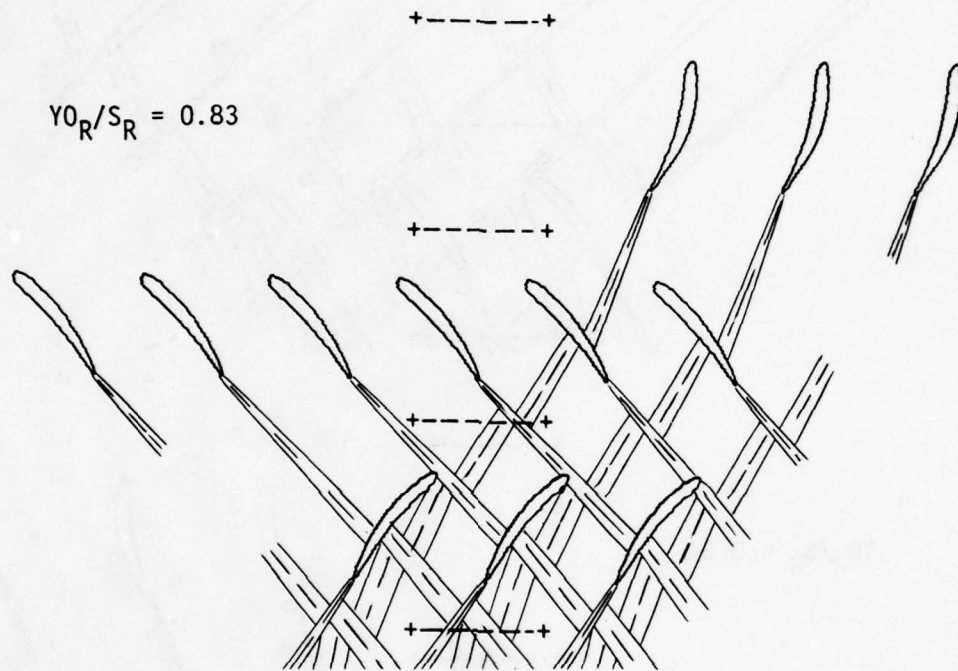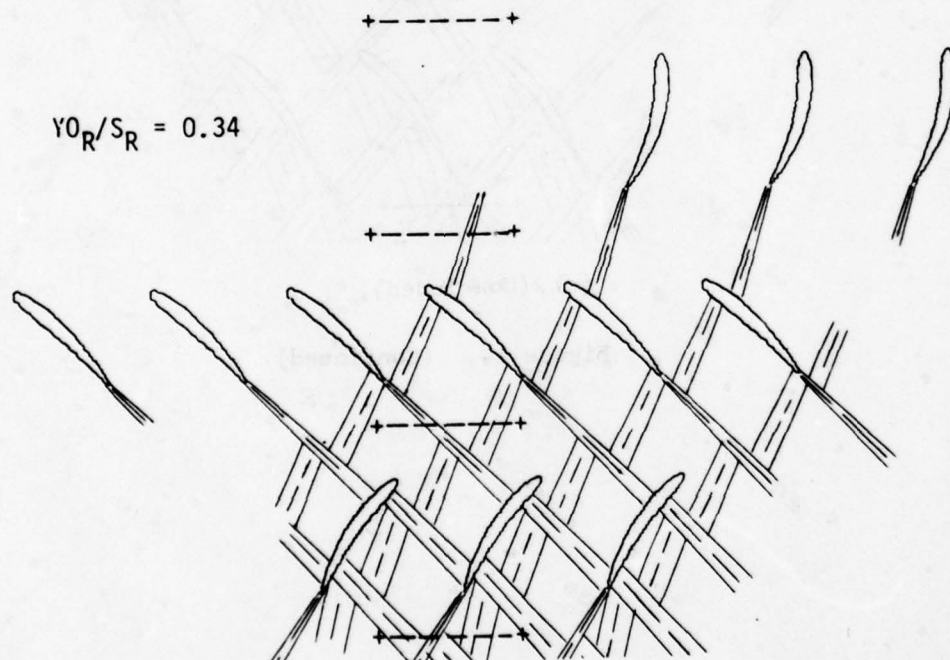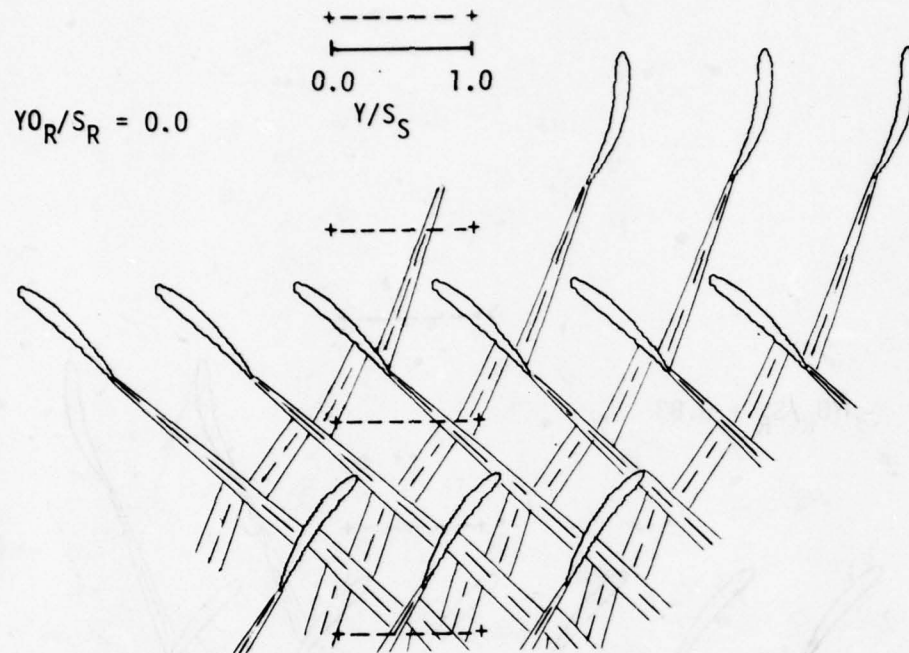
(d) Cascade plots for 70% passage height from hub.

Figure 14. (Continued).

57

$YO_R/S_R = 0.53$
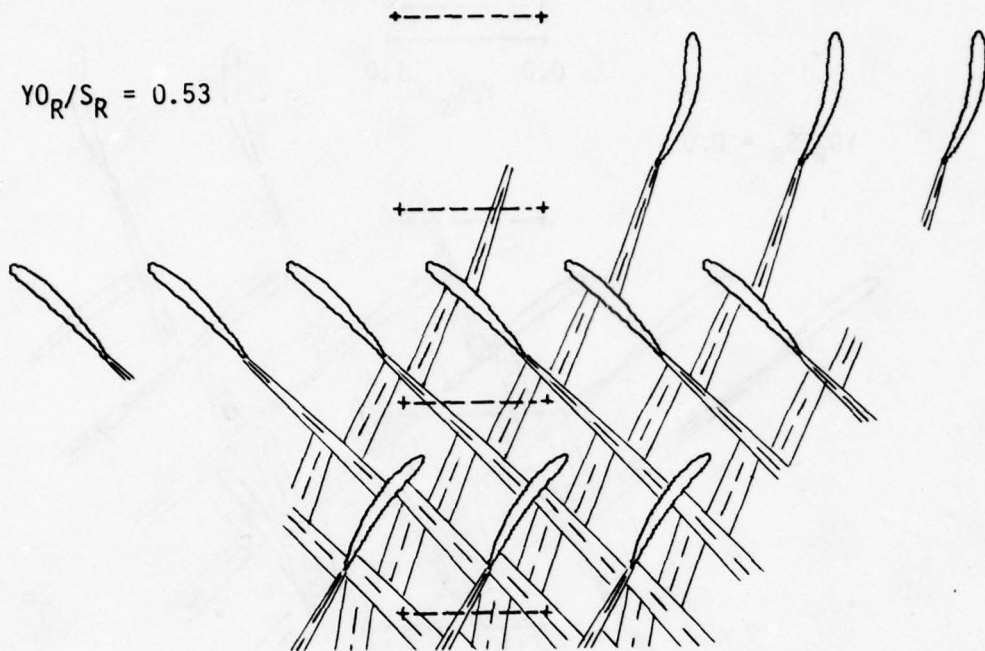
$YO_R/S_R = 0.69$

(d) (Concluded).

Figure 14. (Continued).

58

YO$_R$/S$_R$ = 0.0

Y/S$_S$
0.0 1.0

YO$_R$/S$_R$ = 0.34
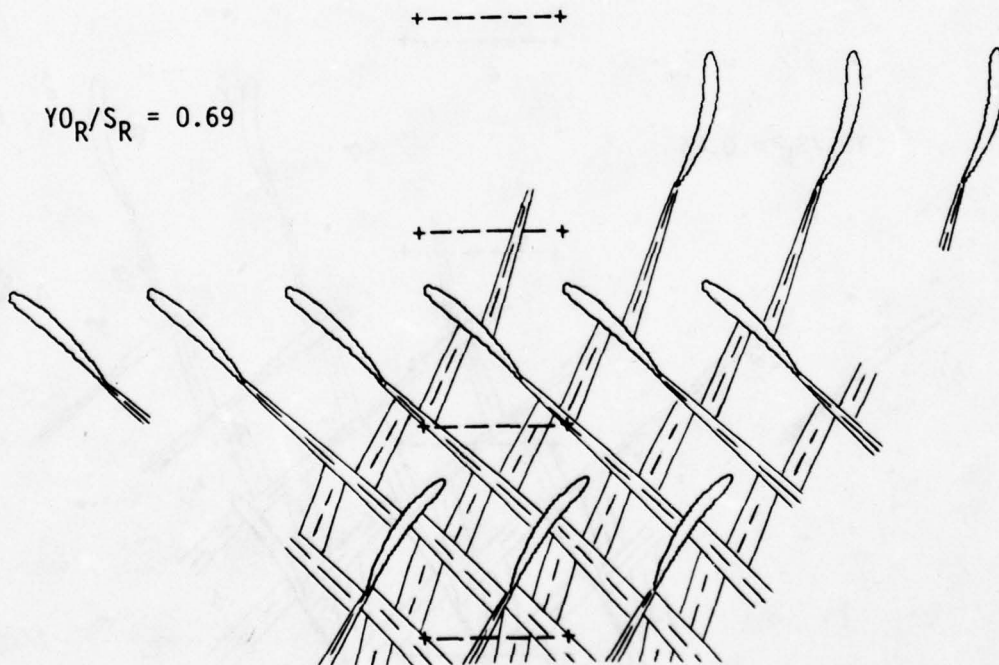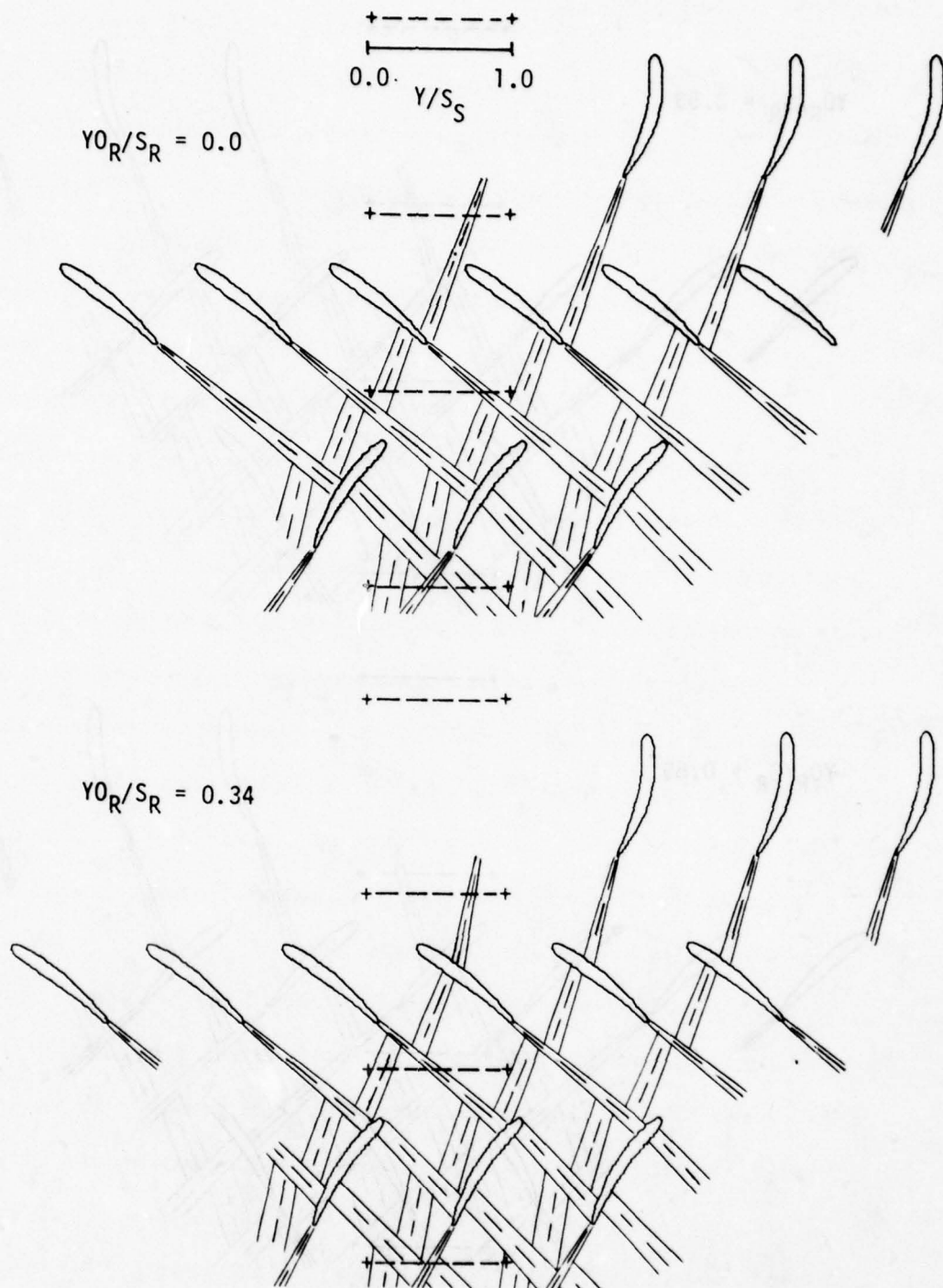
(e) Cascade plots for 90% passage height from hub.

Figure 14. (Continued).

$YO_R/S_R = 0.63$

$YO_R/S_R = 0.69$
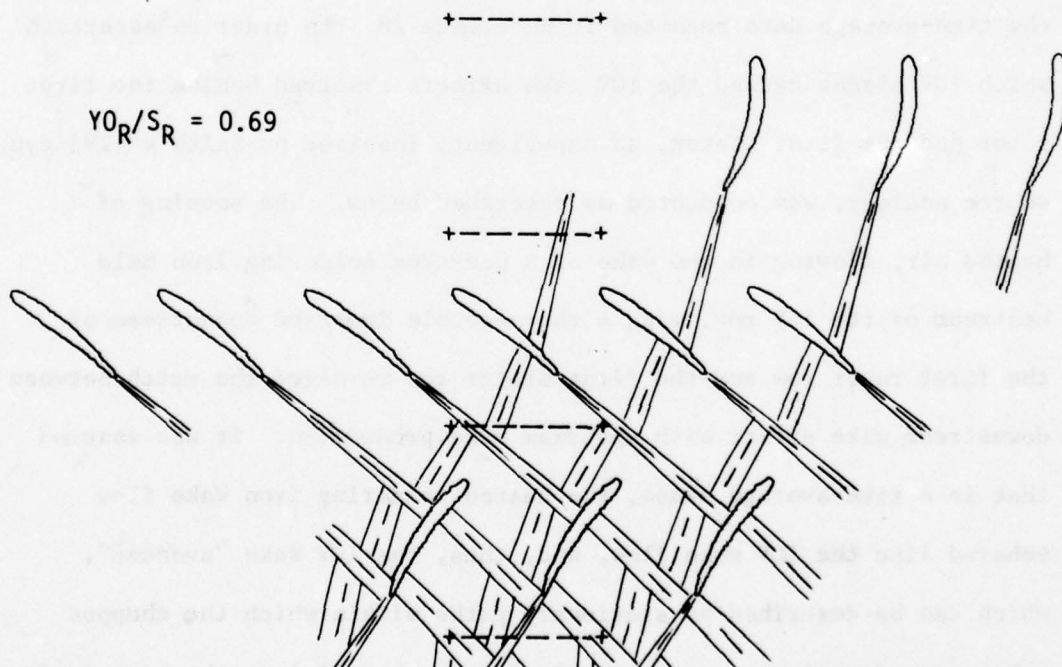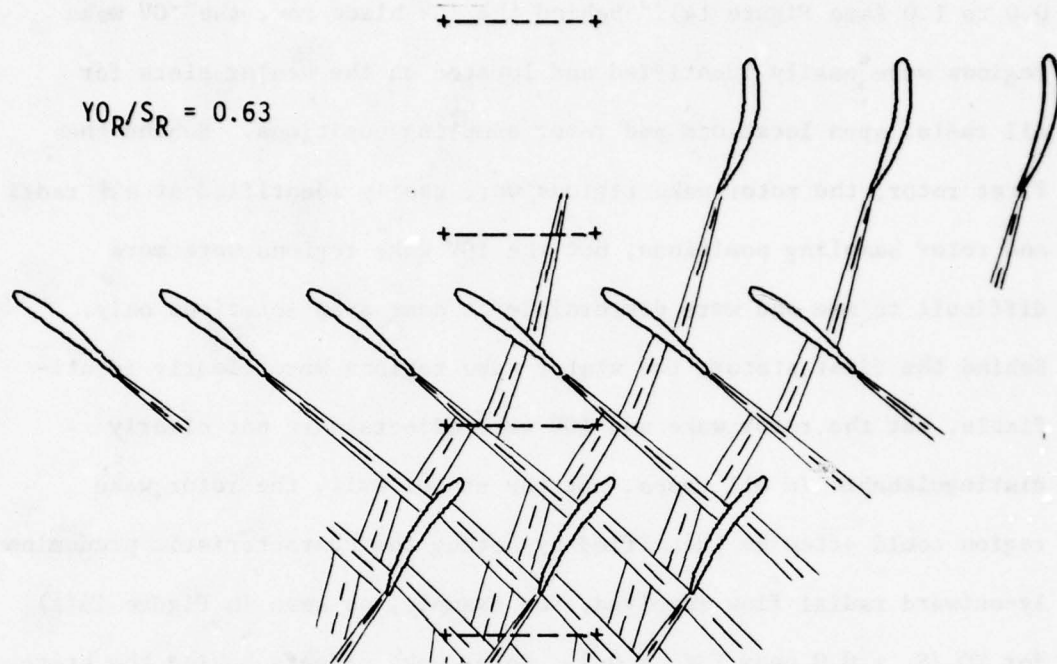
(c) (Concluded).

Figure 14. (Continued).

0.0 to 1.0 (see Figure 14). Behind the IGV blade row, the IGV wake

regions were easily identified and located on the scalar plots for

all radial span locations and rotor sampling positions. Behind the

first rotor, the rotor wake regions were easily identified at all radii

and rotor sampling positions, but the IGV wake regions were more

difficult to see and were discernible at some span locations only.

Behind the first stator, the stator wake regions were clearly identi-

fiable, but the rotor wake and IGV wake effects were not clearly

distinguishable in all cases. At the stator exit, the rotor wake

region could often be identified by noting the characteristic predominant-

ly-outward radial flow involved, for example, as seen in Figure 13(a)

for $YO_R/S_R = 0.0$ near $Y/S_S = 0.2$. Rotor wake effects behind the stator

row were connected to corresponding rotor blades consistently with

the time-average data reported in Reference 28. In order to ascertain

which IGV blades caused the IGV wake effects observed behind the first

rotor and the first stator, an experiment, inspired by Smith's [29] dye

source analogy, was conducted as described below. The sensing of

heated air, flowing in the wake of a pen-type soldering iron held

upstream of the IGV row, with a thermocouple immersed downstream of

the first rotor row and the first stator row revealed the match between

downstream wake effect with upstream wake production. It was assumed

that in a time-average sense, the heated soldering iron wake flow

behaved like the IGV wake flow, and, thus, the IGV wake "avenues",

which can be described as stationary paths within which the chopped

wakes move downstream, were conceived to be parallel to the heated air

flow paths (see Figure 15). The procedure described above resulted
in cascade plots in skeletal form only. Completion of the cascade plots
involved careful interpolation between cascade wake plots for the same
radii and different rotor sampling positions and cascade plots for the
same rotor sampling position but different radii. By using a wake
template involving an increasing wake width, the wake thickening effect,
suggested in References 2 and 3, was approximated. The chopped
segments were caused to reflect Smith's [29] chopping effects by rotat-
ing each bounded wake segment (bounded either by blade surfaces or
wake regions) around its center. The usefulness of these cascade plots
should become evident as the test results are discussed in the next
section.

4.2. Discussion of Data

The results of the periodic-average measurements made behind the
IGV row are presented in velocity and angle component form in Figure
11 and will be discussed first. The two plots of axial velocity
variation from blade-to-blade at 50% passage height from the hub (PHH),
for two different rotor sampling positions, indicate that the rotor
potential flow field could influence the flow at the IGV row exit
measurement plane. Walker and Oliver [3] suggest that 3% to 4%
potential flow effect can be expected for this particular axial spacing
between blade rows. The present data are in close agreement with this
observation. Rotor leading edge locations, as seen in Figure 16 for
rotor sampling positions, $YO_R/S_R = 0.0$ and 0.34, relate to the axial
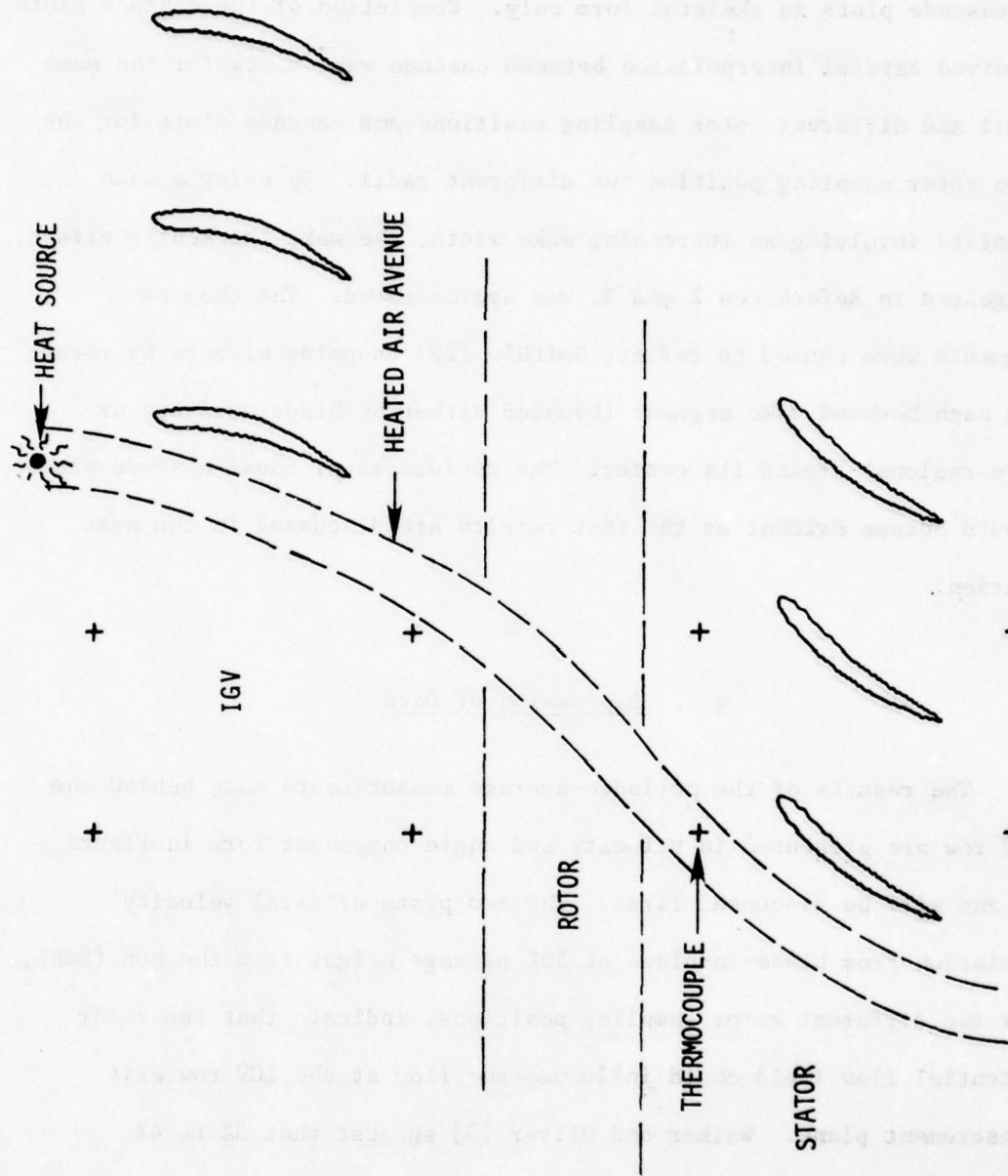
Figure 15. Time-average heated air avenue location in cascade.

63
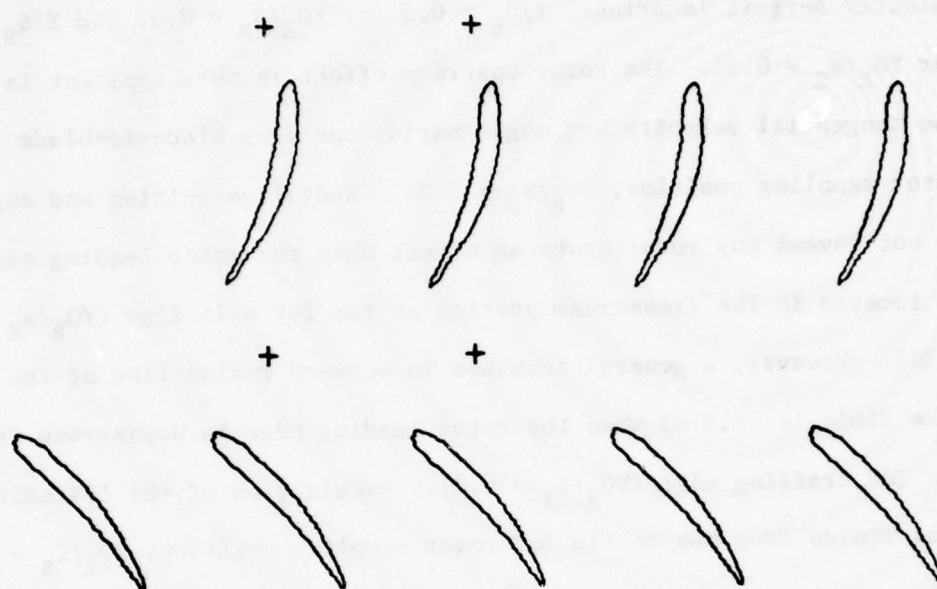
(a)   Rotor sampling position $YO_R/SR = 0.0$.
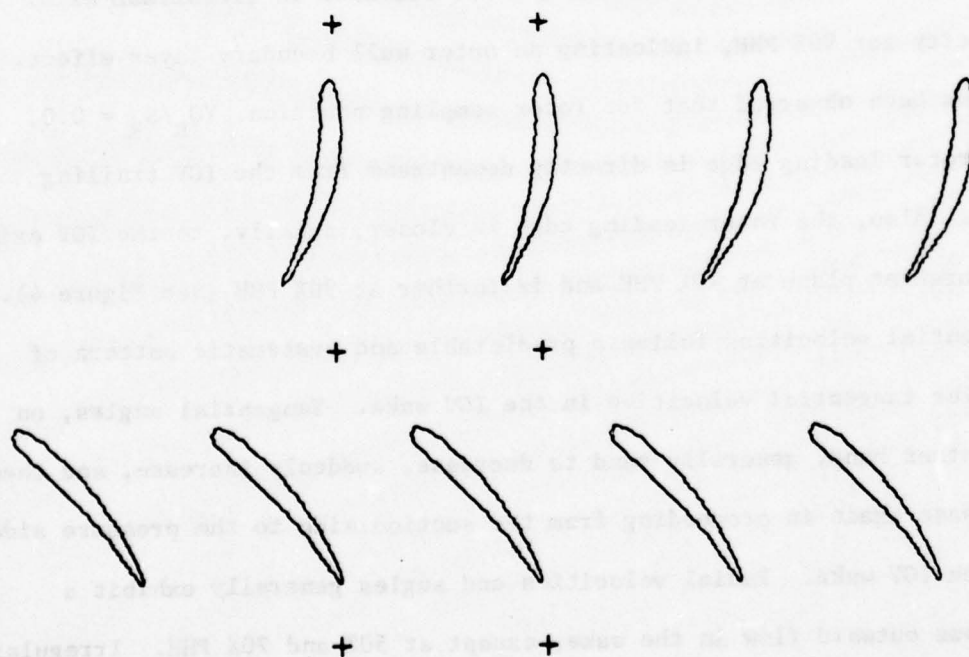
(b)   Rotor sampling position $YO_R/S_R = 0.34$.

Figure 16.   Relative locations of IGV and rotor blades for two
rotor sampling positions at 50% span.

64

velocity deficit locations, $Y/S_S = 0.5$ for $YO_R/S_R = 0.0$, and $Y/S_S = 0.3$ for $YO_R/S_R = 0.34$. The rotor upstream effect is more apparent in the tangential velocity and angle variations from blade-to-blade for rotor sampling position, $YO_R/S_R = 0.34$. Radial velocities and angles do not reveal any rotor upstream effect when the rotor leading edge is located in the freestream portion of the IGV exit flow ($YO_R/S_R = 0.34$). However, a general increase in outward radial flow of the IGV wake fluid is evident when the rotor leading edge is downstream from the IGV trailing edge ($YO_R/S_R = 0.0$). Examination of the IGV exit flow fields from hub to tip for rotor sampling position, $YO_R/S_R = 0.0$, only, suggests that these wakes become narrower from 10% to 90% PHH. At 70% span, the IGV wake is curiously only half as deep as the wakes at 50% and 90% PHH. There is a general decrease in freestream axial velocity for 90% PHH, indicating an outer wall boundary layer effect. It has been observed that for rotor sampling position, $YO_R/S_R = 0.0$, the rotor leading edge is directly downstream from the IGV trailing edge. Also, the rotor leading edge is closer, axially, to the IGV exit measurement plane at 10% PHH and is farther at 90% PHH (see Figure 4). Tangential velocities follow a predictable and systematic pattern of smaller tangential velocities in the IGV wake. Tangential angles, on the other hand, generally tend to decrease, suddenly increase, and then decrease again in proceeding from the suction side to the pressure side of the IGV wake. Radial velocities and angles generally exhibit a curious outward flow in the wake, except at 50% and 70% PHH. Irregular separated flow activity was observed on the suction side of the IGV wake during data acquisition. There did not appear to be any difference

in separated flow irregularity from hub to tip. To obtain meaningful periodic-average data, approximately 2400 instead of the usual 1200, effective samples were obtained for each orientation of the wire.

First rotor periodic-average exit flow parameters for 50% span are presented in Figure 12(a) for six rotor sampling positions and will be discussed next. Corresponding cascade plots are displayed in Figure 14(c). Note that the rotor wake regions shown in the sequence of Figure 12(a) are not from the same rotor blade but rather are from two adjacent rotor blades. This fact may be verified by following the time-sequential movement of the rotor blades in the cascade plots (Figure 14[c]). The chopped IGV wakes seen in the cascade plots follow a fixed avenue. Within this avenue, the wake segments move downstream, as indicated in Figure 14(c). Periodically, the rotor wake region can occupy the same portion of the measuring plane between Y/S_S = 0.0 and 1.0 as the IGV wake avenue. The deepest rotor wake region measured was for a rotor sampling position of YO_R/S_R = 0.69. For this rotor position, the cascade plot (Figure 14[c]) indicates that the rotor wake/IGV wake interaction occurs slightly upstream from the measurement plane. For this rotor position, the circumferential variation of flow parameters in the rotor wake region is characterized by larger deviation and absolute flow angles and by smaller absolute tangential velocities and axial velocities than observed in the rotor wake regions associated with other rotor sampling positions where the rotor wake/IGV wake interaction occurs closer to, at, or downstream of the measurement plane. When the rotor wake/IGV wake interaction occurs slightly upstream or at the measurement plane, the wake region

66

will hereafter be called an "interacted wake region." When the rotor

wake/IGV wake interaction occurs downstream of the measurement plane,

the wake region will hereafter be referred to as a "noninteracting

wake region." The dependence of rotor wake region behavior on rotor

sampling position is explainable in terms of the physical reasoning

proposed by Kerrebrock and Mikolajczak [2] which involved the

relative flow of chopped stator wake fluid moving toward the rotor

pressure surface due to slip (see Figure 17[a]). Such flow in a

chopped IGV wake would tend to result in locally reduced axial velocities

and increased deviation angles on the rotor suction surface side and

in an accumulation of more slower-moving fluid on the rotor pressure

surface side. The mechanism for these interaction effects is best

explained in this way: The collected IGV wake fluid "builds up"

a surplus of fluid on the pressure side of the rotor blade, while on

the suction side of the rotor blade, fluid is drawn towards the rotor

pressure surface of the adjacent blade. Thus, a narrower wake region,

larger deviation angles, and smaller axial velocities occur at the

measurement plane when the suction side wake interaction effects

predominate there, as for $YO_R/S_R = 0.69$. For $YO_R/S_R = 0.69$, the

smaller absolute tangential velocities and larger absolute tangential

angles are explained with the help of a velocity vector diagram

(Figure 18), where three velocity triangles are drawn, one each for

free stream, noninteracting wake, and interacting wake regions. For

rotor sampling position $YO_R/S_R = 0.83$, the rotor blade pressure

surface side interaction effect is stronger at the measurement plane,

resulting in a wake zone spreading effect. For $YO_R/S_R = 0.0$, both
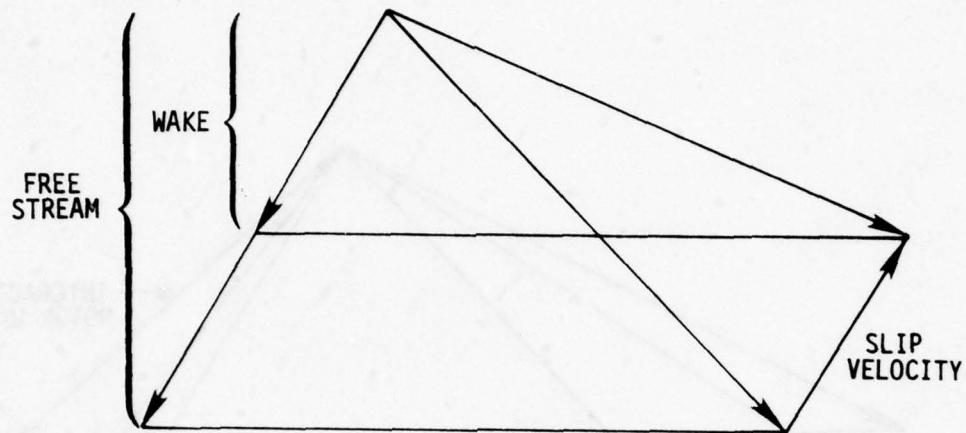
(a) Slip velocity of IGV wake fluid through a rotor row.
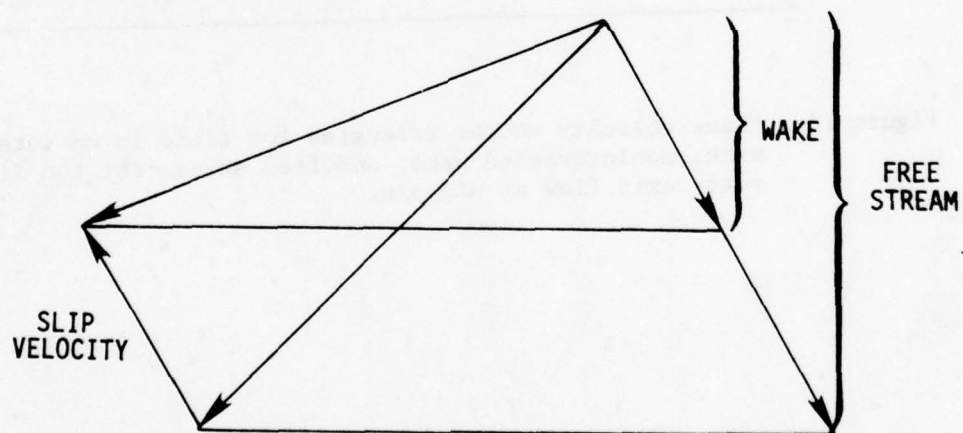
(b) Slip velocity of rotor wake fluid through a stator row.

Figure 17. Velocity triangles showing slip velocities.
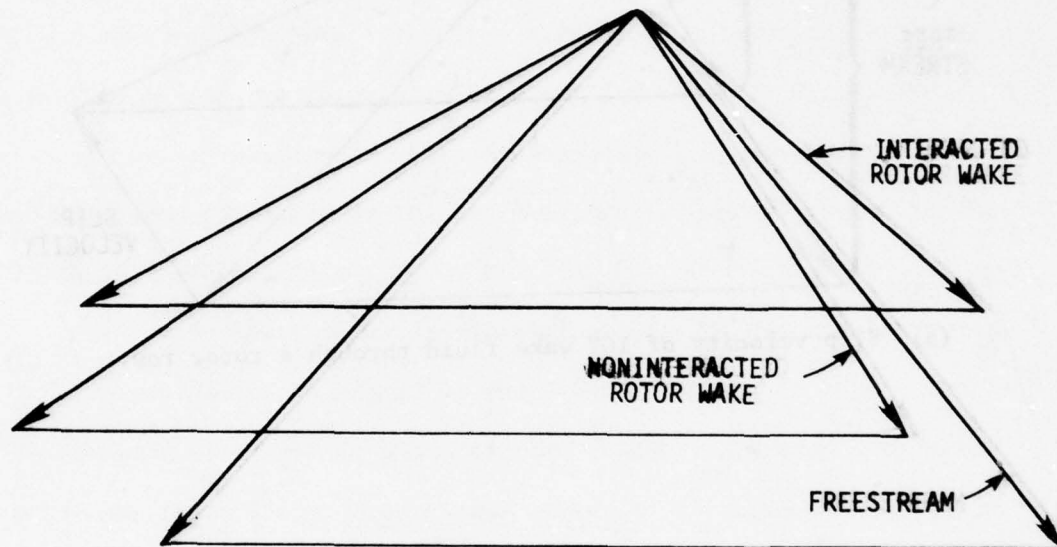
Figure 18. Plane velocity vector triangles for fluid in an interacted wake, noninteracted wake, and free stream for the first rotor exit flow at midspan.

pressure and suction surface interaction effects are noticeable at the measurement plane, the result being a broad shallow wake region. Radial velocity and angle distribution change trends for different rotor sampling positions are not apparent from the data.

Prior to measuring the details of the flow behind the first rotor at other radial locations in the compressor annulus, approximate periodic-average hot-wire oscilloscope traces of a combination of axial and radial velocities were studied to determine which rotor sampling positions should be selected to show the largest changes in periodic-average flow due to rotor wake/IGV wake interaction. For radial locations 10% and 90% PHH, the appropriate rotor sampling positions to use were not obvious because the approximate data were not definitive enough. At the other radial positions, more reasonable rotor sampling position selections could be made with the approximate data.

The rotor exit data for 10% PHH for four rotor sampling positions are shown in Figure 12(b). The related cascade plots are displayed in Figure 14(a). Unfortunately, the data involved only rotor wake/ IGV wake interaction at the measurement plane for rotor sampling positions, YO_R/S_R = 0.0, 0.32, 0.34, and downstream of the measurement plane for YO_R/S_R = 0.69. Data for interaction occurring slightly upstream of the measurement plane, which might have indicated a comparatively deeper rotor wake region, were not obtained. The information shown is consistent with data already discussed.

The periodic-average data for 30% PHH are shown in Figure 12(c) for rotor sampling positions YO_R/S_R = 0.0 and 0.42, which represent

interacted and noninteracted wake regions respectively. The cascade plots (Figure 14[b]) indicate that, for rotor sampling position $YO_R/S_R = 0.0$, a characteristically deeper interacted wake region is produced with the rotor wake/IGV wake interaction occurring upstream of the measurement plane. The flow parameters exhibit the same characteristics as did the rotor exit flow for 50% span, $YO_R/S_R = 0.69$, namely, reduced axial velocities and absolute tangential velocities and increased deviation angles and absolute tangential angles in the interacted wake region.

First rotor exit flow component plots for 70% PHH and two rotor sampling positions, $YO_R/S_R = 0.0$ and 0.53, are shown in Figure 12(d). The corresponding cascade plots (Figure 14[d]) reflect an interacted rotor wake (interaction occurring upstream of the measurement plane) for $YO_R/S_R = 0.53$ and a noninteracted wake for rotor sampling position $YO_R/S_R = 0.0$. For $YO_R/S_R = 0.53$, the rotor wake/IGV wake interaction effects are typical of a deeper interacted rotor wake region except for the tangential angles which are slightly smaller in the interacted wake region than in the noninteracted region. This inconsistency is probably due to the fact that the interacted wake region for $YO_R/S_R = 0.53$ is not the deepest possible and, thus, does not totally possess all of the characteristics exhibited by such wake regions.

The data for 90% PHH rotor exit flow at two rotor sampling positions, $YO_R/S_R = 0.0$ and 0.63, are shown in Figures 12(e) and 14(e). The rotor wake/IGV wake interaction occurs at the measurement plane for $YO_R/S_R = 0.63$ and slightly downstream for $YO_R/S_R = 0.0$. The rotor

wake region corresponding to interaction upstream of the measurement plane was not observed. The trends indicated by the present data are consistent with similar measurements made elsewhere in the compressor annulus.

Rotor exit flow data for seven radial positions but only one rotor sampling position, $YO_R/S_R = 0.0$, are presented in Figure 12(f). Axial velocity variations indicate a general decrease in wake depth from hub to tip and a circumferential shifting consistent with change of blade twist (see Figure 19) except at 95%. The curious circumferential shift at 95% PHH is not clearly explainable, but it possibly is due to tip scraping and clearance leakage effects. Radial velocities and angles show tip scraping and clearance leakage effects at 90% and 95% PHH. The outer casing boundary layer extends to 95% PHH. A hub boundary layer is not apparent in the velocity data for 5% PHH although radial velocities and angles do indicate the presence of secondary flows. At 10% and 30% PHH, deep interacted wake regions are observed while shallower noninteracted wake regions are seen at 70% and 90% PHH. IGV wake effects seem to be more apparent toward the tip, possibly due to the smaller amount of rotation of the chopped IGV wakes involved there.

First stator periodic-average exit flow data for 50% PHH and six rotor sampling positions are presented in Figure 13(a) with associated cascade plots in Figure 14(c). It is obvious that the first stator exit flow is much more complicated than the first rotor exit flow because of the stator, rotor, and IGV wake interactions involved. The stator exit flow variation with rotor sampling position will be discussed

72
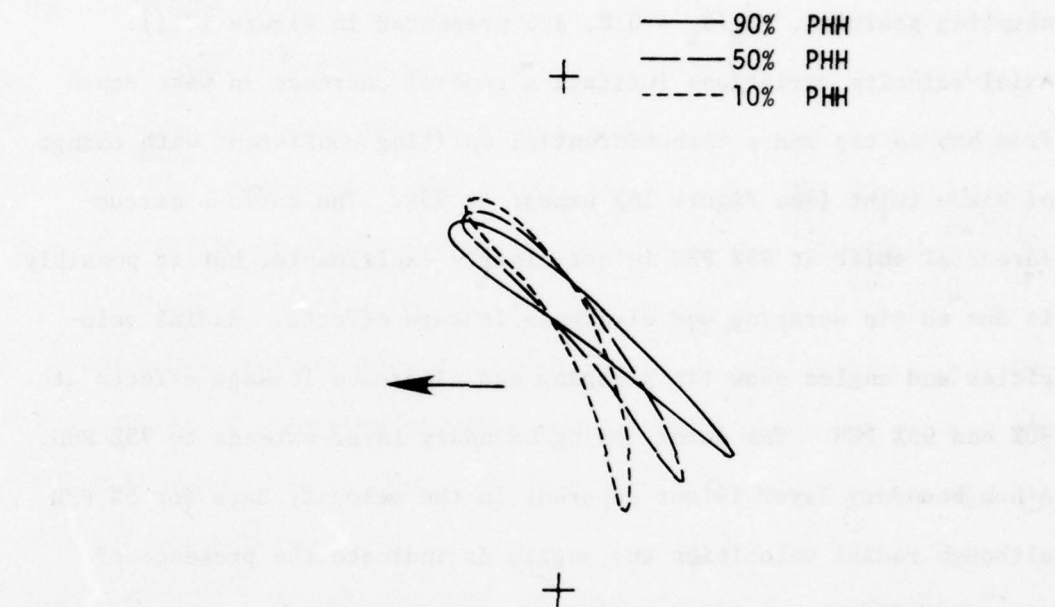
Figure 19. Compressor rotor blade sections at hub, midspan, and tip locations.

first. As mentioned by Kerrebrock and Mikolajczak [2], the chopped

rotor wake fluid tends to move from the stator suction surface to

the pressure surface because of the slip motion in the wake (see

Figure 17[b]). Such flow in a chopped rotor wake would tend to

result in locally-reduced flow and increased deviation angles on the

suction side of the stator blade with an accumulation of more slower

moving fluid on the pressure side. The deeper stator wake regions are

those corresponding to rotor sampling positions YO_R/S_R = 0.0, 0.69,

and 0.83, with the deepest wake region being associated with YO_R/S_R =

0.83. For rotor sampling position, YO_R/S_R = 0.83, the larger tangential

velocities of the chopped rotor wake fluid appear to cancel the

smaller tangential velocities of the stator wake fluid with the result

being only a small amount of circumferential variation of tangential

velocities. Also, the outward radial flow of the chopped rotor wake

fluid cancels the inward flow of the stator wake fluid. The flow angle

tendencies of both the chopped rotor wake and the stator wake seem to

add together. For rotor position YO_R/S_R = 0.5, the stator wake is

least affected by other wake fluid as it is most like an isolated

stator blade wake. Whenever the chopped rotor wake is clearly discerni-

ble at the measurement plane, YO_R/S_R = 0.0, 0.69, and 0.83, it is

interacting with IGV and stator wake fluid, and thus, its distribution

tends to be characteristically spread out and shallow. For rotor

position YO_R/S_R = 0.34, little of the chopped rotor wake fluid is iden-

tifiable at the measurement plane.

First stator exit flow data for 10% PHH are shown in Figure 13(b)

with related cascade plots in Figure 14(a). As the rotor blade passes

in stop-action sequence from YO_R/S_R 0.0 to 0.69, the effect of chopped rotor and IGV wakes on the stator exit flow may be clearly seen. For rotor sampling position $YO_R/S_R = 0.0$, a nearly isolated (noninteracted) stator wake region and a separate and distinct rotor wake/IGV wake interaction region are present at the measurement plane. For $YO_R/S_R = 0.34$, the stator wake region is slightly deeper with a wake sequence of stator-rotor-IGV for $Y/S_S = 0.0$ to 1.0. The rotor wake/stator wake interaction occurs just upstream of the measurement plane, and thus, the stator wake region is of the interacted variety. For $YO_R/S_R = 0.69$, the wake sequence is stator-IGV-rotor, with an appreciably different flow pattern from the ones for $YO_R/S_R = 0.0$ and 0.34. For $YO_R/S_R = 0.69$, the large axial velocity deficit at $Y/S_S = 0.6$ is the result of an IGV wake region. The rotor wake/stator wake interaction occurs downstream of the measurement plane. The rotor wakes are easily identified in the tangential angle plots.

Stator exit flow data for 30% PHH are shown in Figure 13(c). The deepest stator wake region occurs for rotor sampling position $YO_R/S_R = 0.69$. The corresponding cascade plot indicates strong stator wake/ rotor wake interaction at the measurement plane. The least influenced stator wake region occurs for rotor position $YO_R/S_R = 0.34$. In this case, the velocity and angle data reflect expected trends for a noninteracted stator wake region. For all of the rotor sampling positions, the tangential angles are the most sensitive indicator of rotor wake location at the measurement plane.

Stator exit flow data for 70% PHH are presented in Figure 13(d). The rotor wake broadly influences the stator exit flow and makes crisp

delineation of effects difficult. The deepest stator wake region is measured for a rotor sampling position of $YO_R/S_R = 0.0$, consistent with the cascade plot (see Figure 14[d]). For this rotor sampling position, the stator wake/rotor wake interaction is occurring just upstream of the measurement plane. Radial velocities show classical outward rotor wake flow and inward stator and IGV wake flow.

Stator exit flow data for 90% (Figure 13[e]) indicate broad influence of the rotor on the stator exit flow. Thus, as at 70% span, wake interaction effects are relatively difficult to sort out. Deeper stator wake regions are associated with stator wake/rotor wake interaction just upstream or at the measurement plane. Tangential angles are again good indicators of chopped rotor wake influence location.

By looking at the stator exit flow from hub to tip for three rotor sampling positions, namely, $YO_R/S_R = 0.0$, 0.34, and 0.69 (see Figure 13[f-h]), several observations can be made. Boundary layer growth has extended to 90% PHH behind the stator, compared to only 95% PHH behind the rotor. An upstream effect of the second rotor on the flow at the first stator exit measurement plane is not noticeable, although small (less than 4%) upstream effects are probably present.

5. CONCLUSIONS

Summarized below are the conclusions reached after studying the periodic-average flow data acquired to date. Further data analysis and acquisition are being continued.

The IGV suction surface flow is separated at all radial locations. The separated flow appears to involve unusual unsteady effects that deserve further observation. The IGV exit flow is also complicated by noticeable first rotor upstream effects at the measurement plane.

The chopped IGV wakes move downstream within fixed avenues. Imbedded rotor and stator periodic unsteadiness was found to be appreciable in portions of the compressor annulus, depending on the extent of wake interaction involved at the particular location considered. The concept of chopped wake fluid flowing in the general direction of the slip velocity appears to be verified by the present data. Chopped wake interaction with the suction side fluid of a blade section typically resulted in locally large deviation angles and small axial velocities. As a result of wake interaction, tangential and radial velocities were observed to cancel, while tangential angles added. Behind the rotor, large differences in flow fields could result from rotor wake/IGV wake interactions. Behind the stator, stator wake/rotor wake interactions did not lead to as much variation in flow fields. Stator wake/IGV wake interaction effects were difficult to discern, even though IGV effects could be seen at most spanwise locations. Secondary flow effects were noticeable in some cases near the hub, while leakage and scraping effects were discernible near the tip. Outer

casing boundary layer growth was evident from the first rotor exit
flow to the first stator exit flow.

In general, the periodic-average flow was orderly and explainable
with consistent wake transport and interaction plots and physical
reasoning.

6. REFERENCES

1. Mikolajczak, A. A. "The Practical Importance of Unsteady Flow," in "Unsteady Phenomena in Turbomachinery." AGARD-CP-177, April 1976.

2. Kerrebrock, J. L. and A. A. Mikolajczak. "Intra-Stator Transport of Rotor Wakes and Its Effect on Compressor Performance." Transactions of the ASME 92A, Journal of Engineering for Power, 359-368, 1970.

3. Walker, G. J. and A. R. Oliver. "The Effect of Interaction Between Wakes From Blade Rows in an Axial-Flow Compressor on the Noise Generated by Blade Interaction." Transactions of the ASME 94A, Journal of Engineering for Power, 241-248, 1972.

4. Whitfield, C. E., J. C. Kelly, and B. Barry. "A Three-Dimensional Analysis of Rotor Wakes." The Aeronautical Quarterly, 23: 285-300, 1972.

5. Wisler, D. C. and P. W. Mossey. "Gas Velocity Measurements Within a Compressor Rotor Passage Using the Laser Doppler Velocimeter." Transactions of the ASME 95A, Journal of Engineering for Power, 91-96, 1973.

6. Lockhart, R. C. and G. J. Walker. "The Influence of Viscous Interactions on the Flow Downstream of an Axial Compressor Stage." Proceedings of the 2nd International Symposium on Air Breathing Engines, University of Sheffield, Royal Aeronautical Society, London, 1974.

7. Evans, R. L. "Turbulence and Unsteadiness Measurements Downstream of a Moving Blade Row." Transactions of the ASME 97A, Journal of Engineering for Power, 131-139, 1975.

8. Larguier, Robert and Alexandre de Sievers. "Mesures Instation-naires Dans Les Turbomachines." La Recherche Aérospatiale, 267-277, Septembre-Octobre 1975.

9. Paulon, Jacques. "Optical Measurements in Turbomachinery," in "Modern Methods of Testing Rotating Components of Turbomachines (Instrumentation)." AGARD-AG-207. 1975.

10. Weyer, H. and R. Schodl. "Unsteady Flow Measurements in Turbomachinery," in "Modern Methods of Testing Rotating Components of Turbomachines (Instrumentation)." AGARD-AG-207. 1975.

11. Boutier, Alain, Guy Fertin, Robert Larguier, Jean Lefevre, and
    Alexandre de Sievers. "Laser Anemometry Applied to a Research
    Compressor," in Proceedings of the ISU/AGARD Workshop on Laser-
    Anemometry." R-117/76, 1976.

12. Fabri, Jean and Jacques Paulon. "Unsteady Phenomena in Turbo-
    machines as Revealed by Visualizations and Measurements," in
    "Unsteady Phenomena in Turbomachinery." AGARD-CP-177, April 1976.

13. Fleeter, Sanford, L. Jay, W. A. Bennett, "Compressor Stator Time-
    Variant Aerodynamic Response to Upstream Rotor Wakes." Detroit
    Diesel Allison Division, General Motors Corporation. Indianapolis,
    Indiana, 1976.

14. Gallus, G. E. "Results of Measurements of the Unsteady Flow
    in Axial Subsonic and Supersonic Compressor Stages," in "Unsteady
    Phenomena in Turbomachinery." AGARD-CP-177, April 1976.

15. Hanson, Donald B. "Application of Rotor Mounted Pressure
    Transducers to Analysis of Inlet Turbulence," in "Unsteady
    Phenomena in Turbomachinery." AGARD-CP-177, April 1976.

16. Peacock, R. E. and J. Overli. "Dynamic Internal Flows in
    Compressors with Pressure Maldistributed Inlet Conditions," in
    "Unsteady Phenomena in Turbomachinery." AGARD-CP-177, April 1976.

17. Perkins, J. N., L. W. Hardin, F. O. Carta, and W. C. Griffith.
    "Transients in Turbocompressors." North Carolina State
    University, Raleigh, N. C., EDC-76-1, 1976.

18. Raj, R. and B. Lakshminarayana. "Three Dimensional Characteri-
    stics of Turbulent Wakes Behind Rotors of Axial Flow Turbomachinery."
    Transactions of the ASME 98A, Journal of Engineering for Power,
    218-228, 1976.

19. Runstadler, Peter W., Jr. "Special Applications and New
    Technical Aspects of Laser Anemometry," in Proceedings of the
    ISL/AGARD Workshop on Laser-Anemometry, R117/76, 1976.

20. Tompkins, William T., Jr. and J. L. Kerrebrock. "Exit Flow From
    a Transonic Compressor Rotor," in "Unsteady Phenomena in
    Turbomachinery." AGARD-CP-177, April 1976.

21. Weyer, H. B. and H. G. Hungenberg. "Analysis of Unsteady Flow in
    a Transonic Compressor by Means of High-Response Pressure
    Measuring Techniques," in "Unsteady Phenomena in Turbomachinery."
    AGARD-CP-177, April 1976.

22. Dunker, R. J., P. E. Strinning, and H. B. Weyer. "Experimental
    Study of the Flow Field Within a Transonic Axial Compressor Rotor
    by Laser Velocimetry and Comparison with Through-Flow Calculations."
    ASME Paper No. 77-GT-28, 1977.

23. Gostelow, J. P. "A New Approach to the Experimental Study of Turbomachinery Flow Phenomena." 76-GT-47, Transactions of the ASME 99A, Journal of Engineering for Power, 97-105, 1977.

24. Gallus, H. E., D. Bohn, K. Broichhausen. "Measurements of Quasi-Steady and Unsteady Flow Effects in a Supersonic Compressor Stage." Transactions of the ASME 99A, Journal of Engineering for Power, 537-544, 1977.

25. Hirsch, C. and P. Kool. "Measurement of the Three Dimensional Flow Field Behind an Axial Compressor Stage." Transactions of the ASME 99A, Journal of Engineering for Power, 168-180, 1977.

26. Schmidt, D. P. and T. H. Okiishi. "Multistage Axial-Flow Turbomachine Wake Production, Transport, and Interaction." AIAA Journal, 15:1138-1145, 1977.

27. Wisler, D. C. "Shock Wave and Flow Velocity Measurements in a High Speed Fan Rotor Using the Laser Velocimeter," Transactions of the ASME 99A, Journal of Engineering for Power, 181-188, 1977.

28. Schmidt, D. P. and T. H. Okiishi. "Multistage Axial-Flow Turbomachine Wake Production, Transport and Interaction." AFOSR-TR-77-0720, November 1976.

29. Smith, L. H., Jr. "Wake Dispersion in Turbomachines." Transactions of the ASME 880, Journal of Basic Engineering, 688-690, 1966.

7.   APPENDIX A: CALCULATOR PROGRAMS AND STORAGE

Calculator data acquisition and reduction programs used in the present study are listed in this section. All programs and data are stored on cassette tape and are labeled and indexed as specified below:

Flow coefficient program: Calculation of overall flow coefficient from flow rate venturi meter data. Cassette 4C, file 16.

Actuator position correlation program: Linear least squares correlation between actuator potentiometer voltage readout and actuator motion for probe and circumferential positioning actuators. Cassette 4C, file 3.

Hot-wire effective cooling velocity/actual velocity ratio calibration program: Calibration of hot-wire with respect to sensor yaw angle, pitch angle, and velocity for the determination of the ten coefficients in Eq. (6); consists of two parts: 1) calibration data acquisition, and 2) least squares calibration data correlation. Cassette 8B, files 8, 9, 11-13.

Hot-wire linearizer velocity calibration program: Velocity calibration to determine the four polynomial coefficients required by the anemometer linearizer through a least squares correlation of calibration data. Cassette 11B, files 2-4.

Hot-wire second order velocity calibration program: Velocity calibration to determine the three coefficients in the second order velocity calibration Eq. (5) through a least squares correlation of calibration data. Cassette 11B, file 5.

Periodic-average hot-wire data acquisition program: Acquisition of hot-wire, periodic-average, three-dimensional, circumferential survey data. Cassette 11B, files 5-7.

Periodic-average hot-wire reduction program: Reduction of periodic-average hot-wire data to obtain three-dimensional point flow-field parameters. Cassette 11B, files 8-18.

Periodic-average hot-wire data: Storage of periodic-average hot-wire data obtained with the single inclined hot-wire sensor in the research compressor. Cassette 11B, files 57, 58; data cassette #1, files 1-40.

8. APPENDIX B: PARAMETER EQUATIONS

The equations used in the periodic-average measurement system for the calibration procedures and the acquisition and reduction of data are presented below. Symbols and notations are presented on page xii, while sign conventions are generally shown in Figure 10.

8.1. General Parameters

8.1.1. Basic Fluid Properties

Barometric pressure, N/m^2:

$$P_{atm} = h_{hg@t_{baro}} [1.0-0.0018 (t_{baro}-273.15)] \gamma_{hg@273^oK} \quad (B-1)$$

Density of air, kg/m^3:

$$\rho = \frac{P_{atm}}{R \, t} \quad (B-2)$$

Specific weight of water, N/m^3:

$$\gamma_{H_2O} = \frac{g}{g_c} [996.86224 + 0.1768124 (\frac{9}{5} t - 459.67)$$
$$- 2.64966 \times 10^{-3} (\frac{9}{5} t - 459.67)^2$$
$$+ 5.00063 \times 10^{-6} (\frac{9}{5} t - 459.67)^3] \quad (B-3)$$

8.1.2. Blade-Element Quantity

Percent passage height from hub:

$$PHH = (\frac{r-0.14224}{0.06096}) \times 100 \quad (B-4)$$

8.1.3. Miscellaneous

Venturi volume flow rate, m^3/s:

$$Q_v = 0.05229 \sqrt{\frac{2g_c \gamma_{H_2O} \Delta P_{vent}}{\rho}} \quad (B-5)$$
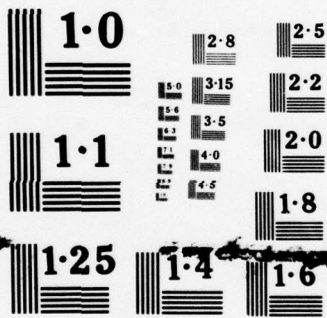
NATIONAL BUREAU OF STANDARDS

Blade velocity, m/s:

$$U = \frac{r\pi RPM}{30.0}$$ (B-6)

Calibration nozzle jet velocity, m/s:

$$V = \sqrt{\frac{2g_c \gamma_{H_2O} \Delta P_n}{\rho}}$$ (B-7)

Venturi flow coefficient:

$$\phi_v = \frac{Q_v}{A \; U_t}$$ (B-8)

8.2. Three-Dimensional Periodic-Average Hot-Wire Parameters

Effective cooling velocity, m/s:

$$V_e = K_1 + K_2 E_\ell + K_3 E_\ell^2$$ (B-9)

Sensor yaw angle relationship (see Figure 8):

$$\cos \alpha = \cos \theta_0 \cos \theta_p \cos \theta_y + \sin \theta_0 \sin \theta_p$$ (B-10)

Effective cooling velocity/actual velocity ratio:

$$V_e/V = b_0 + b_1 \alpha + b_2 \theta_p + b_3 V + b_4 \alpha^2 + b_5 \theta_p^2$$
$$+ b_6 V^2 + b_7 \alpha\theta_p + b_8 \alpha V + b_9 \theta_p V$$ (B-11)

Absolute tangential flow angle (see Figures 8 and 9), degrees:

$$\beta_\theta = \beta_{mv} + \theta_{a,off} + \theta_{y,c}$$ (B-12)

Radial flow angle (see Figure 8), degrees:

$$\beta_r = -\theta_p$$ (B-13)

Radial component of fluid velocity, m/s:

$$V_r = V \sin \beta_r$$ (B-14)

Axial component of fluid velocity, m/s:

$$V_z = V \cos \beta_r \cos \beta_\theta \qquad (B-15)$$

Tangential component of absolute fluid velocity, m/s:

$$V_\theta = V \cos \beta_r \sin \beta_\theta \qquad (B-16)$$

Tangential component of relative fluid velocity, m/s:

$$V_\theta' = U - V_\theta \qquad (B-17)$$

Relative fluid velocity, m/s:

$$V' = \sqrt{(V_\theta')^2 + (V_z)^2} \qquad (B-18)$$

Relative tangential flow angle, degrees:

$$\beta_\theta' = \sin^{-1} (V_\theta' / V_z) \qquad (B-19)$$

9. APPENDIX C: TABULATION OF PERIODIC-AVERAGE HOT-WIRE DATA

The periodic-average circumferential survey data are tabulated in this section. The data represent flow field parameters downstream from the IGV row (station 2), first rotor row (station 3), and the first stator row (station 4). Each vector is completely defined by velocity magnitude, tangential flow angle, and radial flow angle. The computer headings are defined as follows:

Y/SS = circumferential spacing, Y/S_S

V = absolute velocity, V, m/s

BETA Y = absolute tangential flow angle, β_θ, degrees

BETA R = radial flow angle, β_r, degrees

PHH = percent passage height from hub, PHH

YOR/SR = circumferential ratio blade sampling position, YO_R/S_R

Table C-1. Hot wire circumferential survey data obtained with the periodic-average measurement method at minimum noise condition.

STATION 2

PHH=10.00 YOR/SR=0.00

Y/SS	V M/S	BETA Y DEG	BETA R DEG
0.000	15.588	25.046	1.608
0.053	15.642	24.622	1.817
0.103	15.832	24.840	1.018
0.154	15.824	24.588	1.207
0.206	15.679	24.362	1.562
0.257	15.652	24.138	1.527
0.307	15.612	24.060	1.291
0.360	15.511	24.060	1.257
0.411	15.150	23.911	1.455
0.438	14.628	23.536	3.505
0.462	14.371	25.380	2.771
0.488	14.733	24.623	7.771
0.514	11.747	26.262	7.889
0.540	10.353	26.984	9.451
0.565	9.467	26.537	10.906
0.591	9.089	27.050	8.967
0.617	8.565	25.325	10.456
0.642	9.424	24.077	5.327
0.668	10.233	23.170	3.614
0.694	11.806	23.099	0.904
0.720	12.055	21.838	4.701
0.745	13.427	25.679	1.664
0.771	14.142	26.597	2.438
0.796	14.788	26.692	2.002
0.822	15.067	25.916	2.033
0.848	15.389	25.599	1.963
0.874	15.571	25.407	1.570
0.925	15.714	25.769	2.048
0.976	15.753	25.172	1.922
1.000	16.003	25.640	1.085

PHH=30.00 YOR/SR=0.00

Y/SS	V M/S	BETA Y DEG	BETA R DEG
0.001	15.631	21.789	1.502
0.052	15.658	21.389	1.472
0.103	15.676	21.118	1.334
0.154	15.777	21.610	0.984
0.205	15.732	21.177	0.746
0.257	15.550	21.250	0.675
0.308	15.294	20.707	1.371
0.361	15.250	21.240	0.690
0.411	14.977	20.391	1.044
0.462	14.681	20.100	1.639
0.488	14.452	19.161	2.169
0.514	14.262	18.817	2.368
0.539	13.109	17.925	7.376
0.565	11.615	17.899	10.911
0.591	9.832	18.976	16.033
0.617	8.715	23.739	12.337
0.642	8.394	26.223	8.020
0.669	8.812	32.228	8.388
0.693	9.575	24.972	8.600
0.720	11.908	23.656	4.867
0.745	13.194	26.580	6.540
0.771	14.159	25.758	5.341
0.796	14.529	24.122	4.914
0.822	14.874	23.043	3.970
0.848	15.191	23.209	3.536
0.874	15.315	22.911	3.064
0.899	15.601	22.902	3.066
0.925	15.731	22.381	2.229
0.977	15.899	21.754	1.722
1.000	15.906	21.774	1.965

PHH=50.00 YOR/SR=0.00

Y/SS	V M/S	BETA Y DEG	BETA R DEG
0.000	15.548	15.810	1.492
0.051	15.724	20.309	1.044
0.102	15.736	19.426	0.978
0.154	15.831	19.789	0.562
0.205	15.727	19.554	0.902
0.257	15.557	18.962	0.592
0.309	15.492	18.973	0.453
0.360	15.451	18.969	-0.050
0.411	15.199	18.994	0.272
0.462	14.869	18.505	0.946
0.515	14.946	18.211	0.212
0.540	14.846	17.211	-0.148
0.565	14.477	16.636	1.617
0.592	14.139	15.422	1.930
0.616	13.595	17.358	2.834
0.642	11.423	22.207	6.282
0.668	9.546	22.509	5.992
0.694	7.906	25.089	5.672
0.720	8.896	24.302	1.833
0.745	10.145	21.831	1.848
0.771	10.778	21.861	6.831
0.796	12.458	21.776	5.591
0.822	14.058	22.244	5.825
0.849	14.733	23.273	2.656
0.874	15.148	22.876	2.509
0.901	15.251	21.298	2.311
0.925	15.461	21.637	1.530
0.951	15.660	21.835	1.448
0.976	15.815	21.384	0.751
1.000	15.732	21.090	1.243

Table C-1. (Continued).

STATION 2

PHH=50.00 YOR/SR=0.34

Y/SS	V M/S	BETA Y DEG	BETA R DEG
0.000	15.608	21.822	1.228
0.052	15.537	22.187	0.915
0.103	15.253	22.374	1.260
0.154	15.197	20.562	1.135
0.205	15.081	20.220	0.578
0.257	14.859	18.600	1.058
0.308	14.809	18.073	0.625
0.360	14.727	17.694	1.121
0.411	14.887	16.018	1.625
0.463	15.014	15.858	0.385
0.514	15.089	15.009	0.880
0.540	15.024	15.022	0.046
0.565	14.925	14.629	0.625
0.592	14.772	15.432	1.208
0.618	13.578	18.565	2.650
0.642	11.979	17.964	4.708
0.668	10.503	21.209	2.248
0.694	8.737	18.645	2.567
0.720	9.108	20.935	2.740
0.745	10.712	19.110	3.835
0.771	11.751	21.419	0.478
0.796	13.565	22.924	0.858
0.822	15.030	22.071	1.820
0.848	15.206	22.838	3.709
0.874	15.672	22.657	2.506
0.899	15.844	23.529	1.345
0.926	15.757	22.656	1.853
0.951	15.580	22.544	2.544
0.976	15.726	22.647	1.713
1.000	15.789	22.725	1.365

PHH=70.00 YOR/SR=0.00

Y/SS	V M/S	BETA Y DEG	BETA R DEG
0.000	15.225	19.945	-0.106
0.052	15.316	18.869	0.192
0.103	15.432	18.403	0.535
0.154	15.622	18.164	0.461
0.206	15.614	18.247	0.227
0.257	15.596	18.445	0.385
0.309	15.460	18.069	0.107
0.360	15.122	18.815	0.868
0.412	15.019	18.243	0.470
0.463	14.751	17.956	0.616
0.489	14.757	18.197	0.127
0.514	14.728	18.788	0.087
0.539	14.536	17.928	-0.125
0.565	14.440	17.768	0.169
0.591	14.366	17.849	-0.003
0.617	14.C64	17.870	0.588
0.642	13.147	18.981	0.778
0.668	11.955	20.545	1.487
0.694	10.820	22.441	0.016
0.720	10.593	21.907	2.598
0.745	11.087	21.792	3.743
0.771	11.786	19.267	-0.742
0.796	12.909	20.255	1.395
0.822	13.955	21.111	0.482
0.848	14.566	21.518	0.342
0.874	14.895	21.794	0.099
0.900	15.197	21.028	0.241
0.925	15.232	20.391	0.136
0.977	15.499	19.468	0.316
1.000	15.616	19.214	0.294

PHH=90.00 YOR/SR=0.00

Y/SS	V M/S	BETA Y DEG	BETA R DEG
0.000	14.010	18.210	-0.500
0.025	14.238	18.312	-0.889
0.051	14.237	18.705	0.139
0.078	14.496	17.599	-0.360
0.103	14.581	17.565	0.302
0.154	14.415	17.446	0.854
0.205	14.530	17.148	0.986
0.257	14.487	18.275	0.920
0.308	14.578	18.147	0.674
0.360	14.205	17.840	2.353
0.411	14.299	17.486	0.989
0.462	13.736	17.281	3.6C8
0.513	13.684	17.692	3.701
0.566	13.640	16.282	4.031
0.617	13.568	15.651	4.718
0.642	13.538	15.626	5.009
0.669	13.409	15.808	5.748
0.694	12.465	16.754	9.015
0.720	11.071	21.410	6.468
0.746	9.035	24.394	3.123
0.771	9.023	20.477	3.888
0.796	9.532	14.138	2.813
0.822	10.913	18.477	0.964
0.848	12.273	18.233	-2.635
0.874	13.095	18.839	1.648
0.899	13.504	18.934	-0.961
0.925	13.813	18.476	1.537
0.950	14.067	17.608	1.308
0.977	13.984	17.258	0.278
1.001	14.461	16.230	1.394

Table C-1. (Continued).

92

STATION 3

PHH= 5.00, YOR/SR=0.00

Y/SS	V M/S	BETA Y DEG	BETA R DEG
0.000	21.935	49.546	1.073
0.053	21.330	49.312	1.320
0.102	21.171	49.623	0.305
0.129	21.256	49.222	-0.675
0.154	21.172	46.061	-1.811
0.181	21.102	49.598	-3.026
0.206	21.067	54.031	-5.906
0.231	21.067	64.984	-5.459
0.257	21.164	75.861	-2.333
0.282	21.235	81.332	3.559
0.309	21.537	79.924	9.342
0.335	21.971	77.878	11.058
0.362	21.898	75.557	11.435
0.385	21.782	72.410	10.354
0.412	22.023	68.851	8.786
0.436	21.898	68.152	8.173
0.462	22.326	61.324	5.873
0.489	22.466	58.414	5.129
0.514	22.541	57.074	4.938
0.540	23.003	55.844	3.251
0.565	23.042	53.393	3.164
0.616	23.042	53.393	2.550
0.670	23.097	51.889	1.864
0.720	22.921	51.217	1.920
0.772	22.899	50.870	1.122
0.822	22.701	49.455	1.423
0.874	22.281	48.948	1.913
0.926	22.001	48.340	1.369
0.976	21.478	47.201	1.724
1.001	21.455	47.889	1.067

PHH=10.00, YOR/SR=0.00

Y/SS	V M/S	BETA Y DEG	BETA R DEG
0.000	22.434	48.357	-1.516
0.052	21.401	47.655	-0.285
0.103	21.838	48.022	-1.579
0.155	21.547	48.032	-0.664
0.180	21.523	47.736	-0.990
0.206	21.678	48.329	-1.649
0.231	21.587	49.825	-0.971
0.258	20.587	52.875	0.678
0.283	21.161	64.197	-0.101
0.309	21.037	73.123	2.867
0.334	20.775	74.613	6.373
0.360	21.279	73.560	6.359
0.385	21.279	70.402	8.026
0.411	21.906	68.136	9.089
0.437	21.538	63.272	8.259
0.465	22.862	59.094	6.194
0.488	22.862	56.834	5.526
0.514	23.255	54.365	4.036
0.539	23.431	52.212	2.321
0.565	23.244	50.976	1.949
0.592	22.945	49.632	1.859
0.620	23.381	49.545	0.043
0.668	22.965	49.049	-0.088
0.720	23.264	48.597	-0.995
0.772	22.913	47.569	-0.525
0.824	22.768	48.002	-0.833
0.875	22.544	47.754	-0.783
0.925	21.967	46.798	-0.435
0.975	21.759	47.002	-0.116
1.000	21.712	47.737	-0.455

PHH=10.00, YOR/SR=0.32

Y/SS	V M/S	BETA Y DEG	BETA R DEG
0.000	22.829	73.899	3.912
0.025	22.494	77.302	5.779
0.051	21.721	77.391	9.136
0.077	21.455	72.248	9.891
0.103	21.133	68.362	10.387
0.128	20.987	63.684	9.491
0.154	21.190	61.043	6.945
0.180	21.287	56.910	5.769
0.205	21.397	54.057	4.536
0.231	21.844	52.442	2.477
0.257	21.727	49.970	1.293
0.283	21.727	48.449	1.292
0.308	21.946	48.486	0.792
0.359	21.794	47.484	0.386
0.412	21.884	48.229	0.425
0.464	22.086	46.710	0.395
0.514	22.502	47.860	-0.907
0.566	22.477	47.151	-1.153
0.617	22.474	47.539	-1.253
0.668	22.378	47.394	-1.999
0.771	22.378	47.133	-1.819
0.822	21.809	47.187	-0.558
0.848	21.980	48.164	-1.168
0.875	22.258	53.252	-0.991
0.899	22.395	54.933	-0.668
0.926	22.571	65.380	0.964
0.950	22.446	73.897	3.265
0.977	22.421	78.877	5.500
1.000	22.077	79.384	8.215

Table C-1. (Continued).

STATION 3

PHH=10.00
YOR/SR=0.34

Y/SS	V M/S	BETA Y DEG	BETA R DEG
-0.000	22.036	74.190	10.842
0.026	21.453	72.403	13.146
0.051	21.273	68.879	12.238
0.077	21.441	66.163	10.787
0.104	21.694	62.425	8.370
0.129	21.792	59.642	5.935
0.154	21.973	56.218	4.635
0.180	21.966	53.943	3.368
0.205	22.013	51.386	2.134
0.232	21.828	49.514	1.866
0.258	21.801	47.772	1.514
0.308	21.563	46.821	1.348
0.360	21.413	46.873	1.273
0.411	21.852	47.020	-0.145
0.463	21.774	46.955	0.304
0.514	22.151	46.422	0.236
0.565	22.237	46.270	0.371
0.617	22.421	45.818	0.831
0.668	22.375	46.345	1.127
0.720	22.185	46.904	1.261
0.771	22.281	47.525	1.978
0.796	21.778	48.540	1.624
0.822	21.617	50.082	0.135
0.848	21.631	66.690	0.117
0.874	21.933	73.448	3.767
0.899	21.728	76.429	7.277
0.925	21.052	75.049	10.555
0.977	22.052	75.049	10.818
1.000	21.917	72.818	10.483

PHH=10.00
YOR/SR=0.69

Y/SS	V M/S	BETA Y DEG	BETA R DEG
-0.000	22.145	48.527	1.445
0.052	21.884	47.921	1.710
0.103	21.735	47.552	1.130
0.154	21.351	47.635	1.559
0.205	21.228	47.485	1.359
0.257	21.083	47.304	1.234
0.308	21.283	47.348	1.333
0.360	21.229	46.156	-0.212
0.411	21.342	44.946	-0.212
0.463	21.665	45.649	-1.802
0.514	21.742	46.232	-2.008
0.539	21.693	47.190	-2.201
0.565	20.983	50.917	-0.342
0.591	21.121	50.580	0.016
0.617	21.269	60.977	3.163
0.642	21.434	70.553	4.845
0.668	22.157	74.596	5.051
0.694	22.059	72.312	6.179
0.720	22.416	70.868	6.181
0.745	22.592	66.723	6.444
0.772	22.888	64.137	7.873
0.796	22.640	59.635	5.991
0.822	23.253	57.742	4.651
0.849	23.408	55.024	4.139
0.875	23.206	52.644	2.894
0.899	22.969	50.519	2.395
0.925	22.995	49.850	1.977
0.975	22.416	48.312	0.986
1.000	22.493	48.240	0.487

PHH=30.00
YOR/SR=0.00

Y/SS	V M/S	BETA Y DEG	BETA R DEG
0.000	21.739	45.957	0.730
0.051	21.486	46.086	1.060
0.105	21.324	46.071	1.174
0.155	21.182	46.252	0.686
0.205	20.924	45.727	0.443
0.257	20.291	45.580	1.296
0.308	20.185	45.741	0.176
0.334	20.093	45.638	0.831
0.360	19.732	45.038	0.455
0.386	19.500	45.899	1.163
0.411	18.714	45.389	0.329
0.436	18.531	47.755	0.828
0.462	18.619	52.879	3.189
0.490	18.307	61.817	7.502
0.515	13.023	68.657	8.711
0.540	18.118	66.725	8.394
0.555	18.696	62.102	5.543
0.591	19.477	56.903	3.168
0.615	19.692	52.942	3.322
0.642	20.631	49.268	1.401
0.668	20.962	47.399	1.280
0.695	21.392	46.008	0.607
0.720	21.446	45.824	0.970
0.745	21.521	45.928	1.309
0.771	21.608	45.618	1.392
0.822	21.798	45.035	0.831
0.874	21.723	45.473	1.307
0.926	21.748	46.174	1.201
0.976	21.611	45.594	1.250
0.999	21.601	45.828	1.235

Table C-1. (Continued).

STATION 3

PHH=30.00 YOR/SR=0.42				PHH=50.00 YOR/SR=0.00				PHH=50.00 YOR/SR=0.17			
Y/SS	V M/S	BETA Y DEG	BETA R DEG	Y/SS	V M/S	BETA Y DEG	BETA R DEG	Y/SS	V M/S	BETA Y DEG	BETA R DEG
0.000	22.806	54.909	0.301	0.001	20.545	41.928	-0.362	-0.000	20.640	41.854	0.527
0.025	22.560	55.348	2.185	0.052	20.605	41.579	0.210	0.051	20.775	42.147	0.060
0.051	22.333	63.857	4.805	0.103	20.658	42.662	1.026	0.103	20.621	41.897	1.113
0.077	22.410	64.537	5.419	0.154	20.532	42.241	1.096	0.155	20.659	42.375	1.025
0.103	22.065	62.894	7.269	0.206	20.502	42.096	0.649	0.206	20.717	42.564	1.206
0.128	22.021	60.623	5.893	0.257	20.418	41.704	1.172	0.257	20.924	43.312	0.982
0.154	21.538	58.378	5.481	0.308	20.591	42.208	0.457	0.309	20.940	42.964	1.737
0.180	21.046	56.283	5.421	0.359	20.383	42.321	0.272	0.334	21.383	44.971	0.843
0.205	21.011	54.512	5.412	0.411	20.339	41.778	0.636	0.359	21.521	46.045	0.964
0.232	20.228	52.549	3.879	0.462	20.468	42.098	0.009	0.387	21.562	52.351	2.908
0.257	19.697	50.550	4.193	0.489	20.738	42.760	-0.378	0.411	21.244	55.069	5.689
0.308	19.936	48.217	2.541	0.515	20.665	43.288	0.324	0.439	21.359	56.332	5.192
0.359	20.052	46.400	1.818	0.540	21.151	46.413	0.256	0.463	21.083	54.470	5.593
0.412	20.361	46.159	0.150	0.565	20.937	50.680	2.399	0.489	21.433	51.967	3.301
0.463	20.301	45.644	0.058	0.592	21.273	54.557	3.285	0.516	20.938	49.017	3.785
0.514	20.309	45.096	-0.132	0.617	21.533	56.387	4.269	0.539	20.840	48.037	2.818
0.565	20.134	43.948	0.581	0.643	21.186	54.781	5.259	0.565	20.469	46.377	3.005
0.618	20.542	44.345	0.160	0.668	20.233	53.780	5.707	0.592	20.366	46.579	2.371
0.668	21.013	44.212	0.692	0.694	20.501	53.400	5.073	0.617	20.267	45.950	2.842
0.719	21.146	43.485	-0.869	0.723	19.620	51.545	5.204	0.642	19.937	45.034	1.262
0.771	21.535	43.863	-1.040	0.746	19.702	50.597	2.766	0.669	19.744	44.626	0.561
0.797	21.579	44.004	-0.323	0.773	19.526	49.196	1.031	0.694	19.756	44.615	0.045
0.822	21.958	45.047	-0.991	0.797	19.222	47.457	0.668	0.719	19.647	44.051	0.093
0.848	21.883	45.718	-0.395	0.825	19.446	46.023	0.253	0.745	19.638	43.716	-0.757
0.874	22.241	45.444	-0.898	0.848	19.601	43.997	0.696	0.771	19.685	43.507	-0.499
0.899	22.131	46.444	-0.376	0.874	19.572	43.295	-0.209	0.822	19.814	42.314	-0.701
0.925	22.656	49.799	-0.444	0.899	20.076	43.048	-0.887	0.875	20.191	42.238	-0.010
0.950	22.717	52.482	-0.392	0.925	20.169	42.929	-0.490	0.925	20.316	41.693	0.334
0.976	22.809	61.894	1.841	0.977	20.660	42.783	-0.818	0.976	20.586	41.949	0.594
1.000	22.658	65.177	3.195	1.000	20.803	42.814	-0.176	1.000	20.633	42.030	0.595

Table C-1. (Continued).

STATION 3

PHH=50.00 YOR/SR=0.28

Y/SS	V M/S	BETA Y DEG	BETA R DEG
0.000	20.775	42.225	-0.014
0.053	20.483	42.192	0.622
0.104	20.607	43.004	1.027
0.156	20.884	43.469	0.307
0.180	20.775	43.644	1.077
0.206	20.953	44.193	1.304
0.231	21.085	45.268	0.814
0.258	21.417	49.642	2.073
0.283	21.243	53.349	4.534
0.309	21.409	56.574	5.357
0.335	21.512	56.844	5.140
0.361	20.952	51.562	5.391
0.385	21.070	50.371	4.304
0.411	21.120	48.571	2.797
0.436	21.013	46.936	1.585
0.463	20.799	45.868	1.674
0.488	20.696	45.105	1.768
0.515	20.396	44.653	1.983
0.539	20.516	44.755	1.007
0.566	20.174	44.191	1.113
0.591	20.212	44.013	-0.517
0.618	20.213	44.758	-0.294
0.669	19.802	43.889	-0.310
0.720	19.693	43.305	-0.865
0.771	19.909	42.483	-1.427
0.824	20.015	42.698	-1.075
0.874	20.151	42.777	-0.118
0.926	20.416	41.378	-0.097
0.976	20.671	43.078	-0.073
1.000	20.508	42.559	0.968

PHH=50.00 YOR/SR=0.50

Y/SS	V M/S	BETA Y DEG	BETA R DEG
-0.000	20.408	42.426	-0.007
0.027	20.244	43.054	0.260
0.053	20.174	44.873	0.554
0.077	20.066	48.476	1.299
0.103	19.850	52.872	4.041
0.129	20.469	57.066	3.848
0.156	20.587	56.147	5.168
0.181	20.823	52.813	5.199
0.205	21.192	50.312	4.264
0.231	21.609	46.565	2.799
0.257	21.546	44.921	2.205
0.283	21.634	44.207	1.303
0.309	21.481	43.863	0.785
0.334	20.998	43.070	1.433
0.360	20.699	43.132	1.753
0.385	20.676	42.127	1.470
0.411	20.645	43.017	0.904
0.437	20.341	42.314	1.675
0.463	20.374	42.587	1.156
0.514	20.234	43.100	0.731
0.565	19.819	41.603	1.028
0.617	19.847	42.653	-0.169
0.668	19.724	42.319	-0.664
0.719	19.435	41.886	-0.322
0.771	19.843	42.087	-0.810
0.822	19.946	42.144	-0.453
0.874	19.954	41.598	0.094
0.930	19.654	41.140	-0.453
0.976	19.423	41.885	0.299
1.000	19.091	43.919	0.661

PHH=50.00 YOR/SR=0.69

Y/SS	V M/S	BETA Y DEG	BETA R DEG
0.000	18.903	58.122	3.134
0.025	18.610	52.747	5.717
0.052	20.051	49.021	1.049
0.077	20.264	45.230	1.849
0.105	21.053	43.229	-0.016
0.127	21.338	42.955	-0.273
0.154	21.269	42.613	-0.144
0.180	21.122	42.566	0.849
0.207	21.057	42.519	0.462
0.257	20.898	43.138	0.773
0.311	20.673	42.271	1.309
0.360	20.666	42.157	0.609
0.414	20.419	41.392	1.399
0.463	20.400	41.511	0.830
0.514	20.482	42.924	0.254
0.565	20.125	42.845	0.302
0.617	19.940	42.932	0.545
0.668	19.955	43.038	-0.704
0.720	19.869	41.750	-0.144
0.745	20.019	41.346	-0.319
0.771	19.991	41.068	-0.864
0.797	19.577	40.603	-0.149
0.822	19.664	41.661	-0.071
0.846	19.151	45.519	-0.906
0.874	18.615	50.776	2.352
0.899	18.445	58.471	3.029
0.925	17.924	62.382	5.659
0.950	17.627	61.672	5.633
0.977	17.229	56.443	6.193
1.000	17.802	56.018	4.394

Table C-1. (Continued).

STATION 3

PHH=50.00 YOR/SR=0.83

Y/SS	V M/S	BETA Y DEG	BETA R DEG
-0.000	20.311	44.803	0.019
0.026	20.446	42.048	1.548
0.051	21.115	43.497	-0.549
0.077	21.014	42.356	0.708
0.103	21.049	42.803	0.246
0.154	20.813	42.676	1.131
0.206	20.765	42.361	1.092
0.257	20.729	41.968	1.189
0.308	20.543	41.271	1.332
0.361	20.635	41.801	1.520
0.411	20.550	41.904	1.124
0.464	20.655	42.122	0.151
0.514	20.320	42.206	0.190
0.565	20.277	42.222	-0.190
0.617	20.396	41.895	0.389
0.642	20.348	40.777	0.279
0.670	20.620	41.063	0.228
0.694	20.626	43.204	0.523
0.719	20.841	46.921	0.960
0.745	21.033	52.991	3.862
0.771	20.466	55.522	6.073
0.797	20.010	58.235	8.193
0.822	20.073	60.944	6.328
0.849	18.989	59.089	6.947
0.873	18.518	57.721	6.089
0.900	18.724	53.690	3.248
0.925	18.359	50.415	3.191
0.951	18.835	49.814	1.160
0.976	18.561	48.556	2.435
1.000	18.886	47.864	1.156

PHH=70.00 YOR/SR=0.00

Y/SS	V M/S	BETA Y DEG	BETA R DEG
-0.000	18.682	45.370	1.031
0.051	18.797	44.717	1.488
0.103	19.133	45.666	0.986
0.154	19.022	43.541	1.864
0.209	19.109	43.540	1.195
0.257	19.236	42.959	0.839
0.309	19.102	42.134	1.620
0.360	19.142	41.593	1.726
0.411	19.207	41.257	1.771
0.464	19.501	42.508	1.165
0.515	19.499	42.848	2.310
0.541	19.554	42.161	1.957
0.594	19.662	43.438	0.866
0.617	19.724	43.846	1.146
0.642	20.038	43.588	0.365
0.668	20.039	46.013	0.553
0.694	20.206	49.147	1.914
0.720	20.285	52.979	2.646
0.745	19.782	54.491	3.278
0.771	19.969	53.295	5.397
0.796	19.581	51.841	3.506
0.824	19.521	48.979	4.161
0.848	19.338	47.251	2.147
0.875	19.301	46.544	2.295
0.899	19.207	46.761	1.165
0.928	18.809	46.501	0.730
0.951	18.752	45.441	1.588
0.976	19.064	45.437	1.361
1.000	18.846	47.042	0.475
		45.877	1.353

PHH=70.00 YOR/SR=0.53

Y/SS	V M/S	BETA Y DEG	BETA R DEG
-0.000	19.075	41.084	0.383
0.026	18.851	40.337	0.898
0.052	18.750	40.054	-0.119
0.077	18.363	39.254	-0.242
0.103	18.552	39.296	0.558
0.128	18.144	36.583	-0.750
0.155	17.828	40.790	0.093
0.180	17.778	40.143	0.291
0.207	17.783	50.143	0.397
0.231	17.410	52.728	1.545
0.257	17.047	52.152	2.355
0.282	16.634	51.952	3.640
0.309	17.016	48.517	3.916
0.334	17.914	48.505	3.365
0.360	19.074	39.564	1.609
0.385	19.627	38.792	1.317
0.412	19.712	33.779	0.847
0.436	19.657	38.986	1.073
0.463	19.597	38.175	1.228
0.514	19.542	39.278	1.157
0.565	19.511	39.615	1.099
0.617	19.566	41.098	1.521
0.668	19.306	40.509	1.587
0.719	19.124	41.582	0.267
0.772	18.946	41.932	0.512
0.822	18.839	41.833	0.263
0.875	18.837	41.752	0.278
0.925	18.965	41.337	0.099
0.976	19.001	40.674	0.092
1.000	18.966	40.131	-0.092

Table C-1. (Continued).

STATION 3

PHH=90.00 YOR/SR=0.00				PHH=90.00 YOR/SR=0.63				PHH=95.00 YOR/SR=0.00			
Y/SS	V M/S	BETA Y DEG	BETA R DEG	Y/SS	V M/S	BETA Y DEG	BETA R DEG	Y/SS	V M/S	BETA Y DEG	BETA R DEG
0.000	18.138	42.709	4.794	0.000	18.102	49.628	3.651	0.001	17.246	47.657	8.808
0.053	17.487	43.307	3.417	0.026	18.505	47.691	1.426	0.026	16.867	48.735	6.366
0.102	17.083	43.671	2.132	0.052	19.306	45.700	-1.753	0.051	16.232	49.405	6.457
0.154	17.032	43.759	0.819	0.077	19.728	44.734	1.607	0.077	15.729	49.090	6.327
0.205	17.021	42.244	1.997	0.103	19.985	46.603	-0.117	0.102	15.157	48.065	5.170
0.257	17.448	40.010	1.665	0.128	19.820	48.060	2.883	0.129	15.866	50.467	5.158
0.309	17.590	40.074	3.251	0.155	20.695	52.954	1.693	0.153	15.651	50.170	0.064
0.365	18.050	40.822	3.820	0.180	20.481	54.346	1.235	0.180	15.269	50.852	0.254
0.411	18.455	40.295	3.577	0.206	20.145	56.545	0.648	0.204	15.177	48.519	2.245
0.463	18.602	39.740	4.879	0.231	19.479	56.123	2.213	0.258	15.493	49.181	4.167
0.516	19.145	42.014	3.415	0.257	18.915	55.240	1.642	0.310	15.522	49.632	5.503
0.540	19.025	42.097	4.379	0.283	18.590	55.516	1.673	0.360	15.771	48.672	6.149
0.567	19.334	43.466	3.129	0.309	17.974	52.674	0.941	0.411	15.767	48.952	7.923
0.591	19.511	44.928	1.942	0.360	17.653	48.971	0.674	0.462	15.243	49.048	11.083
0.617	19.387	44.743	2.700	0.412	17.586	41.474	1.080	0.514	15.552	55.964	7.515
0.642	20.206	45.465	0.704	0.464	17.973	39.237	1.449	0.565	15.970	50.223	7.062
0.669	19.609	45.664	2.273	0.514	18.214	38.429	1.841	0.616	16.628	57.706	5.003
0.696	19.574	45.907	0.706	0.565	18.261	37.858	2.953	0.668	17.030	65.100	5.519
0.719	19.637	50.651	1.454	0.617	18.322	36.601	4.295	0.721	16.203	66.969	2.406
0.746	19.230	52.272	0.033	0.668	18.819	38.217	5.186	0.746	16.602	67.987	0.231
0.771	19.472	55.354	1.240	0.719	19.038	37.727	6.227	0.771	16.623	67.005	1.693
0.797	19.325	51.823	0.330	0.771	19.332	38.350	6.679	0.796	16.608	64.299	4.289
0.827	19.153	49.597	2.653	0.822	19.487	38.117	6.515	0.822	17.619	61.385	0.534
0.848	18.877	46.345	4.836	0.849	19.577	39.951	5.219	0.848	16.857	54.166	7.458
0.875	18.919	44.662	5.069	0.873	19.557	43.245	5.866	0.874	17.039	48.672	9.808
0.899	19.034	43.823	4.909	0.899	18.840	46.344	4.289	0.899	17.716	48.955	9.808
0.926	18.663	41.724	5.748	0.925	18.151	49.183	3.986	0.925	17.522	43.919	6.205
0.951	18.305	38.748	6.110	0.951	18.169	51.189	2.637	0.950	17.527	43.179	8.458
0.975	17.946	39.372	6.083	0.976	18.558	51.122	-0.515	0.976	17.180	44.868	7.440
1.000	17.936	40.510	4.845	1.000	16.742	49.106	-1.316	1.000	16.423	45.197	7.855
											8.503

Table C-1. (Continued).

STATION 4

PHH=10.00, YOR/SR=0.00

Y/SS	V M/S	BETA Y DEG	BETA R DEG
0.000	16.007	36.358	2.118
0.025	14.836	37.024	3.414
0.051	14.363	37.354	2.124
0.077	13.538	34.904	2.587
0.104	13.721	34.655	1.012
0.130	15.222	33.415	-0.970
0.154	15.222	32.530	-2.353
0.180	16.205	33.140	-2.383
0.205	17.170	34.473	-2.631
0.231	17.576	34.482	-1.960
0.257	17.771	35.923	-0.596
0.310	17.206	36.239	1.178
0.360	16.382	37.435	-0.274
0.412	16.195	36.125	2.548
0.463	16.133	36.047	4.090
0.490	14.085	38.701	2.409
0.514	14.211	38.908	2.395
0.541	14.198	38.323	1.316
0.565	14.496	38.176	1.450
0.592	15.557	38.290	1.354
0.617	16.043	38.047	2.305
0.642	16.572	37.566	2.024
0.668	16.903	36.851	2.075
0.720	17.306	36.903	0.496
0.771	17.632	35.031	-0.496
0.822	17.807	34.241	-2.118
0.874	17.503	34.095	-2.941
0.926	16.977	34.412	-2.792
0.976	17.503	34.412	-0.874
1.000	16.977	35.487	0.699

PHH=10.00, YOR/SR=0.34

Y/SS	V M/S	BETA Y DEG	BETA R DEG
0.000	15.258	37.042	1.515
0.025	14.462	38.207	1.395
0.051	14.060	38.151	-0.664
0.077	13.862	37.488	-1.836
0.103	14.463	36.179	-5.191
0.129	15.202	34.132	-4.952
0.154	15.936	32.001	-3.473
0.180	16.530	32.139	-1.069
0.206	16.509	32.682	5.312
0.257	16.903	38.008	9.010
0.283	15.286	39.036	9.113
0.308	14.954	38.048	8.333
0.334	14.742	40.309	7.693
0.360	14.550	39.903	8.209
0.386	14.736	39.237	9.150
0.411	14.558	38.074	7.290
0.438	15.257	37.765	7.363
0.462	15.681	36.742	6.393
0.489	16.075	35.111	5.393
0.514	16.591	33.728	7.808
0.565	17.087	33.249	0.868
0.617	16.811	32.622	-0.878
0.668	16.830	30.337	-4.287
0.720	16.870	31.814	-5.692
0.771	17.567	32.018	-4.489
0.822	17.653	33.061	-4.072
0.874	17.474	33.957	-3.615
0.925	17.033	34.803	-1.637
0.977	16.642	37.554	-1.842
1.000	16.155	36.857	-0.842

PHH=10.00, YOR/SR=0.69

Y/SS	V M/S	BETA Y DEG	BETA R DEG
0.000	15.098	40.431	4.816
0.025	14.652	38.974	2.667
0.051	14.483	37.479	1.205
0.077	14.321	35.393	-0.248
0.103	14.638	32.731	-0.512
0.128	14.898	30.730	1.227
0.154	15.174	29.240	4.769
0.181	15.799	31.578	6.588
0.206	15.753	33.173	10.089
0.232	16.475	34.923	9.914
0.257	16.961	35.673	6.239
0.308	17.282	33.848	4.778
0.360	17.686	33.392	2.581
0.412	17.797	32.949	1.002
0.463	16.187	32.254	5.122
0.514	15.363	35.733	7.055
0.541	15.198	36.181	6.457
0.565	15.700	36.089	2.015
0.591	15.776	34.518	1.262
0.617	15.861	34.032	-0.514
0.643	15.884	32.985	1.543
0.659	17.135	34.338	3.587
0.694	17.306	34.286	3.904
0.722	17.495	39.170	1.619
0.772	17.488	41.300	3.393
0.822	17.382	40.398	2.606
0.874	17.035	39.304	5.303
0.925	16.541	39.201	4.809
0.976	16.541	38.824	5.527
1.000			

Table C-1. (Continued).

STATION 4

PHH=30.00 YOR/SR=0.00

Y/SS	V M/S	BETA Y DEG	BETA R DEG
0.000	16.219	35.230	-0.478
0.026	15.903	36.493	-0.157
0.051	15.706	37.456	-0.538
0.078	15.124	36.239	0.517
0.104	14.846	36.920	-0.426
0.128	14.127	36.532	-0.364
0.155	13.557	35.720	-0.101
0.180	13.694	33.960	1.001
0.206	13.644	32.377	-0.996
0.232	14.703	31.149	-0.977
0.257	14.422	29.229	-0.742
0.283	15.217	28.229	1.717
0.308	16.923	29.678	2.723
0.334	17.285	32.213	4.221
0.360	17.717	32.755	2.895
0.367	17.755	32.797	2.517
0.411	18.042	33.650	1.686
0.463	18.278	33.208	0.359
0.514	18.096	32.197	-1.121
0.565	17.598	31.935	-0.062
0.617	16.990	31.577	1.242
0.668	16.742	32.376	0.350
0.720	16.677	32.649	-0.528
0.771	16.267	33.571	-0.980
0.822	15.854	34.013	2.026
0.874	16.154	34.306	1.264
0.925	16.092	35.618	1.243
0.951	16.122	34.790	1.313
0.977	16.286	35.162	0.159
1.000			

PHH=30.00 YOR/SR=0.34

Y/SS	V M/S	BETA Y DEG	BETA R DEG
0.000	17.269	36.367	-0.843
0.052	16.461	36.319	0.081
0.078	16.558	36.179	0.028
0.104	15.870	37.816	0.955
0.128	15.168	37.672	0.367
0.154	14.549	39.174	0.367
0.180	13.869	38.834	0.671
0.206	13.891	36.871	2.806
0.232	14.170	34.461	1.013
0.257	14.722	33.214	0.471
0.283	16.047	34.361	3.434
0.308	17.084	33.677	0.079
0.334	17.211	34.193	2.168
0.359	17.823	34.209	2.005
0.386	17.728	36.329	2.095
0.411	17.677	36.092	2.834
0.437	17.453	37.586	2.595
0.463	17.433	37.794	3.663
0.489	17.389	38.237	4.467
0.513	17.103	39.310	3.809
0.566	16.926	38.644	2.697
0.617	16.871	38.099	2.304
0.669	17.035	38.825	2.794
0.720	17.173	37.621	0.442
0.771	17.217	36.621	0.474
0.822	17.214	35.811	0.590
0.874	17.523	36.107	0.360
0.925	17.410	35.426	
0.976	17.255	34.944	
1.000	17.217	35.901	

PHH=30.00 YOR/SR=0.69

Y/SS	V M/S	BETA Y DEG	BETA R DEG
0.000	16.195	34.451	-0.315
0.027	15.805	33.337	-0.108
0.051	15.277	33.979	1.427
0.078	14.726	35.012	0.896
0.104	14.022	36.405	0.837
0.128	13.486	36.465	-1.352
0.154	12.494	37.418	-0.872
0.180	12.345	35.659	-1.216
0.206	12.747	34.061	-0.011
0.232	13.575	34.516	0.726
0.257	14.261	31.677	4.047
0.282	15.101	33.953	5.440
0.308	15.569	33.493	5.657
0.335	15.984	34.807	6.329
0.360	15.859	33.703	6.225
0.385	16.234	35.140	4.844
0.412	16.368	34.911	4.308
0.438	16.312	34.894	4.235
0.462	16.480	34.757	3.264
0.514	16.435	34.360	3.124
0.566	16.522	33.826	1.944
0.617	16.665	33.527	1.034
0.668	16.529	33.516	0.506
0.719	16.377	32.944	0.263
0.771	16.295	32.987	-0.553
0.822	16.109	32.741	-0.775
0.874	15.775	33.020	-0.887
0.925	15.401	33.594	-1.143
0.976	15.068	33.394	-0.535
1.001	15.104	34.109	-0.558

Table C-1. (Continued).

<div style="text-align:center">STATION 4</div>

PHH=50.00 YOR/SR=0.00

Y/SS	V M/S	BETA DEG	Y BETA DEG	R
0.000	18.428	30.844		0.760
0.052	18.166	30.994		2.038
0.077	18.289	31.621		1.301
0.102	18.270	32.181		1.199
0.129	17.952	33.318		1.132
0.154	16.954	33.843		2.827
0.180	16.149	34.538		3.346
0.205	16.055	34.670		2.977
0.232	14.014	35.489		3.405
0.257	13.269	36.724		2.018
0.282	13.010	34.661		1.268
0.308	13.695	32.306		-2.798
0.335	14.054	29.945		-1.185
0.360	14.768	29.585		-0.044
0.386	15.281	30.749		1.094
0.413	15.654	32.189		1.644
0.438	15.783	32.548		2.508
0.462	15.644	32.542		2.154
0.491	15.718	33.191		2.032
0.514	15.674	33.426		0.754
0.566	15.909	32.936		0.713
0.617	16.051	32.164		-0.366
0.663	16.358	30.134		0.516
0.721	16.826	29.645		0.278
0.771	16.982	28.898		0.546
0.822	17.272	29.128		1.537
0.873	17.414	30.355		2.055
0.925	17.688	31.239		2.143
0.977	17.900	31.450		2.232
1.001	17.910			

PHH=50.00 YOR/SR=0.17

Y/SS	V M/S	BETA DEG	Y BETA DEG	R
-0.000	18.666	33.919		1.107
0.052	18.237	33.508		2.682
0.077	18.251	34.585		2.253
0.102	17.969	34.492		2.760
0.129	17.125	34.522		4.598
0.158	16.396	35.255		4.447
0.180	15.661	35.250		4.614
0.207	14.897	34.204		4.964
0.232	14.440	36.212		1.719
0.257	13.909	34.527		1.192
0.285	13.458	33.536		-0.361
0.309	13.252	32.157		-1.299
0.335	13.547	30.022		-3.245
0.360	14.369	30.440		-3.837
0.387	14.828	30.536		-1.253
0.411	15.190	30.890		0.495
0.437	15.526	32.936		0.178
0.462	15.677	32.935		0.953
0.489	15.850	33.934		0.892
0.517	15.898	33.567		0.885
0.567	15.839	33.093		0.899
0.617	16.229	31.323		0.509
0.672	16.608	30.934		-0.034
0.721	16.937	31.420		0.613
0.774	17.060	31.276		1.279
0.824	17.424	32.903		1.954
0.874	17.467	31.900		2.160
0.925	17.774	33.262		2.634
0.977	18.070	33.317		2.032
1.000	18.134	33.550		2.276

PHH=50.00 YOR/SR=0.34

Y/SS	V M/S	BETA DEG	Y BETA DEG	R
0.000	18.335	31.660		1.573
0.053	18.092	32.041		1.711
0.102	17.647	31.938		2.301
0.129	17.265	32.012		2.228
0.155	16.685	31.951		3.045
0.181	16.400	31.996		2.203
0.207	15.514	32.006		3.642
0.232	14.895	32.145		0.786
0.257	14.493	33.404		-1.054
0.283	13.626	33.280		-1.666
0.308	13.299	32.131		-2.383
0.334	13.248	26.711		-3.385
0.361	13.760	28.533		-3.516
0.385	14.545	26.009		-1.439
0.411	14.936	26.302		0.479
0.437	15.299	30.012		1.634
0.462	15.733	30.661		1.470
0.489	15.908	31.447		1.219
0.514	16.002	31.183		1.352
0.540	16.163	30.742		1.092
0.565	16.306	30.456		1.193
0.621	16.708	30.550		0.778
0.669	16.414	29.916		1.894
0.720	16.816	29.779		1.759
0.772	16.876	30.747		1.939
0.822	17.108	31.835		2.154
0.873	17.533	32.271		0.975
0.925	17.832	32.798		1.130
0.974	17.971	31.526		1.324
1.000	17.904	31.793		1.328

Table C-1. (Continued).

STATION 4

PHH=50.00 YOR/SR=0.50

Y/SS	V M/S	BETA Y DEG	BETA R DEG
0.000	17.929	32.512	0.055
0.026	17.751	32.260	0.561
0.053	17.593	32.231	0.264
0.077	17.291	31.687	1.187
0.104	17.293	31.519	0.215
0.129	16.630	31.137	1.706
0.154	16.529	30.985	1.095
0.180	16.255	30.639	0.910
0.206	15.798	30.830	0.426
0.231	14.274	30.539	3.433
0.258	13.539	31.752	1.643
0.283	12.861	30.405	-0.166
0.308	12.727	31.645	-1.390
0.334	12.611	29.663	-1.697
0.362	13.771	29.748	-1.985
0.386	14.666	30.894	-0.509
0.411	15.305	31.564	1.509
0.437	15.798	31.632	2.151
0.463	16.161	32.325	1.398
0.513	16.339	32.230	1.530
0.566	16.479	31.503	0.633
0.617	16.479	31.600	0.639
0.668	16.527	32.725	0.797
0.720	16.423	32.572	1.192
0.774	16.864	33.507	0.301
0.822	17.062	32.783	-0.269
0.874	17.739	32.996	-0.869
0.925	17.949	32.633	-0.464
0.976	17.796	31.688	-0.518
1.000	17.631	31.112	0.016

PHH=50.00 YOR/SR=0.69

Y/SS	V M/S	BETA Y DEG	BETA R DEG
-0.000	17.500	30.148	0.199
0.051	17.411	29.114	-0.101
0.077	17.309	28.880	-0.036
0.103	17.187	28.556	-0.320
0.129	17.015	28.068	0.064
0.155	16.797	28.761	0.083
0.181	16.436	29.310	-0.095
0.205	15.202	29.702	2.528
0.232	14.232	31.226	1.866
0.259	13.375	33.704	0.517
0.285	12.605	35.756	0.773
0.308	12.781	35.379	1.014
0.334	13.742	33.035	-0.445
0.360	14.564	32.965	1.152
0.387	15.491	32.874	2.291
0.412	16.012	33.874	2.533
0.437	16.188	34.107	2.631
0.463	16.389	33.606	2.325
0.489	16.208	33.057	2.392
0.514	16.224	32.821	1.523
0.571	16.218	32.827	0.638
0.617	16.099	33.127	0.533
0.668	16.296	33.668	-0.170
0.723	16.456	33.338	-0.005
0.774	16.691	32.684	-0.095
0.825	17.162	31.843	-0.962
0.875	17.550	31.546	-1.238
0.925	17.473	30.496	-0.258
0.975	17.557	29.746	-0.204
1.000	17.543	28.975	0.197

PHH=50.00 YOR/SR=0.83

Y/SS	V M/S	BETA Y DEG	BETA R DEG
0.000	17.711	28.130	-0.276
0.051	17.875	29.204	-0.859
0.077	17.504	28.385	-0.146
0.103	17.686	29.155	-0.702
0.130	17.219	29.492	0.151
0.155	16.862	31.052	0.273
0.181	15.971	32.370	1.495
0.205	14.973	34.887	1.206
0.231	13.921	38.004	0.839
0.260	13.175	38.981	0.183
0.283	13.133	37.813	-0.505
0.308	13.366	35.606	-0.163
0.334	14.335	34.815	0.541
0.359	15.060	33.618	1.268
0.386	15.556	32.760	2.343
0.413	16.086	34.124	1.557
0.437	15.999	33.195	1.646
0.464	16.282	34.433	0.073
0.488	15.812	33.039	1.047
0.513	15.866	34.265	1.028
0.566	15.556	33.784	1.005
0.617	16.060	34.162	-0.118
0.668	16.327	33.812	-0.459
0.721	16.539	32.717	-0.778
0.772	16.814	32.155	-0.825
0.824	17.104	30.884	-0.915
0.874	17.481	29.800	-1.024
0.926	17.671	28.524	-0.709
0.973	17.636	28.067	-0.006
1.000	17.831	26.789	-0.433

Table C-1. (Continued).

STATION 4

PHH=70.00, YOR/SR=0.00 | PHH=70.00, YOR/SR=0.34 | PHH=70.00, YOR/SR=0.69

Y/SS	V M/S	BETA Y DEG	BETA R DEG	Y/SS	V M/S	BETA Y DEG	BETA R DEG	Y/SS	V M/S	BETA Y DEG	BETA R DEG
0.000	17.012	29.795	-0.436	0.000	16.665	32.309	-1.778	0.000	15.363	33.843	0.973
0.052	17.377	29.250	-0.453	0.053	16.170	32.678	-0.230	0.051	15.615	32.018	1.117
0.103	16.802	28.802	-0.354	0.103	16.674	33.375	-0.370	0.103	16.188	30.679	1.085
0.154	17.209	28.448	1.138	0.154	16.486	33.636	1.397	0.154	16.336	28.547	0.449
0.180	17.155	28.724	1.644	0.180	16.473	32.940	1.134	0.206	15.534	27.266	0.264
0.205	17.349	29.757	1.474	0.205	16.423	34.297	1.574	0.232	16.561	27.002	0.063
0.232	16.992	30.691	1.912	0.232	16.371	31.602	0.701	0.257	16.236	26.167	1.495
0.257	16.465	32.175	1.710	0.257	16.087	31.356	1.230	0.283	15.929	26.200	1.119
0.283	15.146	35.185	6.670	0.282	15.052	31.041	4.018	0.308	15.271	27.304	-0.237
0.308	13.744	37.934	8.112	0.308	14.388	32.229	3.908	0.334	14.507	26.123	3.493
0.334	13.195	37.798	4.623	0.334	13.643	31.906	2.708	0.359	13.877	28.767	3.497
0.359	13.617	36.911	1.374	0.360	12.670	28.235	0.858	0.386	13.623	28.242	2.192
0.387	13.195	32.587	-2.667	0.386	12.871	28.728	0.281	0.412	13.576	22.242	-1.037
0.411	14.834	30.868	1.410	0.411	13.147	25.912	3.013	0.437	15.864	29.735	1.804
0.437	16.156	30.375	2.663	0.436	13.897	24.117	2.638	0.462	16.616	29.190	2.213
0.464	16.769	31.688	3.414	0.462	14.981	24.887	1.598	0.489	16.614	30.172	2.187
0.489	16.897	33.335	2.580	0.489	15.768	27.926	0.924	0.514	16.929	30.294	0.323
0.515	16.790	32.570	4.484	0.514	15.951	28.486	1.802	0.539	17.158	30.857	0.687
0.540	16.393	33.971	4.416	0.540	15.931	28.830	1.656	0.565	17.052	30.826	0.596
0.565	16.397	32.660	3.711	0.565	16.055	29.389	1.082	0.591	16.783	30.821	0.156
0.592	16.140	34.831	3.183	0.590	16.177	29.010	1.255	0.617	16.769	32.083	0.535
0.618	16.073	34.368	3.735	0.617	16.212	28.513	1.103	0.643	16.422	31.840	-0.107
0.668	16.073	34.368	3.084	0.668	16.188	28.289	0.565	0.669	16.020	33.415	1.077
0.720	15.916	32.935	2.497	0.719	16.327	28.960	0.167	0.719	16.753	34.120	0.971
0.771	15.689	31.722	2.697	0.771	16.455	29.306	0.516	0.772	15.456	35.311	1.059
0.822	15.782	29.865	2.681	0.822	16.180	29.447	0.624	0.822	15.329	33.878	0.274
0.874	16.156	29.430	0.947	0.873	16.087	30.880	0.524	0.873	14.977	31.408	1.840
0.925	16.509	28.701	-0.206	0.925	16.032	30.387	-1.559	0.926	15.628	31.045	-0.666
0.976	16.468	28.954	0.874	0.976	15.691	30.784	-0.187	1.000			
1.001	16.506	28.485	1.030	1.000							

Table C-1. (Continued).

STATION 4

PHH=90.00 YOR/SR=0.00

Y/SS	V M/S	BETA Y DEG	BETA R DEG
-0.000	15.089	35.341	1.506
0.052	14.855	34.401	0.849
0.104	14.558	34.521	1.369
0.155	14.475	33.488	1.696
0.205	14.842	33.293	0.544
0.257	14.866	32.045	1.799
0.283	15.077	32.966	1.407
0.309	14.267	31.415	5.857
0.334	14.190	32.958	5.473
0.360	11.342	33.137	11.067
0.386	12.429	33.884	11.162
0.412	10.925	35.783	5.549
0.437	11.472	35.045	11.825
0.462	12.562	34.948	-0.018
0.488	14.208	35.378	-0.411
0.513	14.734	36.024	3.006
0.539	15.453	37.445	2.963
0.566	15.523	38.578	3.409
0.591	15.621	38.941	2.739
0.617	16.716	40.461	2.856
0.642	16.168	39.221	5.015
0.668	15.923	40.773	5.262
0.694	15.869	40.417	5.275
0.719	15.680	39.784	5.604
0.770	15.991	38.212	3.368
0.823	15.745	37.212	3.765
0.875	15.375	35.403	4.989
0.926	15.065	34.651	3.331
0.967	15.119	34.247	1.689
1.000	14.067	32.893	3.847

PHH=90.00 YOR/SR=0.34

Y/SS	V M/S	BETA Y DEG	BETA R DEG
-0.000	14.969	30.861	1.432
0.051	14.717	30.554	-0.099
0.102	14.319	31.021	-1.191
0.155	14.533	32.562	-2.312
0.180	14.523	32.515	-1.119
0.206	14.523	32.364	-1.542
0.231	14.292	31.962	0.415
0.258	14.380	31.603	0.603
0.283	14.063	31.665	2.188
0.309	13.564	31.548	3.952
0.334	12.510	32.252	3.644
0.359	11.382	32.165	1.278
0.385	10.450	34.267	1.843
0.412	10.487	32.174	2.135
0.437	11.458	32.817	2.681
0.463	12.552	31.129	4.707
0.488	13.679	32.292	4.993
0.514	14.212	33.770	4.394
0.540	14.262	34.896	5.099
0.565	14.308	32.361	5.131
0.591	14.908	32.655	2.568
0.616	14.810	33.663	4.680
0.668	15.216	30.648	3.387
0.720	15.487	28.728	4.126
0.771	16.152	28.718	2.593
0.822	16.364	29.046	2.462
0.874	16.181	29.424	2.764
0.925	15.633	28.291	1.757
0.976	14.746	30.250	0.774
1.000	14.444	31.702	0.733

PHH=90.00 YOR/SR=0.69

Y/SS	V M/S	BETA Y DEG	BETA R DEG
0.001	15.169	36.136	-0.102
0.051	14.909	35.500	1.561
0.103	14.638	34.357	1.333
0.154	14.690	32.635	2.498
0.205	14.760	31.293	2.251
0.258	14.325	29.546	3.625
0.283	14.371	29.755	3.873
0.308	13.699	30.422	4.564
0.334	12.908	30.736	5.122
0.361	11.964	30.631	4.762
0.386	11.088	30.035	4.372
0.412	10.865	28.173	4.509
0.437	11.746	28.592	1.337
0.463	12.797	28.143	1.961
0.488	13.934	29.261	0.952
0.515	14.717	30.840	3.687
0.541	14.880	30.490	4.053
0.565	15.118	31.628	3.080
0.591	15.407	31.098	3.399
0.618	16.167	31.836	2.911
0.643	16.167	31.944	2.010
0.668	16.355	31.848	2.636
0.695	16.621	32.124	2.696
0.719	16.497	34.286	3.811
0.772	16.587	35.640	2.897
0.822	16.072	37.026	3.123
0.874	15.619	38.085	1.599
0.925	14.767	36.959	2.633
0.975	13.969	36.568	2.156
1.000	13.931	37.545	1.004